KINETICS OF REFRACTORY SOLUTION

by

Alfred Robert Cooper, Jr.

B.S. Alfred University

1948

Submitted in Partial Fulfillment of the

Requirements for the Degree of

DOCTOR OF SCIENCE

from the

Massachusetts Institute of Technology

1960

Signature of Author
Department of Metallurgy
May 14, 1960

Signature of Professor in
Charge of Research

Signature of Chairman of
Department Committee
on Graduate Students

KINETICS OF REFRACTORY SOLUTION

by

Alfred Robert Cooper, Jr.

Submitted in Partial Fulfillment for the Requirements

for the Degree of

DOCTOR OF SCIENCE

from

MASSACHUSETTS INSTITUTE OF TECHNOLOGY

1960

ABSTRACT

When diffusion in the liquid determines the solution rate, $\overset{*}{J}$, the simplest statement of the relation is the Noyes–Nernst equation[4],

$$\overset{*}{J} = -\frac{D}{\overset{*}{\delta}} \Delta \overset{*}{C} \qquad (a\text{-}1)$$

where $\overset{*}{\delta}$ is an effective boundary layer thickness and $\Delta \overset{*}{C}$ is the concentration difference between the saturated and the bulk solution. Numerous solution experiments in molten metals and aqueous systems have shown quantitative agreement with equation (a-1) with appropriate expressions for $\overset{*}{\delta}$.

Many experiments of refractory corrosion can be interpreted as evidence that diffusion in the liquid controls the corrosion rate and several persons (notably, because of his precedence, Sosman[14]) have arrived at this conclusion. Previously, however, no one has demonstrated the quantitative validity of this premise, nor has it been shown whether the thick boundary layers associated with viscous liquids require modification of the usual boundary layer equations for mass transfer. The other major obstacles preventing a quantitative treatment of refractory solution have been: (1) Complexity of refractories and industrial slags and glasses; (2) lack of sufficient pertinent property (the effective thickness, $\overset{*}{\delta}$, may be a function of diffusion coefficient, kinematic viscosity, and density difference) data to make accurate predictions; and (3) likelihood of considerable change of properties within the boundary layer and no method to take account of these variations.

The development of experimental and analytical techniques for overcoming these obstacles is the major objective of this work.

The first difficulty can be overcome by choosing a simple system in which the solubilities, ΔC^*, are known. These studies are confined to two such systems: sapphire-CaO-Al_2O_3-SiO_2 slag and a model system of rock salt-glycerine. Many of the important properties of the model system are known which, largely, overcomes the second difficulty and the important dimensionless groups the Reynolds, Grashof and Schmidt numbers in the model system have values which correspond to those expected in the sapphire slag system. Thick velocity boundary layers and other incidental variations were examined in the model system and their influence found to be negligible.

It is shown that transient or free diffusion can be considered as a boundary layer process and that the measured rates of solution in this case, together with those for the forced convection and the free convection cases, give three equations with three unknowns--diffusion coefficient, viscosity, and the pressure gradient causing free convection. Thu in a system such as sapphire-slag where the only pertinent property for whic there are reliable values is viscosity, it is possible to perform the three cases of solution experiments and obtain values of the three pertinent properties. The independently measured viscosity gives a quantitative check of the premise of diffusion controlled kinetics.

Simplification of the unsteady state equations for heat flow from internal cylinders proved appropriate with slight correction for the transie case of the sapphire-slag experiments. Methods for dealing with variable diffusivity in transient diffusion are taken from Phillip[110], and Ellenbaas approximation which considers only the diffusivity of the saturated solution used for free convection analysis. For the forced convection case, the effect of variable diffusivity is determined by substituting directly in the differential equation.

The effect of variable viscosity is derived for flow over a flat plate following von Karman's[71] approximate treatment, and assumed to apply to flow generated by a rotating disc. The expected time dependence of corrosion for an experiment in which neither the transient nor the steady state processes can be ignored is derived.

Except for the forced convection experiments below 20° C in the r salt-glycerine system, the results in both systems all showed quantitative agreement with the predictions of diffusion control in the liquid. The exception appears to be caused by the onset of partial interfacial control which is independently evidenced by the development of crystalline facets o originally cylindrical surfaces.

The pressure gradient causing free convection in the rock salt-glycerine system is shown to be the density difference between glycerine saturated with sodium chloride and pure glycerine. In this slag-sapphire system the experimental evidence reveals that the surface forces are more important than density differences in causing the free convection flow. Analyses of the free convection experiments shows qualitative agreement of the driving force for convection (dP/dx) with the surface tension differenc between bulk and saturated solutions.

Interface diffusion coefficients calculated from solutions experiments at temperatures from 1400° - 1550° C in the sapphire-slag system show reasonable agreement with the extrapolated diffusion coefficients for Si^{++++} measured by Towers and Chipman[88]. At 1350° C the calculated coefficient is low by a factor of about 3. The variation of composition within the boundary layer obtained by chemical analysis of slices is in harmony with diffusion of Si^{++++} controlling the solution process.

Thesis Supervisor: Professor W. D. Kingery

Title: Associate Professor of Metallurgy

TABLE OF CONTENTS

LIST OF FIGURES

Page

Figure

LIST OF TABLES

ACKNOWLEDGMENTS

It is a pleasure to acknowledge the financial support for this work which was provided in the form of a fellowship for two years by the Aluminum Company of America and a research grant from the United States Atomic Energy Commission.

The advisor to this research was Professor W. D. Kingery, who initially conceived the possibility of using the Noyes-Nernst Equations to describe solution kinetics of refractories. His suggestions and criticisms were beneficial throughout the course of the research.

Discussions with Professor C. Wagner were especially helpful in the early stages of this work. Several suggestions by Professor F. H. Norton regarding apparatus design proved extremely valuable. Mr. Fred Wilson assisted with many of the experiments and with the construction of the apparatus.

The typing of the manuscript was done by Miss Mary M. Forbes and her co-operation and interest are appreciated.

Most of the illustrations were drawn by the M.I.T. Illustration Service. Photographs of samples and apparatus were made by Mr. D. M. Fellows. Their competence is evidenced by the quality of the figures.

Finally, the patience, understanding, and moral support of my wife, Jacqueline, throughout the long course of this research are gratefully acknowledged.

I. INTRODUCTION

Various mechanisms have been proposed for the rate of solution of refractories in molten slags and glasses. The purpose of this thesis is to quantitatively evaluate these possibilities.

Refractory corrosion is a problem of economic importance in the glass industry, and in the metallurgical industry. The cost of refractories of a typical glass container furnace is approximately one-tenth the glass melting costs. The reason for shutting down glass-tank furnaces is usually the failure of the side-wall block of the tank resulting from solution of the refractory in the molten glass.

A striking example of refractory solution is found in the oxygen steelmaking process where refractories in contact with molten slag have lifetimes less than 30C hours.

In addition to the economic implications of the solution of refractories, it is of academic importance. There has been relatively little fundamental study associated with solution processes in viscous liquids. Indeed, most previous experiments on solution kinetics have been concerned with solution rates in aqueous solutions, molten salts or molten metals, all of which possess viscosities some thousandfold less than typical for slags and glasses.

Solution kinetics at high temperatures likewise have seldom been investigated. When solids are close to their melting points, mobility in the solid phase may play a role in solution kinetics not observed at lower temperatures.

Typically, there is a substantial change of the physical properties within the liquid layer adjacent to dissolving refractories. This introduces complications which have rarely been studied. Analysis of solution kinetics when there are more than two mobile species is an aspect typical of refractory solution which, to a large part, has been ignored. Finally, there are few, if any, recorded instances where solution was slow enough that analysis of the rates during the early transient stages was possible. This is the case when dealing with most slag-refractory or glass-refractory systems.

II. CLASSICAL TREATMENT OF SOLUTION KINETICS

There are excellent reviews[1,2] discussing solution kinetics. The classic work in the field is that of Noyes and Whitney[3] who rotated cylinders of lead chloride and benzoic acid in water and noted the change of concentration from time to time. They found applicable the relation

$$\frac{dc}{dt} = k_1 \ (C_o - C_{oo}) \ A \equiv k_1 \ \Delta C \ A \qquad 2.1$$

where C_o is the concentration of the saturated solution and C_{oo} the concentration of the bulk solution, A is the area of the interface, k_1 is a constant and ΔC is the solubility. While other processes could explain the first order kinetics, they suggested that the rate of solution was governed by the velocity at which solute molecules diffuse out from the interface.

Nernst[4] generalized this idea to a variety of heterogeneous reactions and made the relationship more explicit by postulating that the chemical reaction takes place so rapidly at the surface that liquid at this surface is quickly saturated and remains so during the solution process. Further, he presumed that beyond a finite distance δ the concentration, is that of the bulk solution and equation 2.1 can be rewritten in analogy to Ficks First Law to yield

$$JA = \frac{dc}{dt} = D/\delta^* \ (\Delta C) \ A \qquad 2.2$$

where J is the diffusion flux density, D is a diffusion coefficient and $\overset{*}{\delta}$ is an effective thickness. This sort of relationship has been verified in two ways:[5] First by noting that the temperature dependence of the solution rate bears a close resemblance to the temperature dependence of the diffusion coefficient and second by noting that the value for the effective boundary layer thickness, $\overset{*}{\delta}$, in water is about the same for a variety of solutes.

Stirring can effect solution rates by diminishing the value of $\overset{*}{\delta}$. Thus, if stirring increases solution rates, it is evidence that diffusion in the liquid is of importance. There are numerous evidences of the effect.[1,6,7,8,9]

It is conceivable that the surface reaction might be slow and the diffusion step rapid so that the saturated solution cannot be maintained at the interface. In this case the reaction will be interface controlled and while equation 2.1 could still apply, the proportionality constant k_1 would apply to collision probabilities of solvent and solute molecules. There are examples[10,11] of solution processes which appear to be governed by an interface reaction but the evidence is not as decisive as for the diffusion controlled examples.

For the generalized solution process an expression is needed for the rate of solution when either or both diffusion or interface reaction control. Moelwyn Hughes[1] following the approach of Berthoud[12] derives an expression which can readily be transformed to

$$J = \frac{k_s (\Delta C)}{(1 + k_s(\overset{*}{\delta}/D))} \qquad 2.3$$

where k_s is the rate constant for the interface reaction. When $D/\overset{*}{\delta} \gg k_s$ or $D/\overset{*}{\delta} \ll k_s$ the kinetics simplify into either interface control on diffusion control respectively. There seems to be no experimental study reported where $k_s \approx D/\overset{*}{\delta}$.

It is evident from equations 2.2 and 2.3 that one method for evaluating solution kinetics is to change the effective boundary layer thickness $\overset{*}{\delta}$. This can be done without affecting any of the physical properties of the system by controlling the convection in the liquid.

For multicomponent systems the diffusion equation takes on a much greater complexity. While these more involved relationships are necessary for rigorous analysis, the data required for their use is not available. A more complete discussion of this question is included in the Appendix, "Diffusion in Liquids."

III. REVIEW OF THE LITERATURE ON REFRACTORY SOLUTION

As might be expected from the economic importance associated with the problem of refractory solution there is much published literature dealing with virtually all aspects of the problem. Fortunately, there exists an excellent collection of abstracts[13] of recent literature pertaining to refractories and many of the indexed subjects pertain to the mechanism of refractory solution.

While it would be impractical to attempt a summary of all the articles on this field the following is a brief discussion of the major ideas advanced to explain refractory solution rates.

Diffusion in the Liquid

Among the first writers to seriously consider the problem of refractory solution was Sosman[14]. He, in 1925, concluded that the two main factors which affect the solution rates of refractories were the solubility of refractory in the glass and the mobility or diffusion coefficient of the refractory components in the glass. This idea, which follows directly from the Noyes-Nernst equation 2.2, has had several other advocates in recent years. McCallum and Barrett[15] studied the reaction between sapphire and calcium-aluminum-silicate slag and tentatively concluded that the rate of solution was controlled by the diffusion of oxygen ions in the melt. They also measured the diffusivity of calcium oxide in slag compositions by determining the change of index of refraction.

Weigmann[16] examined the solution of small pellets of refractory in molten glasses with the aid of a high-temperature microscope. He was able to show that the solution of refractory was diffusion controlled. He concluded that high diffusion rates would be preferable in order to eliminate refractory stones from glass.

As noted in the discussion of equation 2.2, when solution rates are influenced by convection, it is a manifestation of control of the solution rate by diffusion in the liquid. While the quantitative relation between diffusion and convection has been obscure to most investigators of refractory solution, it has occurred to many that any convection process which brings unsaturated liquid in contact with the refractory interface will accelerate the corrosion process. Among the early investigators examining or commenting on this point were McCauley[17], Brownlee[18] and Flint and Payne.[19] Flint and Payne, for example, noted the excessive corrosion frequently encountered at horizontal joints on the side walls of glass tanks. They attributed this to the lack of protection of the downward facing surface by refractory saturated glass. They suggested that slag saturated with refractory was denser than that of the bulk glass. Once solution products formed on downward facing interfaces, they would sink and fresh unsaturated slags would be drawn in. This mechanism can also be utilized to explain the excessive metal line corrosion of glass tank sidewalls, illustrated in Figure 3.1. The heavier refractory saturated glass flows down the sidewall bringing fresh unsaturated glass to the upper portion of sidewall.

FIGURE 3.1 PHOTOGRAPH OF THE CONTOUR OF A GLASS SIDEWALL BLOCK (AFTER GOULD[56])

Confirmation of this convection effect is found in a series of solution experiments carried on by Busby and Partridge.[20] They found that, in contradiction to usual refractory materials whose corrosion was most severe at the top of the immersed portion, the solution of fused silica rod by molten glass left a wedged-shaped sample with minimum corrosion at the liquid surface. Presumably, silica solution decreases the density of the glass and hence fresh unsaturated glass was continually flowing to the lower surface of the silica rod.

However, the only careful attempt to measure at glass tank temperatures the density difference between cord glass, i.e. refractory saturated glass, and bulk glass, have not supported this point. Loffler's[21] comparison revealed fireclay cords to be somewhat lower in density and cords from fusion-cast aluminum silicate to almost equal in density to windowglass. The certainty of these results may be subject to question, but if they are correct, they invalidate the explanation for the excessive corrosion of downward facing refractory surfaces and at the metal line in glass tanks.

The influence of convection on refractory solution was examined directly by Reed and Barrett[22] in an experiment in which they rotated rods of sapphire in a molten slag. The scatter was too large to allow any quantitative relationship between solution rates and speeds of rotation but the data clearly indicated that the higher the speed of rotation, the more likely a high corrosion rate. Moore and Heeley[23] rotated the crucibles in which the refractory samples were immersed and found slight increases in the rates of solution with rotation. These evidences all reveal that diffusion in the liquid must affect refractory solution kinetics.

Endell, Fehling and Kley[24] were perhaps the first to suggest the role of viscosity in governing solution kinetics of refractories. They presented a curve for a wide variety of refractory slag systems and showed that, in general, the solution rate is reasonably well determined by the fluidity of the glass. As diffusivity and fluidity both relate to mobility of units in the liquid, this can be taken as support for the premise of refractory solution controlled by diffusion in the liquid. The fluidity of the melt also controls the velocity of convection and Endell, Fehling and Kley emphasized the importance of convection in determining the rate of refractory solution, and they proposed an empirical expression for slag attack which, while undoubtedly useful, gives no insight into the details of the solution process.

The effectiveness of high viscosity liquids in diminishing corrosion rates is supported by noting that zirconium oxide is perhaps the most resistant oxide to solution in alkali silicates. According to the work of Marboe and Wyle[25] the viscosity of an alkali silicate is increased most when ZrO_2 is substituted for SiO_2.

Solomon[26] has attempted to explain the uneven penetration of refractory blocks by suggesting that once an uneven region develops, this serves to cause a vortex in the viscous flow in that vicinity and hence causes an increase in the rate of refractory solution by a stirring process. Analysis of viscous flow behavior in glass tanks[27] does not support this thesis because the flow velocities near the wall are so extremely slow and stream lines closely follow the contour of the wall.

Diffusion in the Solid

There is a rather extensive body of literature suggesting that the solution kinetics are determined by diffusion into the solid. Loffler[28] suggested that alkali ion diffusion into refractory blocks can cause failure by vitrification or liquification of the blocks, and thus implied a mechanism for solution, which is governed by diffusion into the solid. Steinhoff[29] arrived at the same conclusion from composition profiles for various components of glass and refractory, and showed there was a discontinuity in composition between an interfacial layer and the composition of the bulk glass. It is this discontinuity which he associates with the cord formation by refractories.

Konopicki[30] has found alkaline migration half-way through the sidewall block in an operating glass tank. His belief is that the lower temperatures further away from the glass refractory interface diminished the diffusion rates and hence effectively prevented further alkali penetration.

Rigby[31] has shown that, when two spinel bricks of different compositions are placed on one another, the diffusion of iron, for example, from a magnetite brick proceeds faster than does diffusion of chrome from a chrome-magnetite brick. The net effect is a swelling and eventual fracture of the chrome-magnetite brick. While this relates to two solid phases, it is at least conceivable that such a mechanism might occur between a liquid and a solid phase. It requires the diffusion flux in the solid to be greater or approximately equal to the diffusion flux in the liquid. Indeed, the best explanation[32] thus far for the flaking off of discreet particles

of glass when attacked by aqueous solution relates to the diffusion of hydrogen ions into the glass structure and ultimate expansion of the structure causing fracture.

The driving force for this diffusion in the solid has generally been related to the higher activities of some components in the glass than in the solid. A difference in activity coefficients has been demonstrated by the E.M.F. measurements of Plumat[33]. He shows that the potential between oxide and glass decreases from a positive value in this order; silica, alumina, zirconia, until a negative value is achieved for calcia and baria. LeClerc and Peyches[34] have shown that this potential can result in galvanic corrosion. When two refractories of different composition are in electrical contact with one another, the differences in activities can cause one to dissolve while the other grows.

Another aspect of the diffusion of components from the liquid into the solid is the multiphase nature of the solid. It is quite likely that one phase may be more soluble than another. A model experiment elucidating this was performed by Hyslop, Gumm and Biggs[35] in which they suspended a grog-wax composite in a carbon-tetrachloride solution and noticed how the solution of the wax took place in such a manner to permit the falling of grog particles into the liquid.

In a more recent paper Harrison and Wagner[36] have examined the kinetics for the solution of alloys in molten metals. When one component of the alloy is considerably more soluble than the other, the solution rate is initially controlled by diffusion of the more soluble component into the liquid. The surface soon becomes depleted of the

soluble component. Then, it requires diffusion of the soluble component through the solid before more solution can take place. In this case, diffusion in the solid becomes rate controlling and the preservation of a smooth surface is an unstable situation. This is indicated by Figure 3.2 taken from Harrison and Wagner. It shows a perturbation of an originally flat surface. In the region, II, where the surface is recessed, the solid diffusion distance is least and diffusion and solution take place most rapidly in this region increasing the recession. A mechanism such as this may have relevance in the solution of fusion cast refractories which are dense and contain several components of different solubilities.

A similar model has been proposed for the role of mullite crystals in fireclay refractories;[37] the less soluble mullite crystals forming a barrier layer to retard fireclay solution.

Lambelet[38] investigated the equilibrium phases between a soda-lime glass and a fireclay refractory at various temperatures, and in none of his work did he find the presence of mullite. There has as yet been no experimental confirmation of the idea of a barrier layer affecting the solution kinetics of refractories.

The penetration of porous refractories by slags or glasses requires no solid state diffusion.

The extent to which capillary penetration occurs depends upon the wetting properties of the slag on the refractory surface. Comoforo and Hursch[39] examined wetting behavior and found that most silicate liquids wet most alumina-silicate refractories very effectively. Following

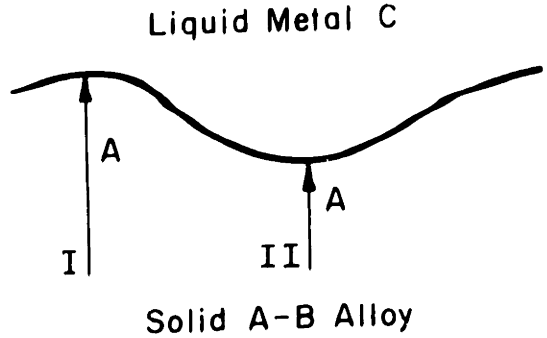

FIGURE 3.2 LEACHING OF COPPER (= METAL A) FROM A SOLID COPPER-NICKEL ALLOY (= A-B ALLOY) BY LIQUID Ag (= METAL C) SATURATED WITH NICKEL AFTER HARRISON AND WAGNER

the work of Adams[40] they discuss the effect of contact angle on the ability for a liquid to penetrate into fine irregular crevices. It is not clear, however, why when capillary pores are not vertical, complete wetting is necessary to achieve penetration.

Because of the importance of wetting behavior on penetration of porous refractories, it has often been suggested that the major task to diminish refractory solution was to find a refractory not wet by glass.

To exploit this idea patents were granted for the use of vanadium oxides as a refractory component based on the poor wetting of vanadium oxide by silicate liquids. This idea proved to be less feasible than initially anticipated because wetting of vanadium oxide increased markedly as the temperature was increased above 1200° C[41].

Parsons and Insley[42], in an examination of corrosion characteristics of optical glass pots, found that glass penetrated the pores of fireclay refractories. They were able to minimize the effect by coating the pot surface with very finely divided clays. This suggests that when the pore size is fine enough, the refractory saturated glass is virtually immobilized in the pores.

Rasch[43] suggested that the liquid phase penetrates into the capillaries of porous refractories and then the cations diffuse into the solid particles. However, it is not necessary to postulate diffusion into the solid grains to explain enhanced solution rates in porous solids.

Interface Control

While the possibility of interface control is allowed by equations 2.1 and 2.3, there have been few suggestions that this is actually the case in refractory solution kinetics. Salmang[44] interpreted his results on the effect of glass composition on refractory solution rates to reveal that an interface reaction was rate controlling.

McCallum and Barrett[45], examining the solution kinetics of single crystals of spinel and sapphire in calcium silicate, sodium silicate, and magnesium silicate, came to the same conclusion, but in their later work in a similar system[15] they concluded that diffusion control in the liquid is dominant.

Surface Forces

Jebsen-Marwedal[46] was first to suggest the possible effects of surface forces in glass making other than the already mentioned role of surface tension in capillary penetration. He advanced the idea that variation in surface tension between refractory saturated and bulk glass affects the way refractories and cords dissolve in glass. His work bears criticism, however, because his analysis and experiments do not apply to submerged refractories or cords and he does not mention this important limitation.

Tress[47] has more explicitly examined the effect of surface properties. He has shown that the variation in surface tension and viscosity with increasing solution of the refractory by the glass can cause a type of convection flow in the neighborhood of the glass-air

refractory surface. This process had been illustrated earlier for the case of soap bubbles and alcohol water solutions.[48]

It has often been observed that bubbles at downward facing surfaces in contact with molten slag of glass appeared to cause acceleration of the refractory solution process. Preston and Turnbull[49] postulated that if the surface tension of the refractory-saturated glass is greater than that of the bulk glass, the surface tension gradient can provide a force opposite to that of gravity. This is a potentially unstable situation which, in their opinion, can cause a motion of the bubbles which carries fresh glass to the refractory surface. With smaller bubbles the bubbles actually jump downward from the surface and float back while large bubbles show no gross motion. Preston and Turnbull were able to confirm their premise by examination of various low temperature model systems.

Loffler[50] proposed a somewhat different explanation for the role of bubbles. In his estimation, the surface active behavior of alkali ions causes its concentration at the surfaee of the bubbles. This greater concentration increases the alkali gradient in the solid and thereby speeds up the "vitrification process."

While Tress and Preston and Turnbull introduced the idea that surface forces may be the dominant driving force for convection at a refractory-melt interface, their premises fit into the general concept of diffusion in the liquid as the rate controlling step for refractory solution. Loffler, on the other hand, sees surface active behavior as

contributing to solid diffusion. It should be pointed out that surface activity of alkali would also increase diffusion gradients in the liquid.

Solubility

Whatever the rate controlling process, the rate of solution will be affected by the solubility. This is revealed by equations 2.1 and 2.3 for diffusion into the liquid or phase boundary control. For diffusion into the solid, solid solubility would play an analagous role.

Except in relatively idealized situations, the solubilities of refractory components cannot be accurately inferred from the phase diagrams. Very little work, however, has been done to measure the solubilities in complex commercial systems. King[51] measured the solubility of zirconia in boro-silicate glasses, but even in this case the work was not motivated by interest in refractories and the temperature level of King's studies was too low to be of direct applicability to refractory solution.

Inferences of the influence of solubility can be found in the literature. Budnikov and coworkers[52] showed that the corrosion rate of alumina fireclay refractories in a glass tank was decreased when the alumina content of the glass was increased. A similar effect is suggested by the work of Barsh[53] in which he suspended refractory samples in glass containing crucibles. He found that the rates of refractory solution of the suspended bars were greater when the crucibles were lined with platinum, thus preventing the solution of the crucible itself from diminishing the solubility of the test bar.

Temperature

Temperature is an important variable in determining the rate of solution of refractories. Many investigators have examined the temperature dependence of refractory solution without analyzing its effect on the details of the solution process. Blau and Smith[54] found for a particular refractory glass system the relationship

$$\log \frac{J_1}{J_2} = .0024 (T_1 - T_2)$$

where J is the solution rate at temperature, T. For relatively small intervals of temperature and when the temperature level is kept relatively constant this expression infers that there is an activation energy for the solution of refractories.

Day and Ambrosini[55] investigated the temperature dependence of the solution of sapphire and fusion cast ZAC. Plots of log solution rate versus reciprocal temperature had identical slopes for both refractories, but sapphire dissolved nearly twice as rapidly as ZAC. The apparent activation energy for the solution process calculated from these results is 80,000 K cal/mole.

Temperature variations within a glass tank can be great. Gould[56] attributes the exaggerated corrosion at the metal line to the vertical temperature gradient in the furnace; the higher temperatures near to the surface causing a faster rate of solution of the refractory. This argument cannot be fully accepted in view of the similar corrosion patterns in glass pots which are virtually at uniform temperature. Brysen[57] made a more detailed examination of the temperature distribution throughout the blocks

of the glass tank furnace and measured temperatures in various positions as a function of time. From this he was able to determine that the solution process took place at a much faster rate initially than after the furnace had been in operation for some time. He attributed this to the cooling effect from the thinning of the sidewalls of the furnace.

There is no doubt that refractory solution is markedly affected by temperature. This is confirmed by experimental results as well as by the evaluation and analysis of the refractory solution in glass furnaces. The difficulty is that both the kinetics of the process and the driving force i.e., the solubility of the refractory, are temperature dependent; and until their separate influences can be distinguished, it is difficult to use temperature dependence for critical analyses of the process.

Time

A final factor affecting refractory solution already inferred is the time of the experiment. In the case of laboratory experiments, the initial solution rate may be decidedly more rapid if diffusion control is dominant because of the virtually infinite diffusion gradient at zero time. Secondly, in the practical case, as pointed out by Brysen, the temperature of the interface is itself, a function of time and its change effects the rate of solution.

Experimental Methods

There have been many laboratory methods devised to evaluate the performance of refractories in contact with corrosive liquids. Both

Norton[53] and Partridge[59] give summaries of methods which are useful. In general, they can be divided into three major categories. In the first, a refractory is actually immersed in the corrosive liquid and allowed to remain in contact for a specified time. Convection currents can be induced[20,22] during the experiment, but as yet there has been no attempt to produce a quantitatively definable flow pattern. Webber, Seifert and Tooley[60] discuss the importance of simulating in such tests the type of convection and temperature distribution that the refractory will receive in practice. To more fully achieve these similarities, both Loomis[61] and McMullen[62] have devised miniature glass tank furnaces for the purpose of refractory evaluation and testing. The problem of maintaining all the necessary dimensional similarities in such a unit is vast and has been discussed by Preston[63].

In a second sort of test, the slag glass can either be sprayed or dripped on the refractory surface and the degree of penetration evaluated after a specified time period.

Finally, tablets can be made of a mixture of refractory and slag and their slumping determined as a function of time and temperature.

Model systems can be used to evaluate refractories. For example, Partridge and Biggs[64] suggest using the solution of fireclay refractories by 50% hydrofluoric acid as a measure of the refractory's resistance to corrosion. This sort of test is one which actually determines the silica content of the brick and implies that the lower the silica content, the higher the resistance to corrosion. Already mentioned in this discussion has been the test of Hyslop in which a grog-wax mixture was used to evaluate corrosion in two-phase systems.

To determine the diffusion patterns, Jaupain[65] has used fluorescent oxides, such as zirconia, in the refractory and measured the decay of fluorescence with distance from the refractory interface. It would be also conceivable, for example, to use a radio-active tracer or a colorant tracer to perform a similar service. The difficulty is that the mobility of the tracer may be different from that of the bulk components. The method of Weigmann using a high temperature microscope to study continuously dimensional changes of a refractory sample seems to be one which should be more thoroughly utilized.

Summary

After examining the available data on refractory solution, Kingery[66] concluded that refractory solution rates are usually governed by diffusion in the liquid. While critical quantitative experiments are not available, the bulk of the experimental data thus far collected can be satisfactorily explained in terms of rate control by diffusion in the liquid. Most convincing in this regard are the experiments which reveal an effect of convection on the rates of refractory solution; no such influence would be expected were the process determined by a phase boundary reaction or by diffusion in the solid. A major reason for the lack of critical experiments is the complexity of actual refractory-glass and refractory-slag systems. It is difficult to separate the various effects that may be present.

IV. GENERAL BOUNDARY LAYER THEORY

Velocity Boundary Layer

The boundary layer concept was first introduced by Prandtl[67]. He reasoned that for flow past a solid object only a small portion of the liquid adjacent to the solid is affected by its presence. He considered this region to be the boundary layer and its thickness is termed, δ_u, the subscript u specifying that reference is made to the velocity boundary layer.

By reducing the Navier Stokes equations[68] to dimensionless quantities and ignoring the terms which are vanishingly small, Prandtl was able to show that

$$\delta_u \sim 1\ (Re)^{-1/2} = \left(\frac{\nu\, l}{u_{oo}}\right)^{1/2} \qquad 4.1$$

where ν is the kinematic viscosity, l is a characteristic length, u_{oo} is the main stream velocity and Re is the dimensionless Reynolds number. Exact numerical solutions for flow past a flat plate[69] and toward a rotating disc[70] confirm this premise.

$$\delta_u \text{ (flat plate)} \approx 5.0 \times (Re_x)^{-1/2} \qquad 4.2a$$

$$\delta_u \text{ (rotating disc)} \approx 4.0\ d\ (Re_d)^{-1/2} = 4.0 \left(\frac{\nu}{\omega}\right)^{1/2} \qquad 4.2b$$

where x is the distance from the leading edge, d the disc diameter and ω the angular velocity.

The reason for the approximate signs in equations 4.1 and 4.2 is that the boundary layer thickness δ_u is not uniquely defined. The ambiguity is based on the fact that the velocity approaches the bulk velocity assymtotically at the outer edge of the boundary layer. Figure 4.1 shows the velocity distributions for flow adjacent to a flat plate. The boundary layer thickness δ_u was arbitrarily selected as that distance for which $u = .99\, u_{oo}$.

There are various other conventions involved in the definition of boundary layer thickness. One of the most convenient for the purpose of this paper is the effective boundary layer thickness δ^*_u which is determined by extrapolating the slope of the velocity profile at the interface to the region of undisturbed flow. This makes δ^*_u entirely analogous to δ^* the boundary layer thickness for diffusion transfer. It is clear from Figure 4.1 that in the exact solution for flow above a flat plate, $\delta^*_u \approx 0.6\, \delta_u$.

One of the methods used to obtain approximate solutions for the flow in boundary layers is to assume a simple functional relationship between the dimensionless velocity $\hat{u} = \frac{u}{u_{oo}}$ and the dimensionless distance $\hat{y} = y/\delta_u$ such that the velocity vanishes at $\hat{y} = 0$ and $\hat{u} = 1$ at $\hat{y} = 1$. A convenient description because it also permits the slope to be virtually constant near $\hat{y} = 0$ and to vanish at $\hat{y} = 1$ is the cubic parabola suggested by Von Karman[71]

$$u = k_2 y + k_3 y^3 \qquad 4.3$$

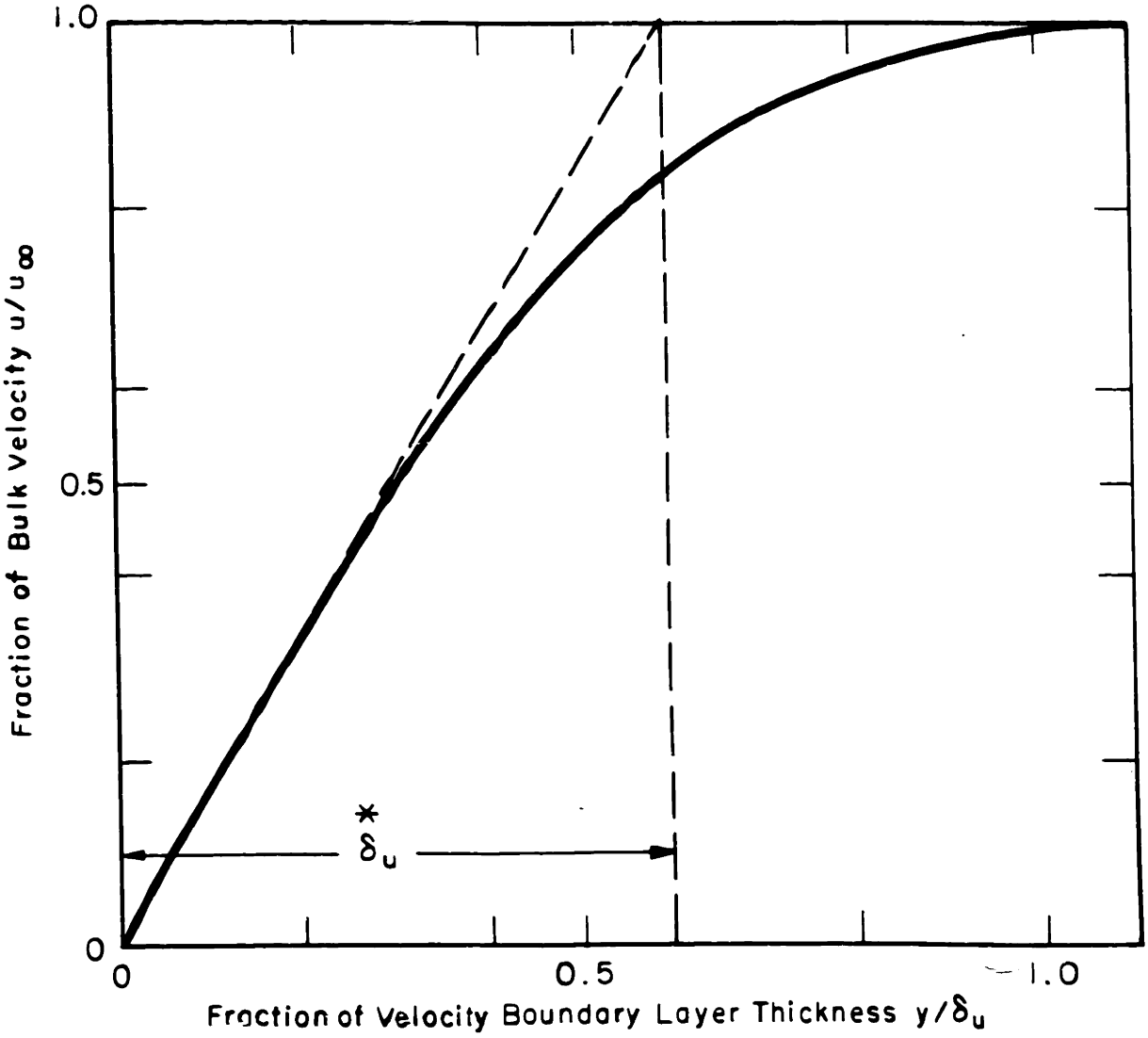

FIG. 4.1 VELOCITY PROFILE IN BOUNDARY LAYER FOR FLOW OVER FLAT PLATE

This permits a relatively simple solution for the boundary layer thickness and leads to very nearly the same value for the effective boundary layer thickness as the exact solution for flow above a flat plate.

According to equations 4.2a and 4.3, within the boundary layer, the velocity u, parallel to a flat plate decreases with distance from the leading edge. From the requirement of continuity there then must be a velocity, v, in the direction normal to the plate.

Diffusion Boundary Layer

So long as the flow velocity has a component in the direction of the diffusion flux, i.e. normal to the interface, the flow will influence the diffusion process. The easiest way to characterize this is to determine the boundary layer thickness for diffusion.

Von Karman's approximation leads to a convenient approximate solution[72] for the effect of fluid convection on the boundary layer thickness for diffusion provided the boundary layer for diffusion is less thick than the velocity boundary layer and the concentration profile is described by a cubic parabola. Then the effective boundary layer thickness for diffusion for flow above a flat plate is given by

$$\overset{*}{\delta} = 3.09 \left(\frac{\nu x}{u_{oo}}\right)^{1/2} \left(\frac{D}{\nu}\right)^{1/3} = 3.09 \times Re^{-1/2}\, Sc^{-1/3} \qquad 4.4$$

where Sc the Schmidt number is a dimensionless quantity, the ratio of the kinematic viscosity to the diffusivity. In general, the boundary layer thickness for forced convection can be expressed as a product characteristic length and a function of dimensionless numbers

$$\overset{*}{\delta} = x \; f(Re,Sc) \qquad 4.5$$

Solution in the absence of a velocity field gives rise to fluid flow due to density changes which have their thermal analogy in natural convection about heated objects. The other dimensionless number of importance is the Grashof number, (Gr), which includes the buoyancy forces causing fluid flow.

$$(Gr) = \frac{g x^3}{\nu^2} \left(\frac{\rho_o - \rho_{oo}}{\rho_{oo}}\right) = \frac{g x^3}{\nu^2} \Delta\rho \qquad 4.6$$

where ρ_o = density of saturated solution, ρ_{oo} = density of bulk solution, $\Delta\rho$ = fractional change in density and g = gravitational acceleration. The thickness of the boundary layer can be represented for the general case of free convection flow by

$$\delta_3^* = x\, f\,(Gr, Sc) \qquad 4.7$$

An approximate analysis similar to that used for forced convection above a flat plate has been used[72a] to determine the boundary layer thickness for free convection. For high Schmidt numbers

$$\delta_3^* = 1.96\, x\, (Gr, Sc)^{-1/4} = 1.96 \left(\frac{D\nu x}{g\,\Delta\rho}\right)^{1/4} \qquad 4.8$$

Recent experimental studies in heat[73] and mass[74] transfer confirm this equation with lower values for the constant probably resulting from values of the Schmidt number too small for the complete validity of equation 4.8.

In addition to the diffusion boundary layers that are associated with steady state mass transfer under the influence of forced or free convection there is an analogous situation that applies in the early

stages of a free diffusion process without convection, i.e., during unsteady or transient mass transfer process. While this situation has not typically been referred to as an example of a boundary layer, for the purpose of this work it has all the necessary characteristics.

For example diffusion from a surface into a semi-infinite medium[75] has the concentration profile shown in Figure 4.2 in which δ is defined by the condition when $y = \delta$, $\hat{C} = \frac{c_o - c}{c_o - c_{oo}} = .99$. It is clear that the general appearance of concentration profiles in the transient case is similar to the velocity profiles from forced convection (Figure 4.1).

The boundary layer thickness taken from the solution of the diffusion equation for this case is

$$\delta_1 = 3.6\ (Dt)^{1/2} \qquad 4.9$$

or since from Figure 4.2

$$\overset{*}{\delta}_1 = 1/2\ \delta$$

$$\overset{*}{\delta}_1 \approx 1.8\ (Dt)^{1/2} \qquad 4.10$$

From exact calculations

$$\overset{*}{\delta}_1 = (\pi\ Dt)^{1/2} \qquad 4.11$$

In combination with the Noyes-Nernst equation 2.2, equations 4.4, 4.7 and 4.11 reveal the properties on which the rate of solution depends when diffusion in the liquid is the rate-controlling step. The following functional relationships summarize this information.

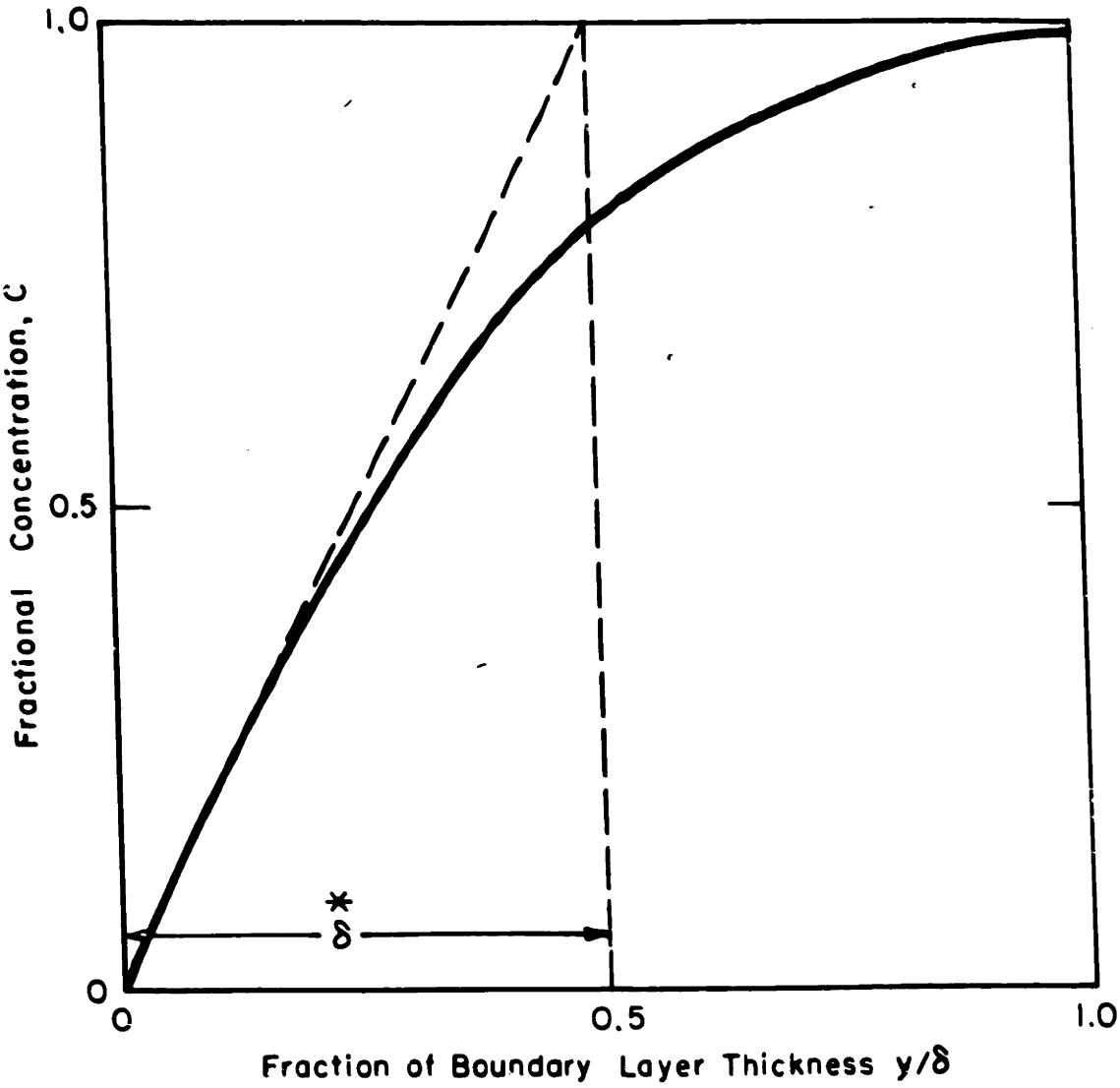

FIG. 4.2 CONCENTRATION PROFILE IN BOUNDARY LAYER FOR FREE DIFFUSION

$$J_1 = t^{-1/2} f(D)(\Delta C) \qquad \text{(i)}$$

$$J_2 = x^{-1/2} f(D)(\Delta C)(\gamma)(u_{oo}) \qquad \text{(ii)} \qquad 4.12$$

$$J_3 = x^{-1/4} f(D)(\Delta C)(\gamma)(\Delta \rho) \qquad \text{(iii)}$$

Often what is measured is not the rate of solution J but the total amount of solution M. The set of equations, 4.12, are readily transformed to:

$$M_1 = \int_o^t J_1\, dt = t^{1/2} f(D)(\Delta C) \qquad \text{(i)}$$

$$M_2 = \int_o^t J_2\, dt = x^{-1/2} t\, f(D)(\Delta C)(\gamma)(u_{oo}) \qquad \text{(ii)} \qquad 4.13$$

$$M_3 = \int_o^t J_3\, dt = x^{-1/4} t\, f(D)(\Delta C)(\gamma)(\Delta \rho) \qquad \text{(iii)}$$

Equations 4.12 and 4.13 reveal that transient diffusion, forced convection and free convection require respectively 2, 3 and 4 physical properties of the system to describe the rate of solution and that 4.12 (ii) and 4.13 (ii) have parameter u_{oo} that can be varied experimentally. Also it is easy to distinguish the processes by noting different dependences on x and t.

If solubility is known and the system is simple succeeding experiments of transient diffusion, forced convection and free convection permit all the pertinent physical properties to be determined without their direct measurement.

Similarity Solutions

Even though solutions for the boundary layer equations are only available for a limited number of simple geometries, experimental or approximate solutions can be extended to a variety of cases by the use of equations 4.5 and 4.7. As long as the pertinent dimensionless numbers and the geometry are unchanged the functional dependence, once determined, is appropriate in all other cases[76]. This suggests the use of models as a means of determining the governing relationships in cases for which analytical solutions, are unavailable. As an example of this approach, Eisenberg, Tobias and Wilke[77] studied the solubility of benzoic acid cylinders rotated in a liquid bath at velocities corresponding to Reynolds numbers of 10^3 - 10^5. They found experimentally that data could be correlated by the relation (rearranged from their results),

$$\overset{*}{\delta} = 12.64\, d\, (Re_d)^{-.7}\, (Sc)^{-.356} \qquad 4.14$$

V. MATERIAL PROPERTIES

Introduction

Among the simple refractory oxides (R_xO_y) only sapphire (Al_2O_3) is readily available as a single crystal in a wide range of shapes and sizes. There is one stable phase, corundum, of alumina from room temperature to its melting point. For these reasons single crystals of sapphire were used for the majority of the solution experiments.

The most widely studied simple system including Al_2O_3 is the $CaO-Al_2O_3-SiO_2$ system. It has large liquid regions of high viscosity and is an idealization of industrial silicates important in glass, metallurgical and boiler technology. This explains its choice for this study.

The properties which are of interest in solution kinetics have already been discussed. They are: a) solubilities, b) activities, c) diffusivities, d) density and partial molar volumes, e) viscosity and f) surface tension.

A possible source of confusion is the several means of specifying composition in a ternary system. There seems to be no accepted convention regarding the distinction between mol % and wt %. In addition, for alumina, both mol % Al_2O_3 and mol % $AlO_{1.5}$ are used. Figure 5.1 shows the relations between these three ways of specifying Al_2O_3 content.

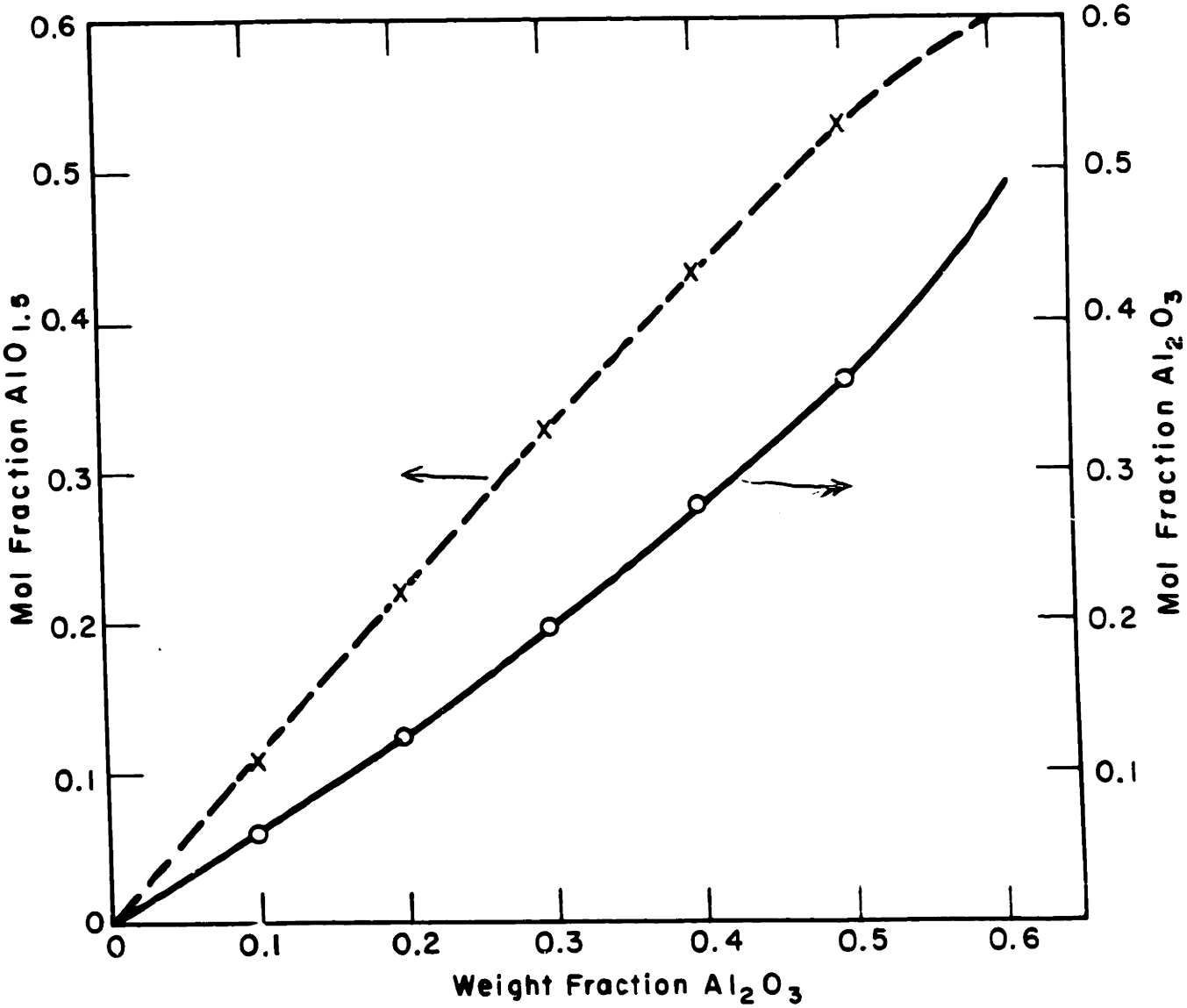

FIG. 5.1 NOMOGRAPH SHOWING RELATIONSHIP BETWEEN SEVERAL WAYS OF SPECIFYING Al_2O_3 CONTENT

Solubility

When the mass transfer is written as a diffusion equation, the driving force for flow is the concentration difference between the saturated and bulk solution. The saturation temperature and composition of a given component is termed the liquidus of that component. The liquidus surfaces in the system $CaO-Al_2O_3-SiO_2$ are rather well established up to 1600° C by the work of I. W. Greig and G. A. Rankin and F. E. Wright as summarized in the ternary phase diagram.(78)

The portion of interest is summarized in Figure 5.2 where the primary field of Al_2O_3 is enclosed by the bold line. The liquidus surface in equilibrium with Al_2O_3 is indicated by dashed isothermal liquidus curves. These are extrapolated beyond the boundaries of the Al_2O_3 field as dotted lines to suggest that Al_2O_3 may be in contact with a liquid with which it is not in equilibrium but from which the equilibrium phase has not crystallized. The shaded region on the ternary plot gives the general range of bulk compositions utilized in this study.

As the compositions all lie very near to the binary $Al_2O_3-CaO-SiO_2$ it may be possible to simplify the system. Figure 5.3 shows the equilibrium relations in this psuedo binary. Below 1380° C the system cannot truly be considered a binary because phases are present that cannot be described in terms of the end members. However, the dashed line indicating Al_2O_3 in equilibrium with liquid below 1380° C on the diagram may be appropriate if the crystallization of anorthite and gehlenite is a slower process than the solution of alumina. If this is the case, it is not wrong to treat the system as a binary.

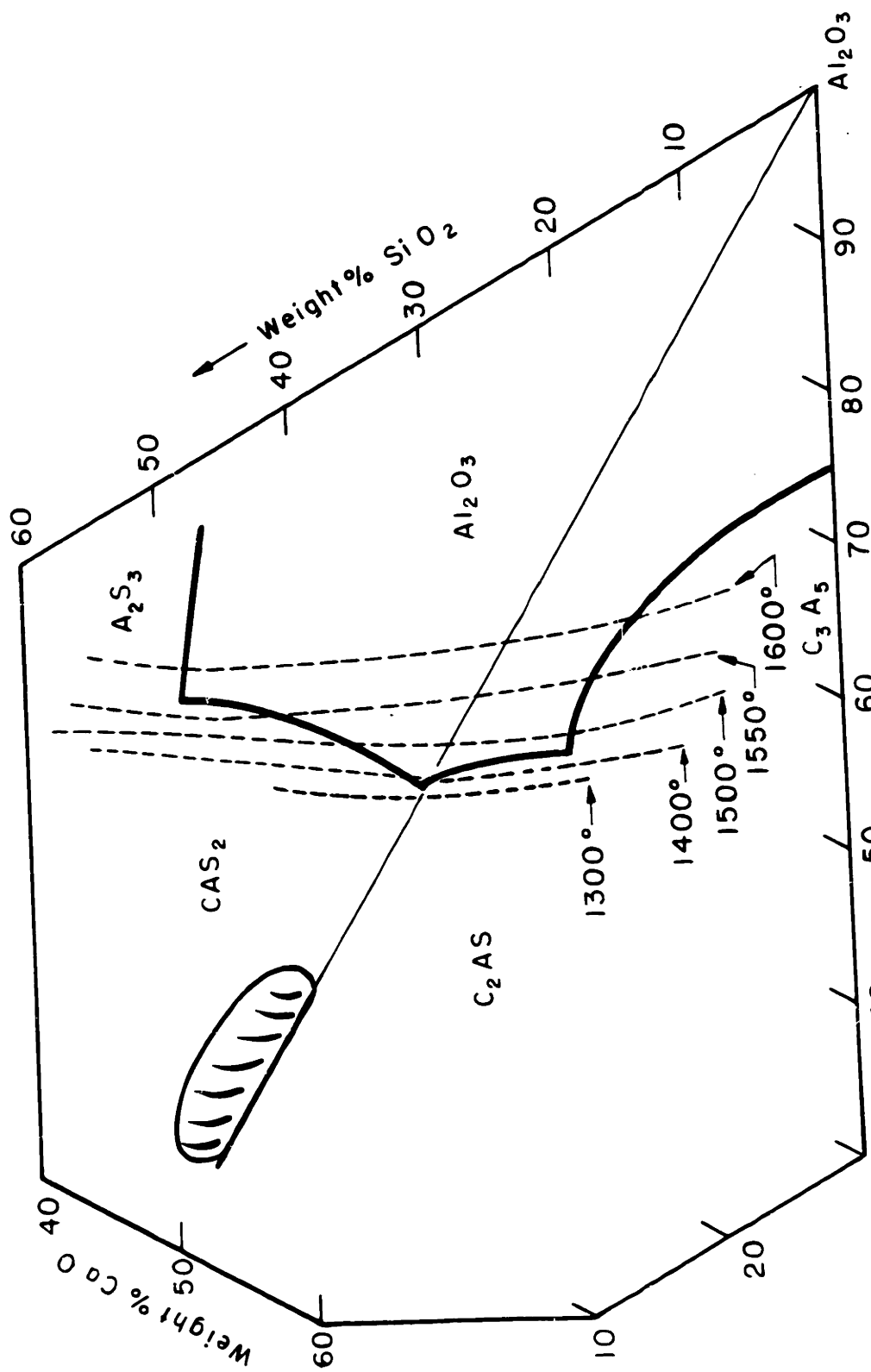

FIG. 5.2 PORTION OF $CaO—Al_2O—SiO_2$ EQUILIBRIUM DIAGRAM

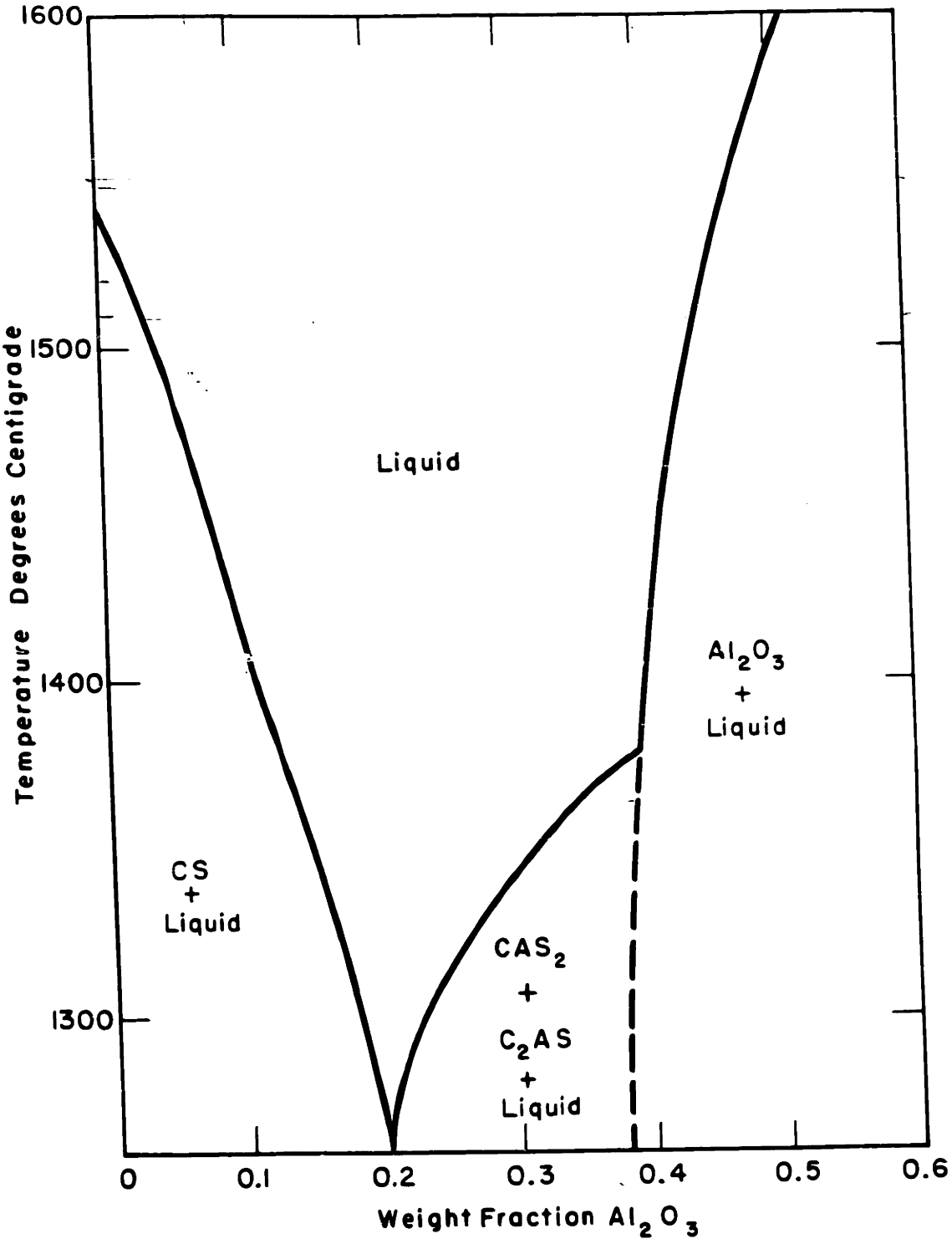

FIGURE 5.3 PORTION OF PSUEDO BINARY SYSTEM (Ca SiO_3-Al_2O_3)

For solution studies, the general equation has the form (equation 2.2 etc.)

$$J_i = -\frac{D}{\delta} \Delta C_i \qquad 5.1$$

The value of the flux, J, depends on the convention used for specifying the concentration, C_i. The equilibrium diagrams give concentration in terms of weight, w, fraction as

$$C_i = \frac{w_i}{w_{slag}} \qquad 5.2$$

which means that J is expressed as $\frac{\text{gms } Al_2O_3}{\text{gm slag}}$ $(\frac{cm}{sec})$. Multiplying both sides of equation 5.2 by the same quantity

$$(C_i \frac{\rho_{slag}}{\rho_i}) = \frac{V_i}{V_{slag}} \qquad 5.3$$

one obtains concentration as a volume fraction. Volumetric concentration will be designated by $\overset{*}{c}$ i.e.

$$\overset{*}{C} = C_i \frac{\rho_{slag}}{\rho_i} = \frac{V_i}{V_{slag}} \qquad 5.4$$

or to close approximation for alumina

$$\overset{*}{C}_{Al_2O_3} \approx .72\, C_{Al_2O_3} \qquad 5.5$$

which will be the value used for $\overset{*}{C}_{Al_2O_3}$ through the remainder of the thesis.

Equation 5.1 can now be rewritten

$$\overset{*}{J}_i = - D/\delta \Delta \overset{*}{C}_i \qquad 5.6$$

At the interface of the solid and liquid conservation of volume of the solid constituent, i, requires that

$$\overset{*}{J}_i = -\frac{\Delta y_i}{\Delta t} \qquad 5.7$$

where Δy_i is the change in dimension of the solid normal to the interface. Therefore, $\overset{*}{J}$ is a direct measure of the corrosion rate in cm/sec.

Activity Data

The activity of all components is necessary for two reasons. First to adequately reduce the number of independent diffusion coefficients in equation 1 in the Appendix it is necessary to use the set of conditions in equation 13 in the Appendix which requires knowledge of the rate of change of free energy of each constituent with concentration. Secondly, extrapolation of diffusion data requires knowledge of the rate of change of activity with change in concentration.

The activity of all components as oxides have been measured.[79-84] A basic problem to the application of the activity data to diffusion coefficients is that all activity data has been obtained as oxide activity while with only one exception the diffusion data is for the ions.

There are two possible ways, neither completely satisfactory, to cope with this difference between ways of specifying activity and diffusivity.

It could be assumed that since all activity measurements are made at a specific oxygen pressure then the oxygen activity is constant and the oxide activity uniquely determines the cation activity. The possible error here is that it is the atomic oxygen activity that is constant which gives no assurance that activity of the oxygen ion is constant.

It could also be assumed that oxygen ion diffusivity is (Figure 5.8) greater than that of any cation and hence the diffusivity of an oxide would be essentially the same as the diffusivity of the cation. Making this assumption leads to negative values of the diffusion coefficient of calcium oxide.

Part of the difficulty may be in the activity data itself. For both calcia[79,82] and silica[80,81,82,83,84] different investigators obtained contradictory results. Only for alumina[79,83] do the results of the research show the same pattern and even here there is not close agreement.

There is surely a need for an integrated study of the activity, a_i, of all components in this system with sufficient detail to permit the slopes $\frac{da_i}{dc_j}$ to be determined and with sufficient checks ("Gibbs Schuimann" relation) so that the self consistency of the study is assured. Lacking this, a complete quantitative assessment of solution kinetics is impossible.

Density

Density of the slag is necessary to convert dynamic viscosity to kinematic viscosity, to determine the driving force for free convection flow and to calculate the partial volumes necessary according to equation 13 in Appendix A to reduce the number of independent diffusion coefficients. The only measurements of density in this system are those obtained by Barrett and Thomas[85] from bubble pressure experiments. They measured density of only ten compositions but three of these lie on the Ca SiO_3-Al_2O_3 binary. Figure 5.4 shows density variation along the binary. The linear dependence

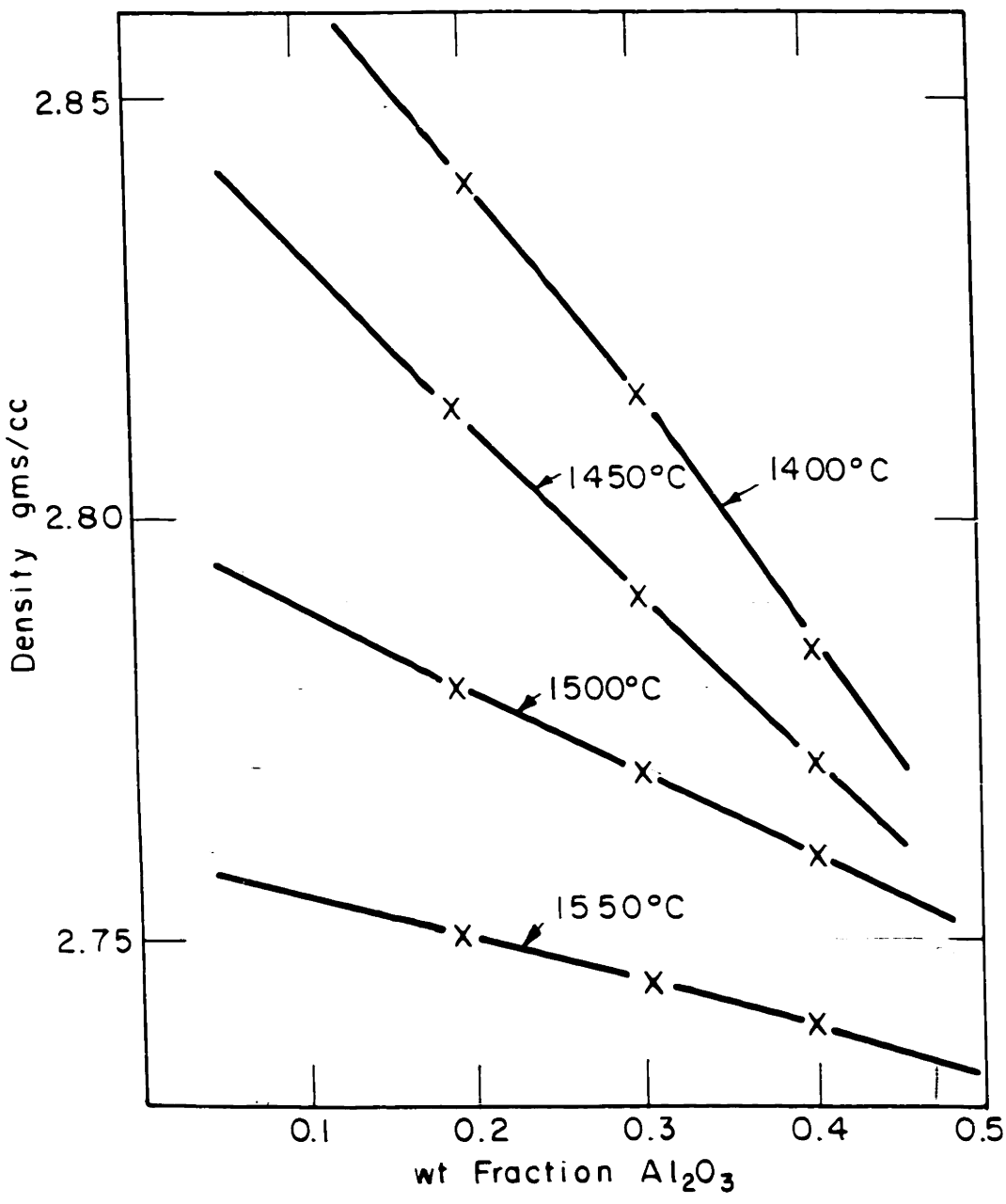

FIGURE 5.4 DENSITY VARIATION ALONG THE ($CaSiO_3$-Al_2O_3) BINARY

on Al_2O_3 content shown in these curves is not consistent with the change in structure with increasing Al_2O_3 content suggested by the activity and viscosity data. Calculation of partial volume of Al_2O_3 and Ca SiO_3 along the binary gives: $\bar{V}_{Al_2O_3} = .368$ and $\bar{V}_{CaSiO_3} = .356$.

Viscosity

From equation 4.12 (ii) it is clear that kinematic viscosity is of direct importance in determining steady state rates of solution under forced convection. Dynamic viscosity is vital to extrapolate the limited diffusion coefficient data to different compositions. For these purposes it is essential to know the viscosity right up to the liquidus composition. While no one has measured viscosity in this system close to the Al_2O_3 liquidus, it is fortunate that two extensive series of viscosity measurements have been made. Machin and Tin Boo Yee[86] have measured viscosity below 1500° and Kozakevich[87] has measured a wider range of compositions at temperatures primarily 1600° C and higher. The importance of the Kozakevich study to lower temperature studies such as this is that it gives the general shape of the viscosity composition curve in the composition range of the lower tmperature liquidus.

This is illustrated in Figure 5.5 showing the viscosity as a function of the weight percent Al_2O_3 with the CaO and SiO_2 weight percents equal. The crosses represent data from Kozakevich and the circles data from Machin. Assuming liquid configurations remain unaltered with temperature, the high temperature data can be utilized to give the shape of the curves at high Al_2O_3 content and the low temperatures data to give a clearer picture

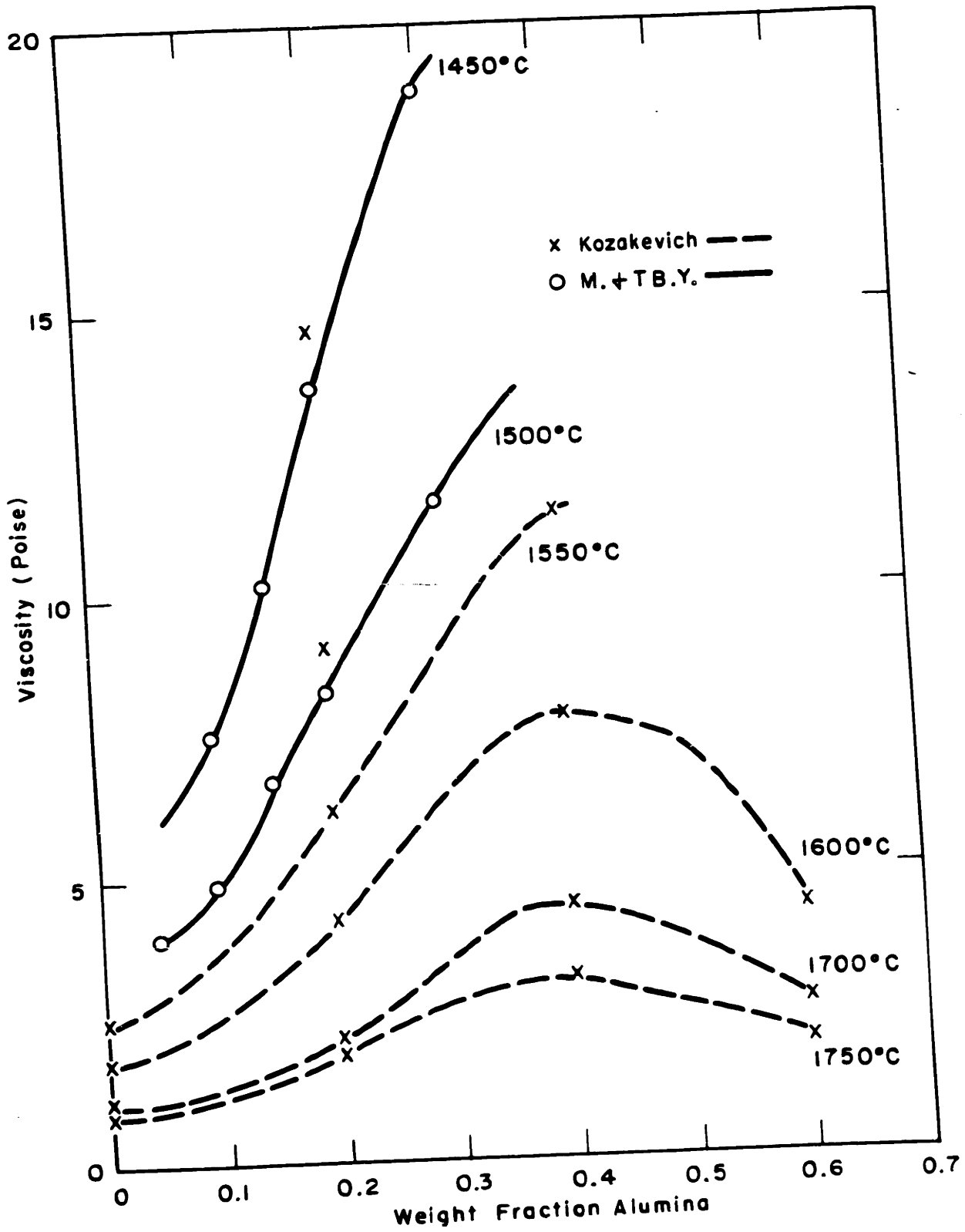

FIGURE 5.5 DYNAMIC VISCOSITY OF CaO-Al_2O_3-SiO_2 SLAGS OF EQUAL WEIGHT FRACTION CaO AND SiO_2

of the shape at low Al_2O_3 content. The maximum in viscosity at approximately 45% Al_2O_3 corresponds with an equal molar ratio of CaO and Al_2O_3. Beyond this point there are insufficient oxygen atoms present to permit additional aluminum atoms to assume tetrahedral coordination with oxygen, to contribute to network extension and to increase viscosity. Thus the data seems to correspond well with a likely physical model.

The discrepancy between Kozakevich and Machin's results is indicated by the "X" at 20% Al_2O_3 on the 1500° and 1450° C isotherms. It suggests that Kozakevich's results give a 10% higher value for viscosity than Machin's.

Figure 5.6 was constructed assuming validity of Machin's absolute values. It differs also from Figure 5.5 in that rather than the weight ratio the molar ratio of CaO and SiO_2 is kept at unity.

Utilizing the density data already presented, the variation of kinematic viscosity ($\nu = \frac{\eta}{\rho}$) is shown in Figure 5.7.

Diffusion

The value of the appropriate diffusion coefficient is necessary for quantitative confirmation of the rate of solution experiments. Measurements have been made of the diffusion coefficients in all the ionic species in the $CaO-Al_2O_3-SiO_2$ system. A single composition has been closely examined, 20 wt. % Al_2O_3 80 wt % $CaSiO_3$. The results of Towers and Chipman[88] for Si^{++++} and Ca^{++}, Koros and King[89] for $O^{=}$ and Henderson, Yang and Derge[90] for Al^{+++} are summarized in Figure 5.8. In all cases the results were obtained using a tracer atom. Only the Al^{+++} data are available on another composition in the $CaSiO_3-Al_2O_3$-binary.

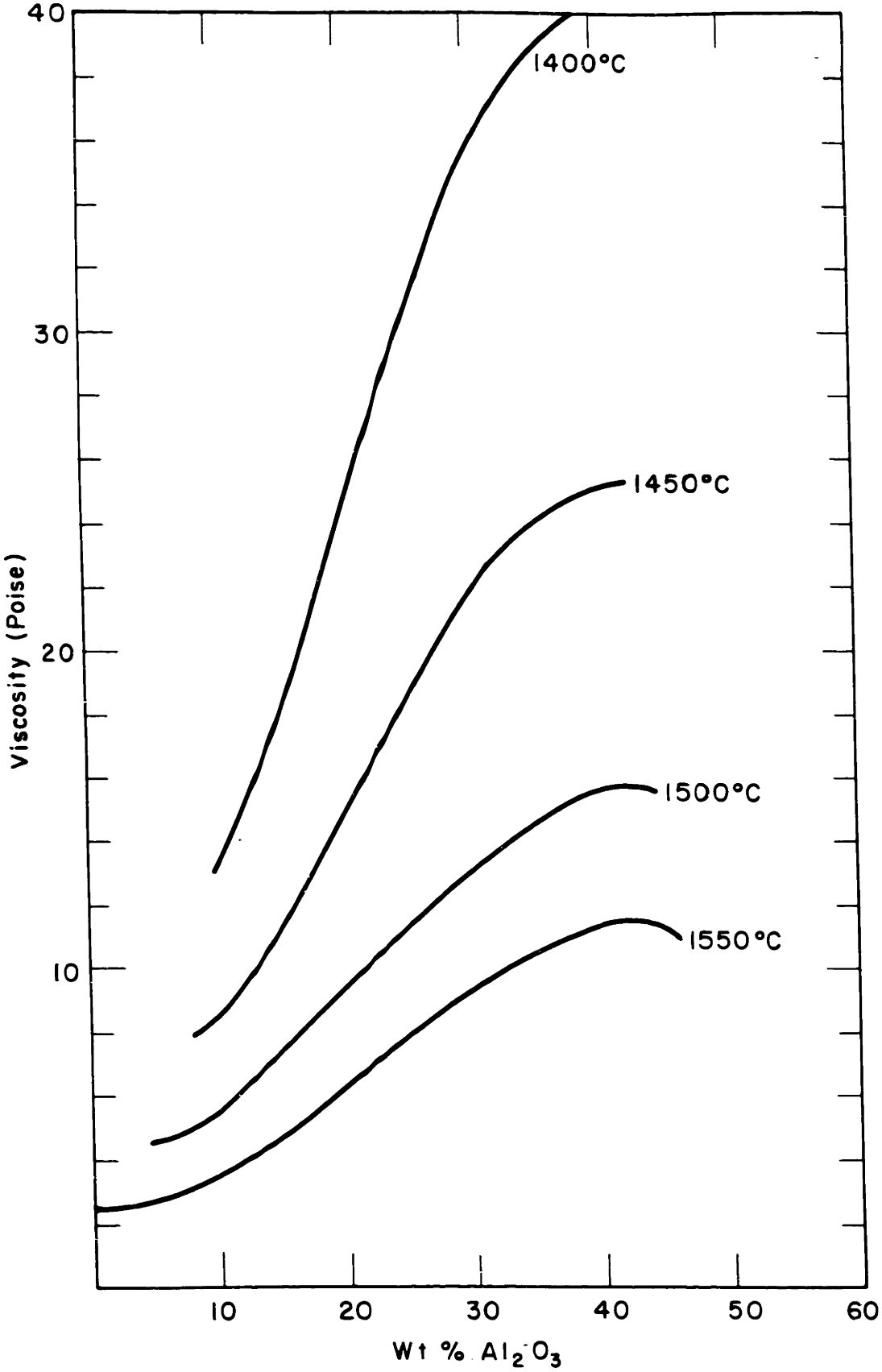

FIGURE 5.6 DYNAMIC VISCOSITY ALONG THE BINARY Ca SiO_3-Al_2O_3

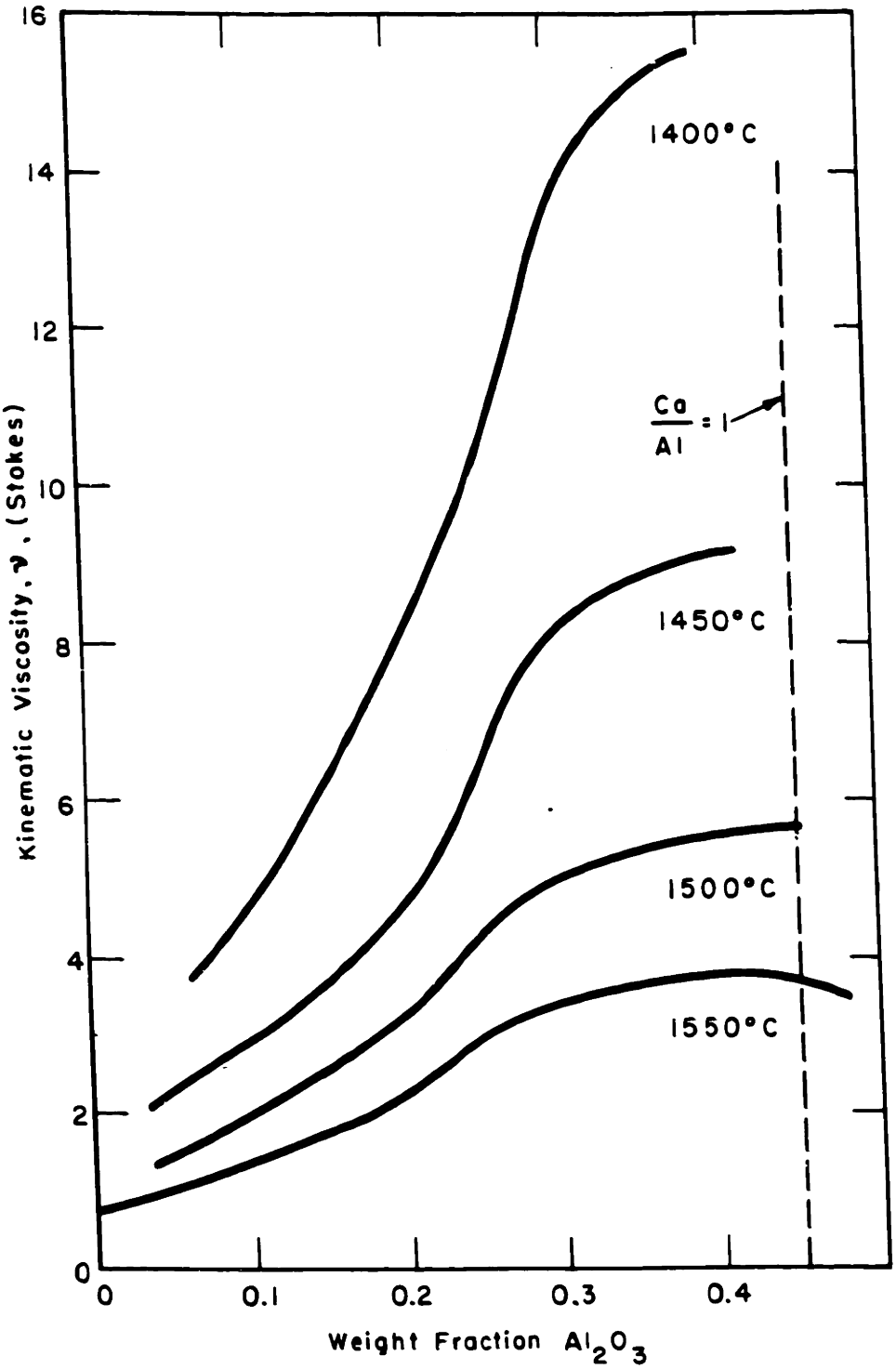

FIGURE 5.7 KINEMATIC VISCOSITY ALONG THE BINARY Ca SiO_3-Al_2O_3

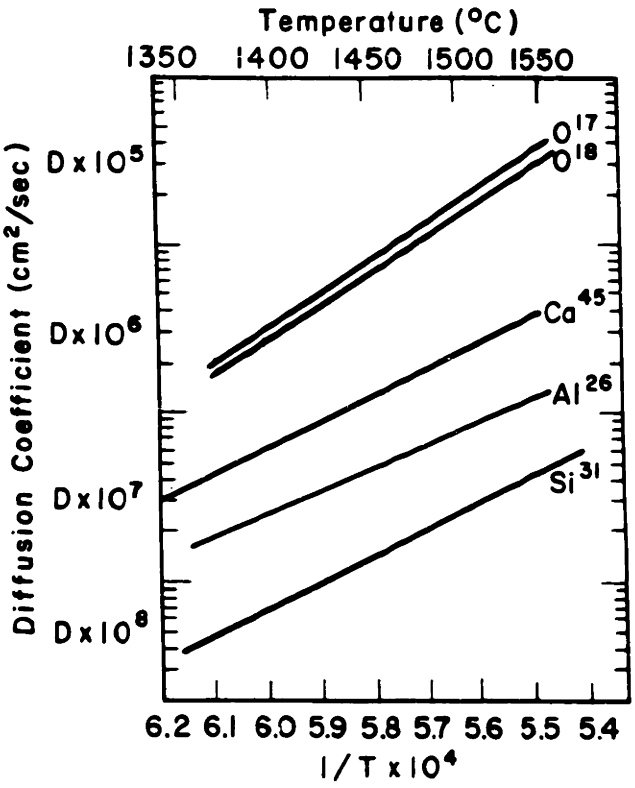

FIGURE 5.8

TRACER DIFFUSION RESULTS AT 20 WT% Ca SiO_3 80 WT% Al_2O_3

It is well to consider the corrections necessary to convert from diffusion coefficient obtained by radioactive techniques to the chemical diffusion coefficient. For crystalline lattices, it has been shown[91] that when diffusion occurs by a interstitial or vacancy mechanism, it is necessary to make an upward correction of diffusion coefficients obtained by tracer technique. The correction is related to correlation of a tracer atom with a vacancy or interstitial site, this correlation increases the probability of a return jump and thus diminishes the apparent diffusion compared with that which would be obtained in regular chemical processes.

While glasses and liquids do not possess vacancies in the same strict sense as crystalline solids, modern thinking of the liquid state requires the presence of "holes" in liquids and it is not incorrect to consider glasses or liquids to possess interstitial positions which can probably only be defined statistically. In any event Haven and Stevels[92] have reconciled the discrepancy between tracer diffusion results for Na^{+}_{24} and electrical conductivity in the vitreous system, Na_2O–CaO–SiO_2 by making appropriate corrections for return jumps.

The correlation factor m as defined by Bardeen and Herring[91]

$$m = \frac{D_T}{D_{AA}}$$

where D_T is the diffusion coefficient of the tracer and D_{AA} is the true self diffusion coefficient.

Bardeen and Herring show that the value of m is approximately equal to $(1 - 1/z)$ where z is the coordination number of sites surrounding atom A. Compaan and Haven[93] have shown that an error of a factor of 2 exists in Bardeen and Herring's calculation and that approximate relation is more nearly

$$m = 1 - 2/z$$

Estimating a value for Z for Al^{+++} we might select 5 as an appropriate average value taking into account that the aluminum may exist in either tetrahedral or octahedral coordination with oxygen, giving values of next nearest sites of similar type of 4 and 6 respectively. Following the same argument an appropriate value for Z for Si^{++++} is 4. With these assumptions the self diffusion coefficient of Al^{+++} is 5/3, the measured tracer diffusion coefficient, and for Si^{++++}, the self diffusion coefficient is twice the tracer value.

Extrapolation of diffusion data is discussed in Appendix A. According to equation 20 in Appendix A activity data is required to extrapolate with any confidence. Lacking this, one must utilize equation 18 in Appendix A realizing that his results are subject to larger errors.

When only the variation of viscosity is taken into account, the shape of diffusivity vs concentration curves are the same for all constituents. Only the magnitudes vary. In Table V-1 are shown the diffusivity of Al^{+++} and Si^{++++} according to the viscosity results of Figure 5.8 with corrections for correlated jumps according to equation 5.7 and extrapolated using equation 18 of the Appendix.

Surface Tension

Surface tension of the liquid does not enter directly into the expressions for solution rate but, as pointed out by Tress[47], differentials of the surface energy between saturated and bulk solution can cause a convection at the surface. The values of surface tension obtained by Barrett and Thomas[85] show an increase of surface tension with increasing Al_2O_3 along the $CaSiO_3$-Al_2O_3 binary. There is a difference of about 30 dynes/cm between the surface tension at the liquidus and the surface tension

TABLE V-1

Extrapolated Interface Diffusion Coefficient, D_o, of Silicon and Aluminum Ions Corrected for Correlated Jumps

Temperature	Diffusion Coefficient	
	Si^{++++}	Al^{+++}
1550° C	5.2×10^{-7}	1.6×10^{-6}
1500° C	3.4×10^{-7}	9.0×10^{-7}
1450° C	1.6×10^{-7}	5.2×10^{-7}
1400° C	8.4×10^{-8}	2.8×10^{-7}

Summary

While numerous physical property measurements have been made in the system $CaO-Al_2O_3-SiO_2$, they are not self consistent nor extensive enough to provide an acceptable theory to explain this system. Lacking that, confident extrapolation of physical property data is impossible and attempts such as Table V-1 are of limited value.

Model System

As already mentioned, a model system provides an important method of evaluating experimental set ups, and even to determine the functional relationships of dimensionless quantities that affect the solution rate.

Glycerine has a kinematic viscosity which suggests its use as a corroding liquid in a simple model system. It varies from 12 stokes at room temperature to 90 stokes at the ice point. This range can be extended further by addition of water with a resulting decrease in viscosity. Alkali halides are soluble in glycerine and available as single crystals. As Wagner[74] has already shown that solution of sodium chloride by water is diffusion controlled in the liquid, the much lower diffusion coefficients in glycerine indicate diffusion control for solution of sodium chloride by glycerine. Thus if each of the dimensionless number (Re, Sc, Gr) are of the same magnitude as those of refractory corrosion, the sodium chloride-glycerine system would serve as a satisfactory room temperature model for refractory solution.

Many of the necessary data are available. The solubility of sodium chloride in glycerine-water mixtures[94], the density of pure and sodium chloride saturated glycerine[95] and the viscosity of ycerine[96] have all been measured. They are summarized in Table V-2 with solubility data converted to volumetric units.

TABLE V-2

Pertinent Data on System NaCl Glycerine-H_2O

Wt. % Glycerine	Viscosity 25° C stokes	Solubility C* 25° C cm^3/cm^3	Density Change
55.00	.05	9.9×10^{-2}	.085
84.00	1.02	5.9	.044
100.00	7.5	4.5	.029

The remaining important physical property is the diffusion coefficient. Measurements by Wolkows[97] show that D is a linear function of the dynamic viscosity, η, for glycerol-water mixtures of greater than 60% glycerol at 15°, 20° and 30° C. For NaCl in glycerine, $D \times \eta = 6.5\ 10^{-7}$.

Provided that dimensions and fluid flow velocities are the same, the Reynolds number depends on the viscosity. In Table V-3 the Reynolds, Schmidt and Grashof numbers attainable in the NaCl, glycerine-water system are compared with those likely in the sapphire, $CaO-Al_2O_3-SiO_2$ slag system.

TABLE V-3

Comparison of Model System with High-Temperature System

	Reynolds Number (Re) $u/\nu l$	Schmidt Number (Sc) ν/D	Grashof Number (Gr) $gl^3 \Delta\rho/\nu^2$
NaCl-glycerine water	max value 20 Ul	2×10^{10}	$3\ gl^3$
	min value 0.01 Ul	4×10^{3}	$4 \times 10^{-6}\ gl^3$
Sapphire-$CaO-Al_2O_3-SiO_2$ slag	max value 1 Ul	5×10^{7}	$.2\ gl^3$
	min value 0.02 Ul	10^{5}	$2 \times 10^{-4}\ gl^3$

This shows that the characteristic dimensionless quantities in the suggested model system completely encompass those of the actual system affirming the utility of the model.

The data pertaining to property variations is less well established. Very little has been published on the variations with temperature of sodium chloride solubility in glycerine. Measurements of Holm[98] indicate a nearly constant solubility of sodium chloride in glycerine from 20-25° C. Variations of density with temperature are more completely established. An empirical relationship has been established[99] for the variation of glycerine density with temperature.

The variations of density difference between saturated and bulk solution with temperature $(\frac{d\Delta\rho}{dT})$ is not known but with the relatively constant solubility of sodium chloride in glycerine it seems reasonable that this variation also is slight.

The affect of sodium chloride concentration on diffusion and viscosity are only poorly established. Davis and Jones[100] report that most cations including sodium increase the viscosity of glycerine.

VI. EXPERIMENTAL APPROACH

Introduction

The set of equations 4.12 reveals that the most complete method to study solution kinetics is to examine separately the transient case, the forced convection case and the free convection case. The transient and the free convection case can be examined satisfactorily by immersing cylindrical samples in a melt. Forced convection experiments require more detailed consideration. Levich[101] was the first to suggest the desirability of using a rotating disc for forced convection transport experiments and showed that the effect was calculable from Cochran's[70] solution of the flow pattern. Burton, Prim and Schlicter[102] used a rotating disc to affect a diffusion controlled crystallization process and Wagner[103] calculated heat transfer from a rotating disc. Model experiments showed rotating disc experiments to be practical in viscous liquids. They proved to be, by far, the simplest way to generate a describable flow.

As seen in the set of equations, 4.12: for the transient case, the only physical property to affect the solution rate is the diffusion coefficient; for the forced convection case, both the diffusion coefficient and the kinematic viscosity affect the rate; and for free convection, all three properties--diffusivity, viscosity and density difference influence the rate of solution. Reliability is considerably enhanced when an independent value for these properties is available to test the results.

The preceeding section revealed that dependable data for viscosity was available. Considerable uncertainty exists, however, regarding density differences and diffusivity at the liquidus composition. In complex silicate systems of industry where refractory solution is an important problem, virtually nothing is known of the pertinent properties. Density and viscosity can be measured with relative ease compared with measurements of diffusivity and since a major objective of this thesis is to provide a general experimental approach to the problem of refractory solution kinetics, provision to measure density and viscosity as well as the rate of solution adds to the value of the apparatus, and to the meaningfulness of results.

Description of Apparatus

Schematic drawings of an experimental arrangement designed to measure density and viscosity and permit the three cases of solution to be examined are shown in Figures 6.1 and 6.2.

The liquid is contained in an approximately 3 inch $\overline{ID}$ by 5 inch high alumina crucible lined with 0.010 inch platinum. Powdered alumina acts as a cushion between the liner and crucible. Details of the crucible arrangement are seen in Figure 6.3. The crucible is supported by and cemented to a high alumina pedastal which in turn is pinned by a sapphire rod to an alumina tube.

Beneath the furnace the alumina tube fits into a steel "upper flange." Six set screws in the collar of this flange permit adjustment of the alumina tube to give minimum eccentricity. The upper flange and the alumina tube are both keyed to the lower flange on which is welded a steel shaft. The shaft is supported by two flange type ball thrust bearings

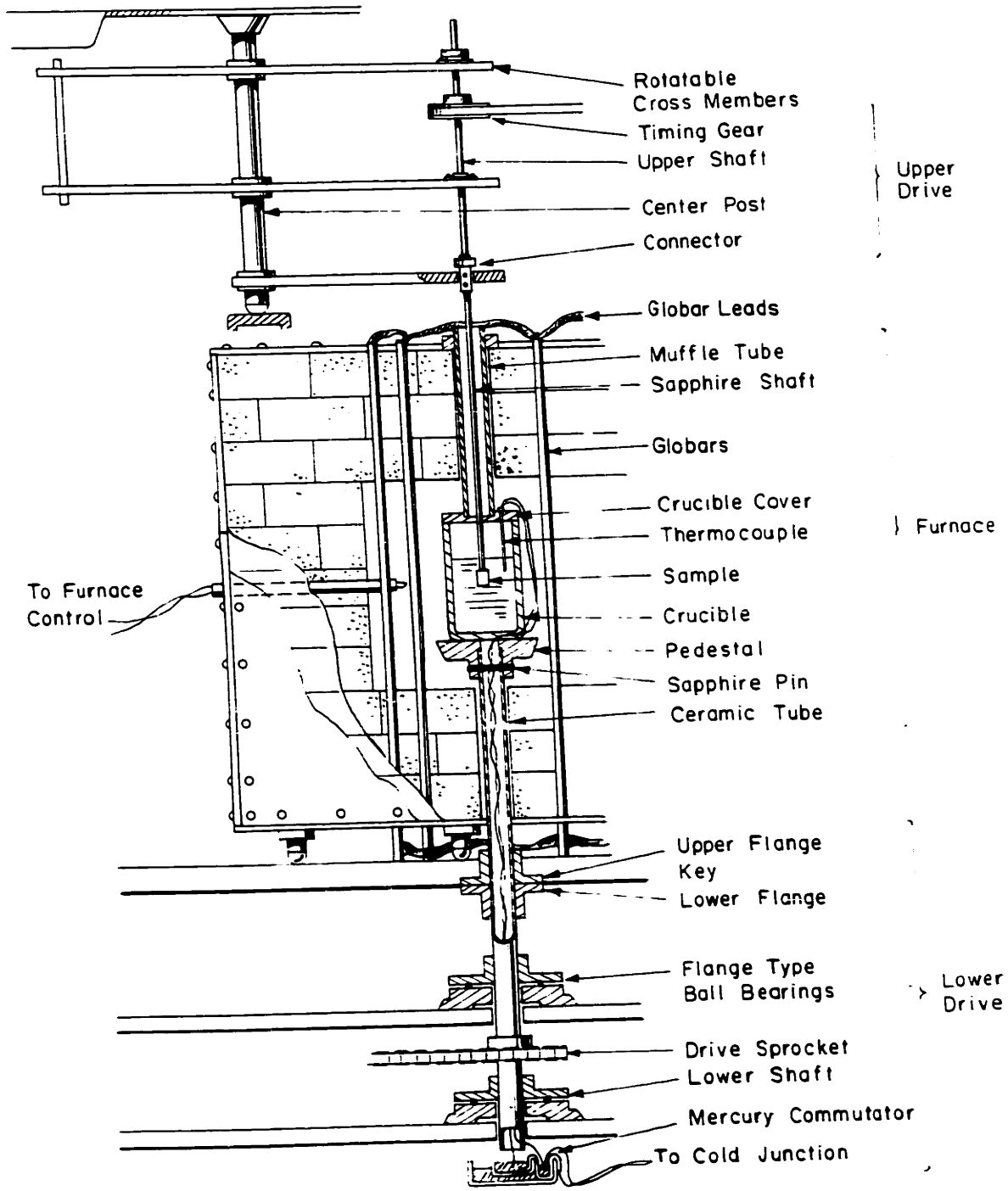

FIGURE 6.1 SCHEMATIC CROSS SECTIONAL DIAGRAM OF APPARATUS FOR STUDYING SOLUTION OF SAPPHIRE BY SLAG

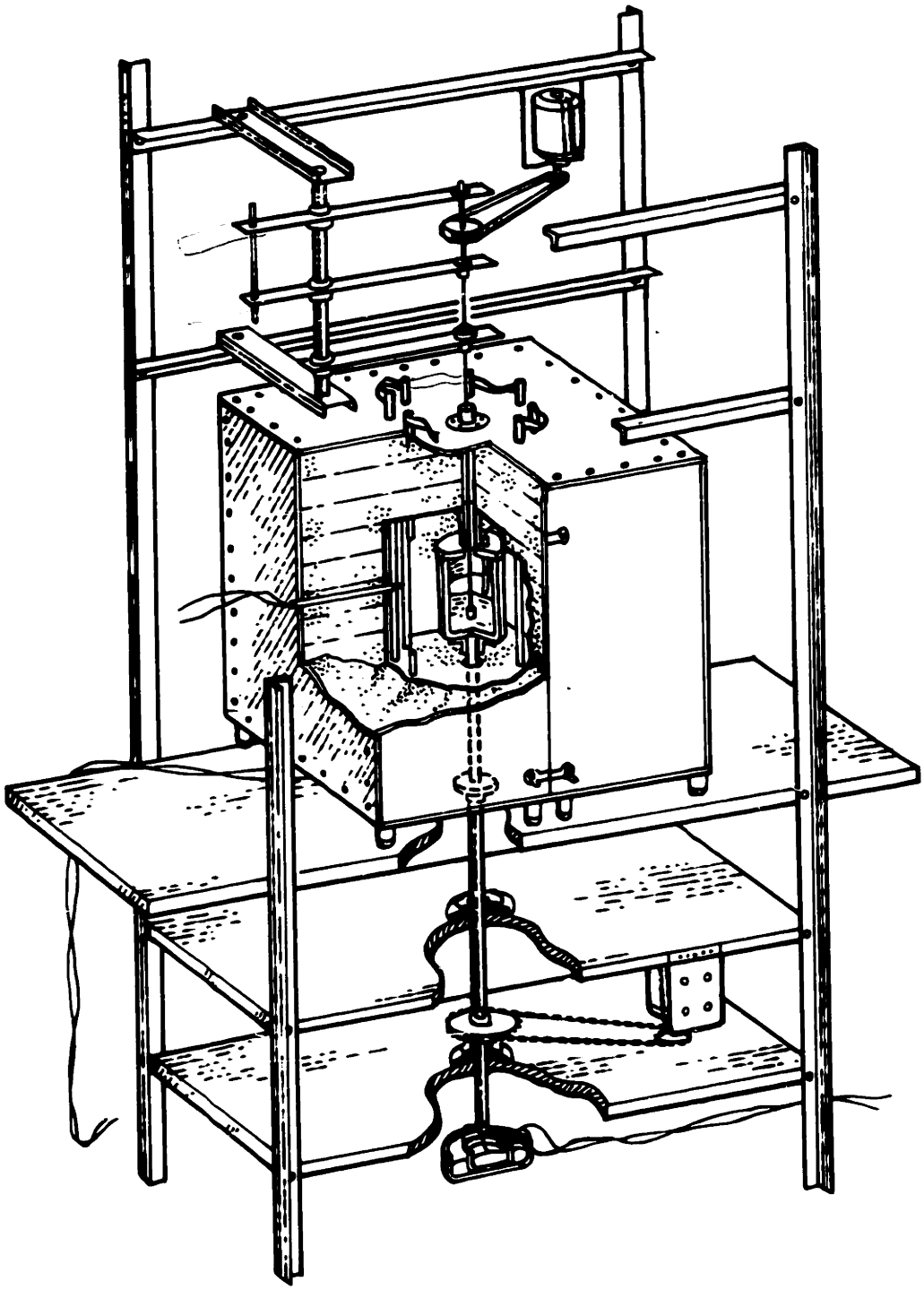

FIGURE 6.2 SCHEMATIC CUT AWAY DRAWING OF APPARATUS FOR STUDYING SOLUTION OF SAPPHIRE BY SLAG

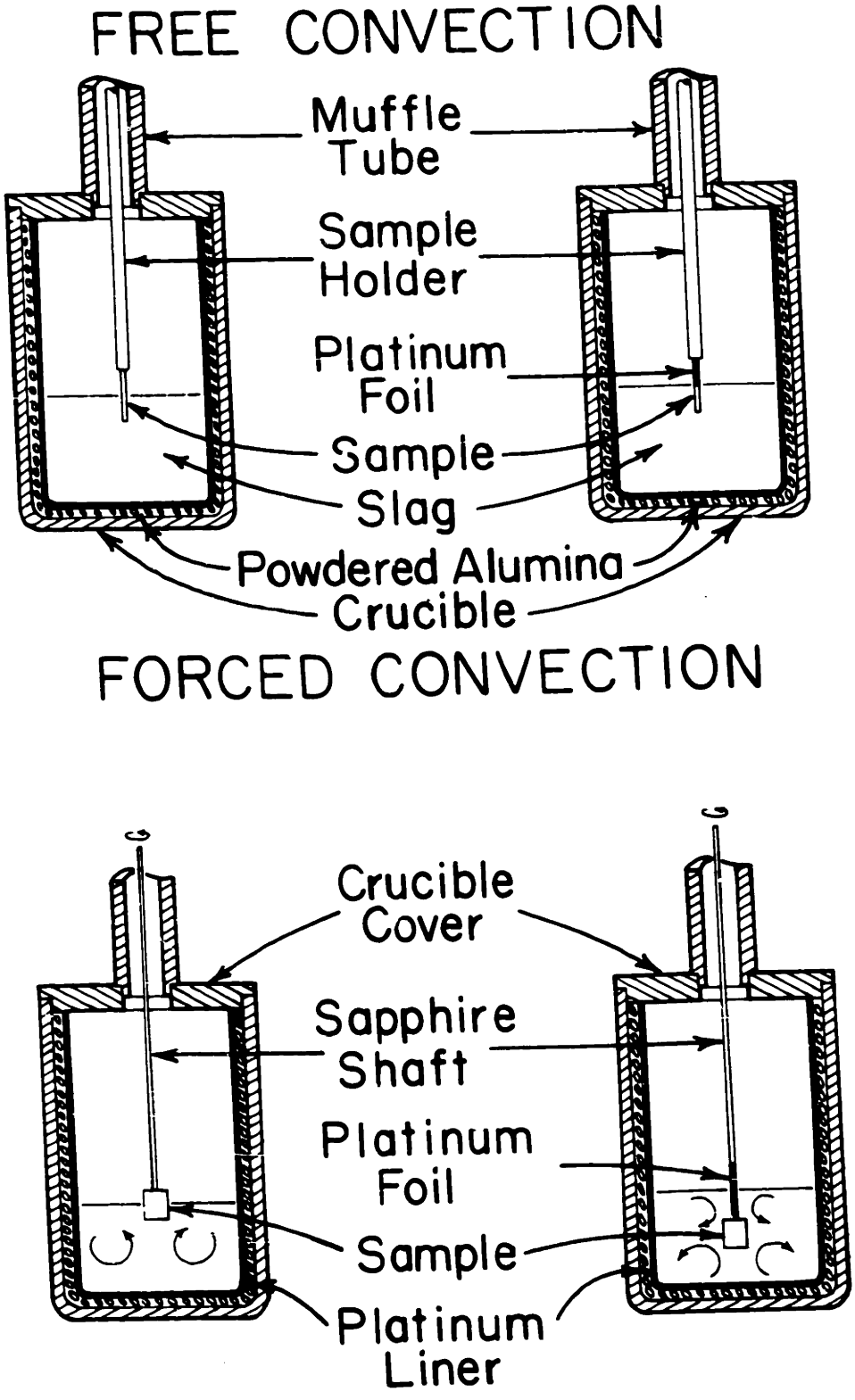

FIGURE 6.3 DETAILS OF THE DIFFERENT TYPES OF EXPERIMENTS

approximately 30 inches apart and is rotated when necessary by means of a sprocket which is driven by a speed reducer. Four speeds from 4 RPM to 50 RPM are possible from a pulley belt arrangement between the motor and speed reducer.

Above the crucible is an alumina muffle tube which fits into the crucible cover to make possible sealing the crucible and to minimize temperature gradients. Through this muffle tube the samples are introduced into the melt.

The furnace itself is made in two halves, which horizontally interlock. This is illustrated in Figure 6.4 by a photograph of the half furnace and crucible arrangement. Each furnace half is mounted on casters making it relatively easy to bring the furnace together without disturbing the concentricity of the crucible and its alignment with the sample rotation and viscosity measurement mechanism. The furnace chamber is octagonal in horizontal section with an area of 125 square inches. Its height is 10 inches making the furnace chamber volume about 2/3 cubic feet. The walls are made with three layers of insulating firebrick. The three-piece composite insulating firebrick lower plug surrounding the alumina shaft and one block of the three-piece upper plug surrounding the muffle tube are visible in Figure 6.4.

The furnace is heated with eight 1/2 inch diameter silicon carbide heating elements of 10 inches heated length and 25 inches overall length. They are arranged in an octagonal arrangement around the crucible and are wired in series—parallel with two series connected legs of four elements each. Temperatures up to 1600° C have been attained for several hours. A power input of 3.5 kw is necessary to maintain 1500° C.

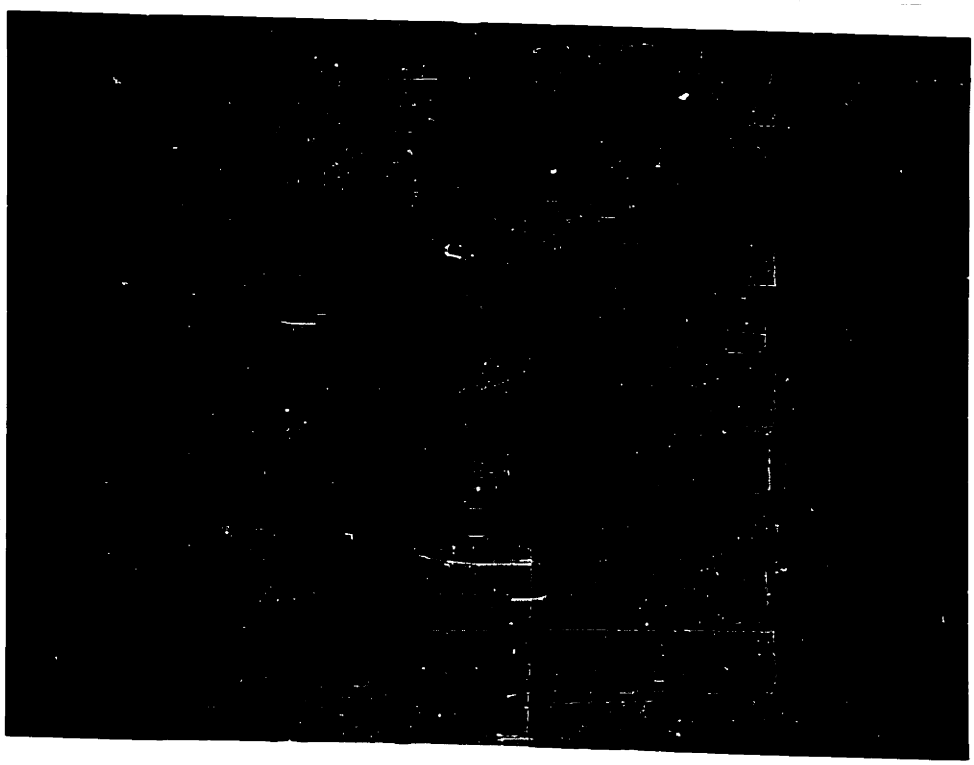

FIGURE 6.4 ARRANGEMENT OF CRUCIBLE IN THE FURNACE

Casters keep the bottom of the furnace about 1 1/2 inches above the transite base plate. Stuffing this gap with glass wool markedly minimizes air drafts through the furnace.

Temperature is controlled with a Celect-ray controller. The circuit is so arranged that only 10% of the load is added or eliminated by the controller. This prevents "overcontrol" and cycling of temperature. The control temperature is measured by a platinum-platinum rhodium thermocouple horizontally introduced through the furnace walls. Its position in space about 1 inch from the crucible at a height nearly equal to the melt level is seen in Figure 6.4.

In addition to the control couple, the temperature is measured in two other ways. A thermocouple is permanently installed in the melt, is threaded out the cover, down the crucible sides, through the alumina shaft and steel shaft to a two-dish mercury commutator at the bottom of the apparatus just beneath the end of the steel shaft.

A reference thermocouple can be inserted through the muffle and down into the slag to periodically check the permanent thermocouple and to make temperature surveys.

Melt temperature is read on a Leeds and Northrup Model K-2 potentiometer. At times fluctuations of more than 10° C are indicated by the permanent thermocouple. These are markedly diminished when the furnace power is turned off suggesting that stray fields are affecting the readings. No such variation distorted the control couple.

A typical result of a temperature survey of the furnace is shown in Table 6.1. It is evident that there is a vertical region extending to almost 3 inches above the glass line where the temperature is constant within ± 1° C. This is essentially the region enclosed by the crucible. The temperature difference between the control thermocouple and the probe thermocouple is typical. The temperatures used for this study represent the probe readings If the difference between the probe thermocouple and permanent thermocouple represents a real temperature gradient in the crucible then stirring should increase the temperature indicated by the permanent couple; since this does not occur, it is concluded that the difference between the probe thermocouple and permanent thermocouple does not represent a horizontal gradient. In fact, the insensitivity of temperature of the permanent couple to stirring suggests that the entire melt is virtually constant in temperature.

Free Convection and Free Diffusion Technique

The samples employed are cylinders of Linde sapphire (though other materials have been tested) which are typically 0.180 inch diameter initially. These have a reasonable fit to Norton Company thermocouple protection tubes RA 186 OD 3/8 $\overline{\text{OD}}$ and 3/16 $\overline{\text{ID}}$ to which they were cemented with aluminum phosphate cement.

The sample is rather rapidly (two minutes) introduced into the furnace just above the melt. There it is permitted to remain in contact with the ambient temperature above the melt for about 5 minutes. The sample is then dropped into the slag to a prescribed depth and allowed to remain

TABLE VI-1

Temperature Survey in Furnace

Inches above glass level	Temperature inserting	removing
- 2	1440° C	1439° C
- 1	1439	1439
0	1400	1440
+ 1	1440	1440
2	1439	1440
3	1437	1436
4	1425	1411
6	1338	1339
8	1191	1219

Controller: 1450° C

Permanent Thermocouple: 1426 $\pm$ 1° C

for a specified period. At the end of this test period the sample is pulled from the liquid gradually, taking about five seconds, in order to permit most of the slag to drain off. The sample is then rapidly lifted to a cooler (200° C) region of the furnace. After a few minutes the sample is removed from the furnace and allowed to cool in air. When cool it is immersed in 48% hydrofluoric acid to dissolve the slag and leave only the uncorroded sapphire.

The sample is measured before and after corrosion across nearly the same diameter, at intervals of 1/8 inch along the length of the crystal with an 0-.500 inch L. S. Starrett Company micrometer with vernier to read to $\pm$.0001 inch. To obtain an accurate zeroing, the sample diameter is read beforehand above, as well as on the region to be immersed. After corrosion a remeasurement of the uncorroded region provides a good check.

Samples have also been measured making use of an optical comparator or by using a filiar eyepiece microscope. In neither case was the reproducibility as satisfactory as with the micrometers. Optical means have the advantage that the contour of the sample can be determined in regions of minimum diameter.

After each experiment the melt was stirred before conducting another free convection or transient diffusion run.

Forced Convection

Forced convection samples are short cylinders of Linde sapphire one half inch long and .280 inch in diameter. These samples have a centrally located hole concentric with the outer cylindrical surface.

A sapphire shaft of .120 inch diameter is cemented into the central hole with aluminum phosphate cement.

The upper end of the sapphire shaft is fastened to a connector by six set screws. These set screws permit alignment of the shaft to provide maximum concentricity of the sample. A Boston collar is held to the outside of the connector by a set screw; the collar rests on a brass arm with a single hole which the remainder of the connector easily clears. This permits the connector (with shaft and sample attached) to be supported above the glass, allowing the drive shaft to be joined to the connector. Raising the collar allows the sample to be lowered into the slag and rotation can begin a second or two after the sample is immersed. After the required time for solution the sample is removed from the melt by lifting the drive shaft. Five seconds are utilized for removing the sample from the melt to obtain a substantial degree of draining of the slag. It proves impractical to rapidly quench the sample to a lower temperature region. (This is less important in forced convection than free convection experiments because the boundary layer thickness is substantially less.) Instead the sample is removed to a cooler region in about thirty seconds, removed from the furnace shortly thereafter, cooled and placed in hydrofluoric acid.

Two types of forced convection experiments have been conducted. In the first, the sample is totally immersed in the slag, in the second, only one disc face is immersed. Each of the methods has advantages. When the sample is totally immersed a rather symmetrical flow pattern occurs in the liquid as shown in Figure 6.3. This provides interesting

information regarding the contour of the cylindrical face. The main disadvantage is that the measurement of length change is relatively uncertain. This is because the sample finally assumes a profile as shown in Figure 6.5. The curvature introduced by the edge effect and from the inside corner effect minimizes and finally eliminates the flat region on the upper disc surface from which length measurements can be made with certainty. This problem is avoided by only partially immersing the samples preserving the original upper reference surface. The sapphire shaft for the partially immersed samples is notched to permit introduction of the micrometers very near to the centerline of the disc face.

The rotation mechanism for the forced convection experiments is shown in Figure 6.6. Rotation is provided by a Bodine 1/75 horsepower constant speed motor linked by a timing belt and gears to the upper drive shaft. The bearings of the drive shaft are mounted in two cross members independently adjustable around a center post permitting careful centering of the sapphire shaft in the muffle and vertical alignment of the upper drive shaft. Speeds from 300 to 10,800 RPM are attainable.

The cross members are easily swung out of the way while the sample is being inserted or removed. Rotating the drive shaft toward the observer in Figure 6.6 releases the tension on the belt and permits its removal.

When the cross members are rotated 180 degrees, the drive shaft extends substantially beyond the extremities of the furnace. Concentricity of the sample is obtained by adjustment of the six set screws in the connector with the sample outside the furnace under equivalent conditions to those during an experiment.

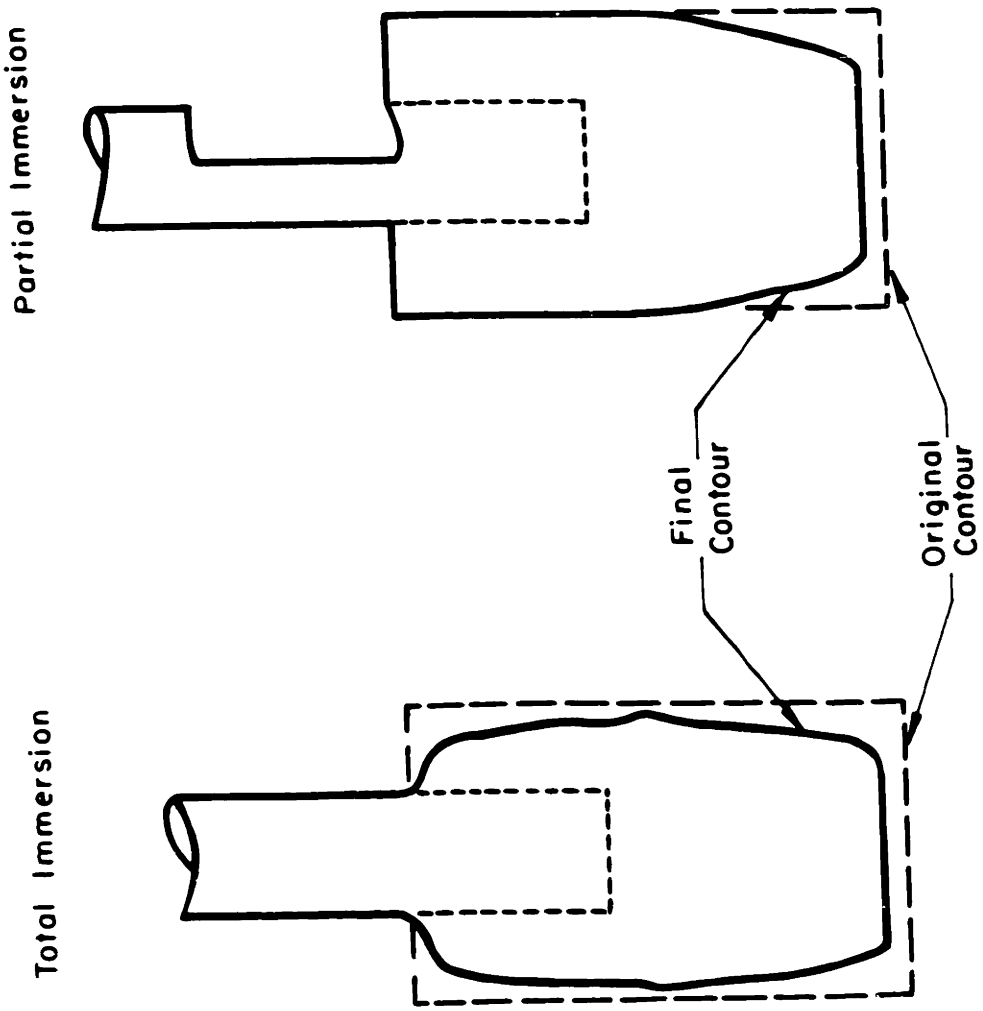

FIGURE 6.5 CONTOUR BEFORE AND AFTER CORROSION OF TOTALLY AND PARTIALLY IMMERSED SAMPLES

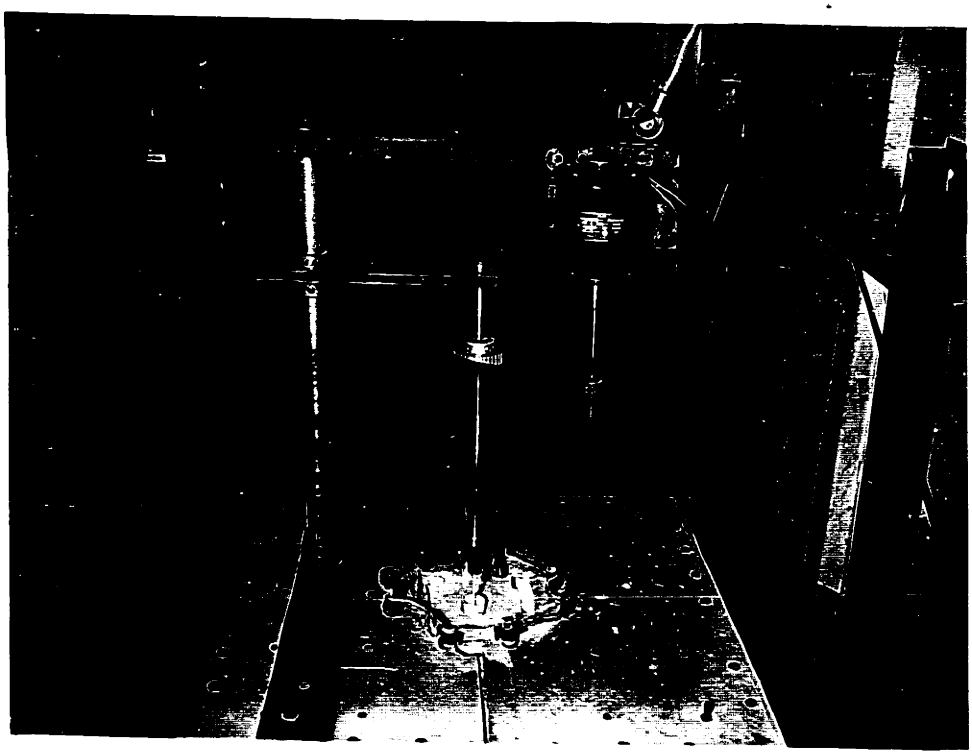

FIGURE 6.6 VIEW FROM ABOVE FURNACE SHOWING MEANS OF ROTATING FORCED CONVECTION SAMPLE

The center post itself is mounted on a frame which is independent of the furnace. It is adjustable at both top and bottom in all horizontal directions which allows a proper positioning with respect to the crucible and vertical alignment to be achieved. The entire apparatus showing the frame is seen in Figure 6.7.

Viscosity Measurements

The viscosity measurements are made using a bob geometry almost identical with that used for the forced convection experiments. A sapphire shaft is cemented into such a platinum cylinder and protection sleeve. At its upper end this sapphire shaft is joined with six set screws to permit alignment to a connector which in turn is screwed into a compass wheel. The connector also has provision for securing, by set screws, a brass bob that is soldered to the torque measuring piano wire of .004 inch diameter.

At its upper end the wire is clamped to a holder that can be moved up and down in a cross piece to immerse the bob in the slag to a specified depth or to remove it. The cross member in which the holder is mounted can be rotated about the center post to obtimize the centering of the sapphire shaft. A water cooled ccpper coil is mounted directly on the furnace roof to diminish the temperature of the viscosity measuring apparatus. These are all illustrated in Figure 6.8.

Viscosity is measured in two ways; either by rotating the crucible using the lower drive mechanism illustrated in Figure 6.1 and measuring the angle of twist of the compass wheel, or by measuring the damping of the rotation after a rotational displacement is introduced.

FIGURE 6.7 PHOTOGRAPH OF ENTIRE APPARATUS

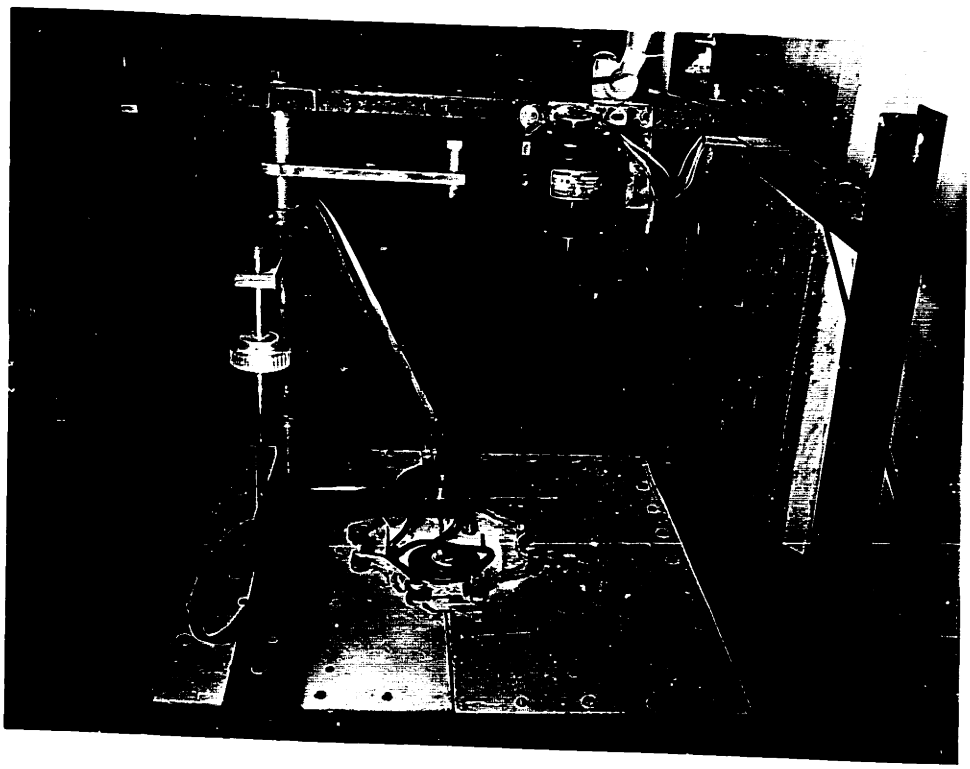

FIGURE 6.8 VISCOSITY MEASURING ARRANGEMENT

Sapphire shafts are never without camber and the readings of torque are very sensitive to any deviations of alignment. For this reason, the damping does not decay logarithmically when the amplitude of the swing becomes small. Neither does the amount of rotation of the compass wheel bear a linear relationship to the speed of rotation of the crucible as would be expected if the alignment were perfect. Deviations of this sort are not mentioned explicitly in papers dealing with measurements of viscosities of glass and slags.

In any event a correlation of the viscosity bob and shaft is required. This can be done by substituting a beaker of the same dimensions for the crucible when the furnace is cool and measuring the angular displacement of the compass wheel for the various speeds of rotation with castor oil of known viscosity in the beaker. Temperature of the castor oil can be varied to extend the range of correlation. The damping correlation can similarly be attained..

Details of alignment during correlation should be identical with those of the anticipated measurement. Such apparently trivial considerations as arrangement of the screws used to fasten compass wheel to the connector and the angular orientation of brass cylinder to connector give significant differences in the correlation.

To permit correlations to be made (in the case of a broken sapphire shaft for example) while the furnace is in operation, an additional pedastal, rotated by the same lower drive mechanism, is placed outside the furnace, in a position such that by rotating the cross member 180° the torque wire is directly over the pedastal cente

This is also convenient to permit correlations to be made prior to an experiment in which the torque change with time is measured while a regular sapphire sample dissolves. Such an experiment gives a torque decay which is influenced both by the change of viscosity and by the change of size of the sample.

Density Measurements

Measurements of specific gravity are made by the Archimedean method following the technique of Bockris, Tomlinson and White[104]. A platinum bob was fabricated by fusing platinum into a roughly spherical shape. This is fused to a platinum wire of .020 inch thickness long enough to extend way above the furnace. At its other end the wire is clamped to a brass connector. The connector is capable of sliding vertically on a thin brass shaft that in turn hooks onto an adapted analytical balance with a sensitivity of $\pm$ 1 milligram.

Figure 6.9 shows density measuring apparatus in place. It is mounted about 5 inches above the furnace on a heavy transite sheet, the underside of which is covered with aluminum foil.

The procedure is to weigh the bob in air and in distilled water at 20° C and from this calculate the bob volume at room temperature and to use the coefficient of expansion for platinum presented by Shartis and Spinner[105] to calculate the bob volume at measuring temperature. Then the loss of weight of the bob in the melt is determined. The effect of surface tension on the wire is calculated using Barrett and Thomas'[85] data. This tended to make the weight reading in slag high and thus it is a positive

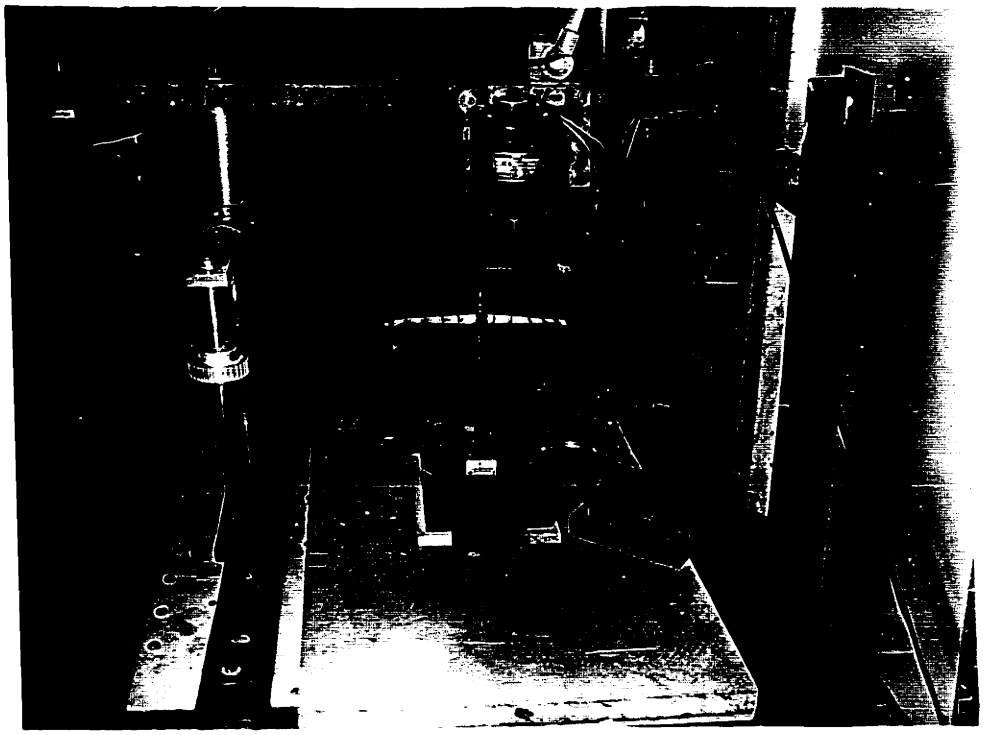

FIGURE 6.9 DENSITY MEASURING ARRANGEMENT

correction to the loss in weight. The density is calculated according to

$$\rho_T = \frac{B + \sigma}{E_p V_p}$$

where ρ_T is slag density at temperature T

B is bouyancy at temperature T

σ is the surface tension correction

E_p is volume expansion of platinum between 20° C and T

V_p is volume of platinum at 20° C

Experimental difficulties are experienced from recrystallization, embrittlement and weakening of platinum leading to several fractures of the platinum lead wire. Also the bob occasionally sticks to the muffle tube cemented there with molten glass.

Materials

The melt is prepared from glass sand, reagent grade calcium oxide, and Linde A-100 Al_2O_3. Chemical analysis of melt is made at approximately weekly intervals. The samples are primarily single crystals of Al_2O_3 supplied by the crystal products division of Linde Air Products Company. Also investigated have been polycrystalline Al_2O_3 sintered from Norton Company X-100 Al_2O_3, polycrystalline mullite sintered from Babcock and Wilcox mullite, and polycrystalline CaO sintered from reagent grade calcined calcium carbonate.

Model System

A number of model system experiments were conducted using glycerine. These were used initially to determine suitable convection patterns from a variety of types of flow generation. Colored particles of ink and bubbles proved valuable for tracing flow lines. Initial experiments utilized mounting samples far from the axis and rotating a liquid bath. These proved to be only poorly reproducible and not suitable to analysis. By using a drill press to provide rotation it was determined that flow to a rotating disc face was fully developed in glycerine at the lowest rotational speed of the press (approximately 1200 RPM) and only at the highest speed (approximately 5000 RPM) did substantial turbulence develop. Laminar flow about the rotating cylindrical surface does not produce a velocity component normal to the cylindrical surface and hence does not affect the solution rate.

When it becomes evident that rotating disc experiments were most suitable for this study, an apparatus was constructed to perform these experiments in the system NaCl-glycerine. This is illustrated schematically in Figure 6.10. A coil of copper tubing of similar capacity to an evaporator on a house-hold refrigerator was soldered to a copper cylinder about 5 inches in diameter and 5 inches high. A bottom plate was soldered to the cylinder, and a cover plate fitted at the top. The compressor from a household refrigerator was connected to the coil providing a means of chilling the copper cylinder to temperatures as cold as - 15° C. A brass container with a glass liner of similar dimensions to the platinum liner for the slag was centered in the copper cylinder by means of rubber tubing. The cover of the brass container has two openings, a central circular hole used for introducing the sample and a second hole providing for a chromel alumel thermocouple. Mallenchrodt reagent grade glycerine was placed in the brass container.

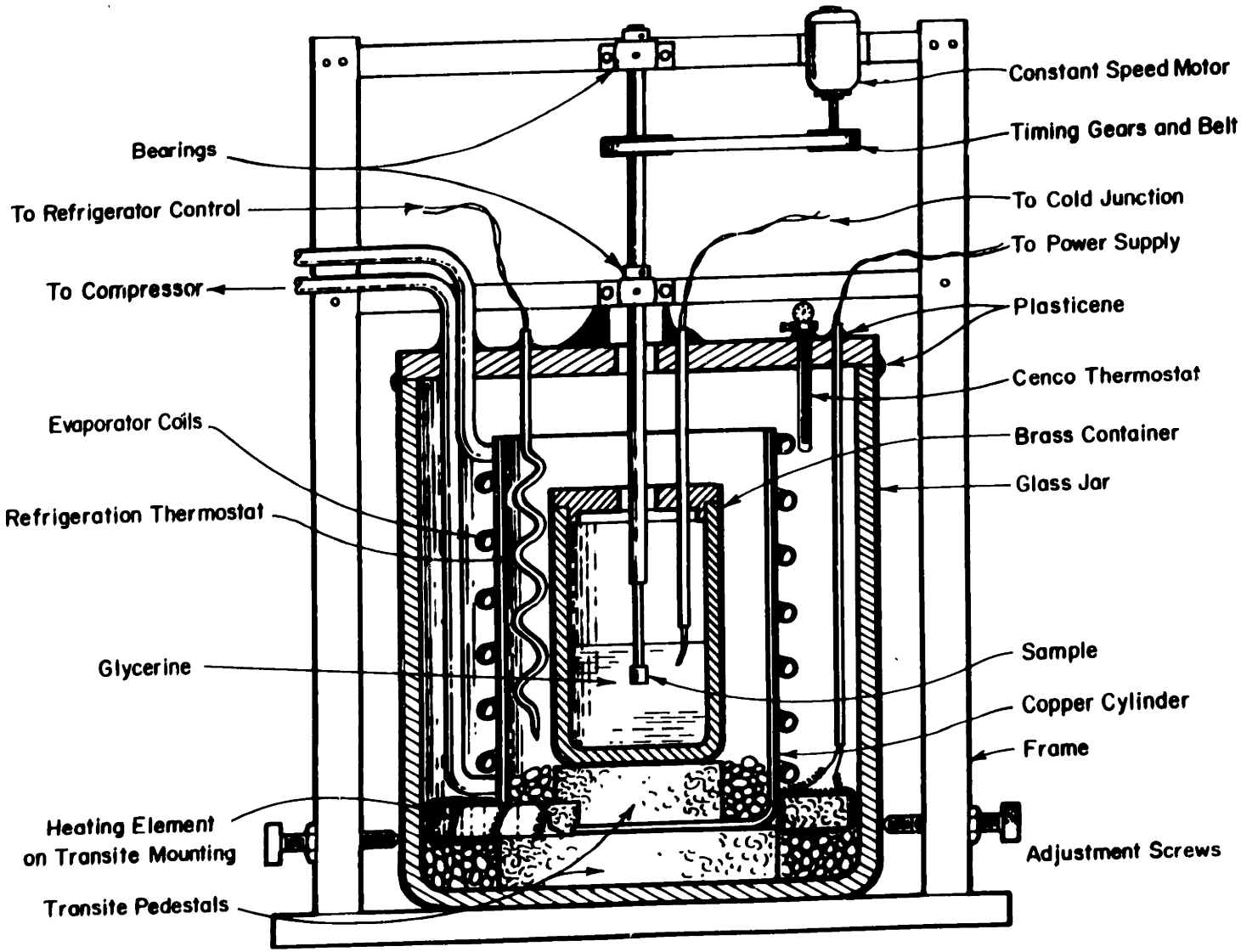

FIGURE 6.10 SCHEMATIC DIAGRAM OF APPARATUS FOR STUDYING SODIUM CHLORIDE SOLUTION BY GLYCERINE

The refrigerator thermostat was inserted between the brass container and copper cylinder . A substantial quantity of drierite was also placed in the void space between the brass container and the copper cylinder to maintain a dry atmosphere and prevent water pickup by the glycerine. The entire assembly was then placed on a transite platform in a large glass vessel. A wire wound transite ring at the base of the glass vessel served as a heating element. Its power supply was regulated by a variable resistance and the air temperature was maintained constant by an on-off control of this power.

The glass vessel was covered with a transite plate and the various connections, refrigerant, power and control circuits taken out through the transite top. Plasticene was used to seal the transite plate to the glass vessel and to seal all the openings except for the center opening used for introducing samples.

An independent frame containing the rotating mechanism was constructed to fit over the glass vessel. A Bodine Electric 1/75 HP motor and a timing belt and gears were utilized to provide the rotation.

The frame was made slightly larger than the glass vessel and mounted around the glass. Adjustment screws permitted locking the glass vessel in proper position to align the openings in the brass container cover and the transite cover with the drive shaft of the rotation mechanism.

Single crystal sodium chloride was supplied by Harshaw Chemical Company as cylinders of .275 inch diameter. The cylinders were sliced to 1/2 inch lengths and a centrally located hole .120 inch in diameter and one quarter inch deep was drilled in one side. Monsanto Chemical Company Arochlor

Number 4465 resin was used to cement the sodium chloride samples to the steel drive shaft. The enclosure was made relatively air tight by using the plasticene to form a seal between the lower bearing of the rotation mechanism and the transite cover.

Samples were introduced by lowering them through the bearings into the glycerine. As in the high temperatures case, the samples were allowed to reach equilibrium with the temperature above the glycerine before starting the experiment. They were removed as rapidly as possible and the excess glycerine wiped off with toweling. Samples measurement is made in precisely the same way as with the sapphire samples.

The temperature measurement of the glycerine was made with a Leeds and Northrup Speedomax recorder. Using full scale to represent one millivolt, precision of temperature measurment to 0.1° C was possible with chromel alumel thermocouples.

Measurements of glycerine viscosity were made with the Brookfield RVF viscosimeter which was also used to measure viscosity of the castor oil used for high temperature calibration,

VII. DETAILS OF ANALYSIS

Introduction

The object of this section is to examine the analytical solution for diffusion flux for the three cases of solution experiments. As was noted in the section on material properties, diffusivity and viscosity vary within the boundary layer in both the sapphire-slag system and the rock salt-glycerine system. Therefore, to make a thorough analysis of the experimental results it is vital that cognizance be taken of the variable properties. In the slags and glasses of industry where refractory solution is of importance, the pertinent properties certainly vary within the boundary layer. Thus in addition to the necessity to understand the role of variable properties in order to evaluate the experimental results of this study, it is also essential to have this clear understanding to apply the principles of solution kinetics to other more complex refractory slag systems.

The major effort in this section is to examine diffusion equations for the transient case, the forced convection case and the free convection case for the geometries used in the experimental approach and to evaluate the effect of variable properties. Other deviations from ideality are briefly considered as is an method for treating the interaction of unsteady and steady state diffusion.

The entire analysis assumes that diffusion rather than viscous relaxation governs the flux. This is equivalent to the assumption that viscous relaxation is a faster process than diffusion in all cases, a premise that seems reasonable but which will not be demonstrated.

Transient Case

For cylindrical samples it is most convenient to use cylindrical coordinates. Fick's second law is

$$\frac{\partial^2 C}{\partial r^2} + \frac{1}{r}\frac{\partial C}{\partial r} - \frac{1}{D}\frac{\partial C}{\partial t} = 0 \qquad 7.1$$

For a sample of radius R dissolving in a liquid, the boundary and initial conditions are

$t = 0 \qquad r > R \qquad C = C_{oo}$

$t \geqslant 0 \qquad r = R \qquad C = C_o$

A solution to the analogous problem in transient heat flow from an internal cylindrical surface of constant temperature was presented by Jaeger[106] and summarized by Carslaw and Jaeger[107]. The flux at the surface can be calculated,

$$\overset{*}{J}_1 = -D\left(\frac{\partial \overset{*}{C}}{\partial r}\right)_{r=R}$$

$$= \frac{4(\Delta \overset{*}{C})D}{\pi^2 R}\int_0^\infty \exp(-Dw^2 t)\,\frac{dw}{w\left[J_{o(Rw)}^2 + Y_{o(Rw)}^2\right]} \qquad 7.2$$

where w is a dummy variable and J_o and Y_o represent zero order Bessel functions of the first and second kinds. This integral has been tabulated by Jaeger and Clarke[108]. For small values of the dimensionless time,

$$\hat{t} = \frac{Dt}{R^2} :$$

$$\overset{*}{J}_1 = \frac{(\Delta \overset{*}{C})D}{R} \left[(\pi \hat{t})^{-1/2} + 1/2 - 1/4 \left(\frac{\hat{t}}{\pi}\right)^{1/2} + 1/8\, \hat{t} \ldots\ldots \right] \qquad 7.3$$

At extremely small values of t,

$$\overset{*}{J}_1 = \frac{\Delta \overset{*}{C}\, D}{R} \quad (\pi t)^{-1/2} \qquad 7.4$$

$$\overset{*}{J}_1 = (\Delta \overset{*}{C}) \quad \left(\frac{D}{\pi t}\right)^{1/2}$$

When the time is very short the flux is identical with the expression for mass flux obtained from equation 4.11 from a plane surface. So long as $t \ll 1$ the effect of the increase in area presented for diffusion with increasing r is of negligible consequence.

The values of $\overset{*}{J}$ given in equations 7.3 and 7.4 are the instantaneous values of the flux at time, t. Of more direct applicability to the solution experiments is the total amount of solution, M, per unit area.

$$M_1 = \int_0^t \overset{*}{J}\, dt$$

Integrating both sides of equation 7.3 reveals

$$M_1 = (\Delta \overset{*}{C}) \quad D \frac{2}{\sqrt{\pi}} \left[\left(\frac{t}{D}\right)^{1/2} + \frac{t}{2R} - \frac{1}{6\pi^{1/2}} \frac{D^{1/2}\, t^{3/2}}{} \ldots \right] \qquad 7.5$$

When time is sufficiently short, only the first term need be considered and the amount of solution per unit area is independent of the radius R. Such an approximation is valid provided $(\hat{t} \ll \frac{\pi}{4})$. The error involved is most clearly seen by defining a correction factor $\beta_{(\hat{t})}$ such that

$$M_1 = \frac{2}{\sqrt{\pi}} \beta_{(\hat{t})} (\Delta C^*) (D) \left(\frac{t}{D}\right)^{1/2} \qquad 7.6$$

The value of $\beta_{(\hat{t})}$ is readily determined from equations 7.5 and 7.6 and is plotted in Figure 7.1. For $\hat{t} \leq 0.01$ the value of $\beta_{(\hat{t})}$ is within 5 % of unity, and it can be dropped from equation 7.6 without significantly diminishing the precision of these results.

Equation 7.1 can be rewritten for $\hat{t} \leq .01$ and variable diffusivity,

$$\frac{d}{dy} \left(D \frac{dC^*}{dy}\right) - \frac{dC^*}{dt} = 0 \qquad (\hat{t} \leq 0.01) \qquad 7.7$$

where $y = (r - R)$ is the direction normal to the interface measured from the interface.

Defining a new variable $\phi = y\, t^{1/2}$, Boltzmann[109] showed that equation 7.7 can be rewritten

$$\frac{d}{d\phi} D \frac{dC^*}{d\phi} = -\frac{\phi}{2} \frac{dC^*}{d\phi} \qquad 7.8$$

This is appropriate provided the boundary conditions for equation 7.7 can be expressed in terms of ϕ alone. The boundary conditions are the same as those for equation 7.1 with the transformation $\phi = (r - R)\, t^{1/2}$

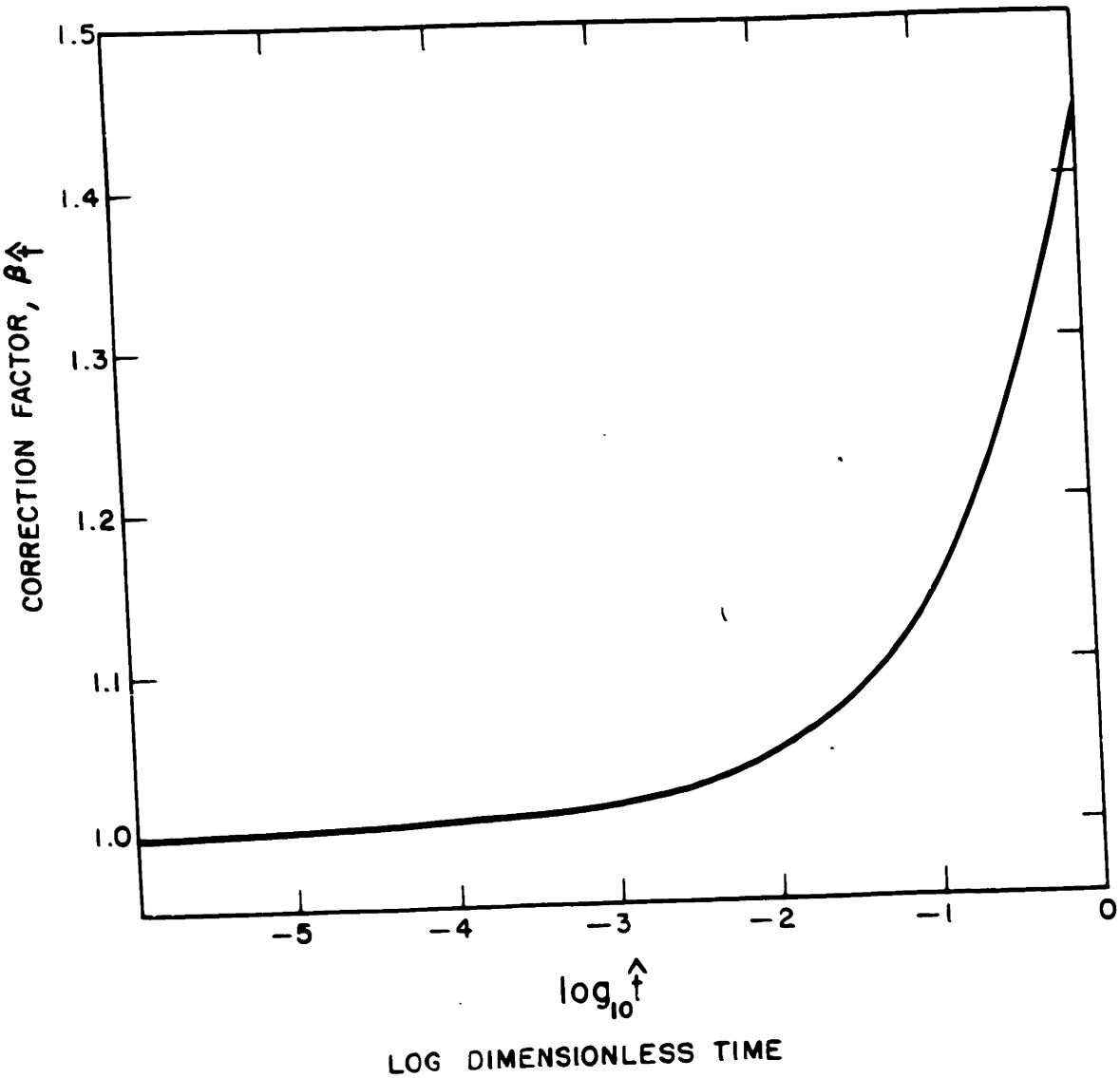

Figure 7.1 Correction Factor for Transient Diffusion for Cylindrical Surfaces.

$$\phi = 0 : \qquad \overset{*}{C} = \overset{*}{C}_0$$

$$\phi \rightarrow + \infty : \qquad \overset{*}{C} \rightarrow \overset{*}{C}_\infty$$

which implies

$$\phi \rightarrow + \infty : \qquad \frac{d\overset{*}{C}}{d\phi} = 0$$

A numerical solution for equation 7.8 can be obtained using a method suggested by J. R. Phillip[110]. Essentially, it consists of integrating 7.8 once to obtain

$$\phi \, d\overset{*}{C} = - 2 D \, d\overset{*}{C}/d\phi \qquad 7.9$$

This can be solved by an interative process in which a step function is substituted for the variation of D with $\overset{*}{C}$. A main feature of the suggested technique is an independent calculation at $\phi = \infty$ where D is assumed to be varying so little as to be constant.

The result of this approximate solution is the value for

$(d\overset{*}{C}/\overset{*}{C}\phi)_{\phi = 0}$

$$(d\overset{*}{C}/d\phi)_{\phi = 0} = (\Delta\overset{*}{C}/\overset{*}{D}^{1/2}) \qquad 7.10$$

in which the value of the effective diffusion coefficient, $\overset{*}{D}$, is given explicitly by the numerical solution.

A good approximation[110] which proves satisfactory is

$$\overset{*}{D} = \frac{2}{(\Delta\overset{*}{C})^2} \int_{\overset{*}{C}_\infty}^{\overset{*}{C}_0} D(\overset{*}{C} - \overset{*}{C}_\infty) \, d\overset{*}{C} \qquad 7.11$$

Then since

$$\left(\frac{d\overset{*}{C}}{dy}\right)_{y=0} = \left(\frac{d\overset{*}{C}}{d\phi}\right)_{\phi=0} t^{-1/2} = \frac{\Delta \overset{*}{C}}{(Dt)^{1/2}} \qquad 7.12$$

$$M_1 = \frac{2}{\sqrt{\pi}} \beta_{(\hat{t})} (\Delta \overset{*}{C}) D_o \left(\frac{t}{\overset{*}{D}}\right)^{1/2} \qquad 7.13$$

is obtained in the same manner as equation 7.6 giving the expression for the total amount of solution for short times in the case of variable diffusivity where D_o is the value of D at y = O, is obtained from Figure 7.1 and $\overset{*}{D}$ from equation 7.11. Since the dependence of D with C is not well established in the systems studied in this work, the added effort of obtaining a numerical solution to equation 7.8 is not justified.

A source of error are the end effects. While end effects are difficult to calculate, it is easy to take account of them experimentally and confine the measurements to regions far from the edge.

Forced Convection (Rotating Disc)

Variable Diffusivity

For steady state mass transport in one direction the requirement of continuity leads to the expression

$$\frac{d}{dy} D \frac{d\overset{*}{C}}{dy} = v \frac{d\overset{*}{C}}{dy} \qquad 7.14$$

where the lefthand side expresses rate of accumulation due to diffusion, and the right hand side expresses the rate which material is carried away by convection. For steady state, these must be equal.

Equation 7.14 can be rewritten as

$$D \frac{d^2\overset{*}{C}}{dy^2} + \frac{dD}{dy} \frac{d\overset{*}{C}}{dy} - v \frac{d\overset{*}{C}}{dy} = 0 \qquad 7.15$$

For flow near a rotating disc Cochran[70] has determined through rigorous numerical solution the dependence of v, the velocity normal to the disc on y. Expressed as an infinite series this is

$$\frac{v}{(\nu\omega)^{1/2}} = (-5.10 (\omega/\nu) y^2 + 0.333 (\omega/\nu)^{3/2} y^3 - 0.103 (\frac{\omega}{\nu})^2 y^4 + 0.0127 (\omega/\nu)^{3/2} y^3 - 0.00283 (\frac{\omega}{\nu})^3 y^6 \ldots.)$$

The boundary conditions for equation 7.15 appropriate for flow to a rotating disc are:

$y = 0 \qquad \overset{*}{C} = \overset{*}{C}_o$ and $v = 0$

$y \to \infty \qquad \overset{*}{C} = \overset{*}{C}_{\infty}$ and $v = -.886 (\nu\omega)^{1/2}$

$y \to \infty \qquad d\overset{*}{C}/dy = 0$

The value of v at $y = \infty$ comes from Cochran.

When D is constant, the second term drops out of equation 7.15 and the solution is relatively easily attained for these boundary conditions. This case has been solved by Levich[101] and Gregory and Riddiford[111] by making use of Cochran's solution for v. For high values of the Schmidt number ($Sc > 10^3$) as is the case of our interest, only the first term of the series determined by Cochran is required and:

$$\overset{*}{\delta}_2 = 1.611 (D/\nu)^{1/3} (\nu/\omega)^{1/2} = 1.611 D^{1/3} \nu^{1/6} \omega^{1/2} \qquad 7.16$$

For the general case where diffusivity is not constant equation 7.15 requires a more intricate solution. Following the procedure of Gregory and Riddiford for the constant property case, a method solving equation 7.15 in its entirety develops.

First equation 7.15 is rewritten

$$\frac{d^2C^*}{dy^2} + \left(\frac{d \ln D}{dy} - \frac{v}{D}\right) \frac{dC^*}{dy} = 0 \qquad 7.17$$

Now it can be integrated once using an integrating factor[112] to give

$$\frac{dC^*}{dy} = K_6 \exp - \int_o^y \left(\frac{d \ln D}{dy} - \frac{v}{D}\right) dy \qquad 7.18$$

$$\frac{dC^*}{dy} = K_6 \exp (\ln D_o - \ln D) \int_o^y \frac{v}{D} dy \qquad 7.19$$

By definition of δ^*:

$$\left(\frac{dC^*}{dy}\right)_{y = 0} = - \left(\frac{\Delta C^*}{\delta^*}\right)$$

K_6 can thus be eliminated and after simplification equation 7.18 becomes

$$\frac{dC^*}{dy} = - \left(\frac{\Delta C^*}{\delta^*}\right) \frac{D_o}{D} \exp \int_o^y \frac{v}{D} dy \qquad 7.20$$

Integrating equation 7.18

$$C^* = - \frac{\Delta C^*}{\delta^*} \int_o^y \frac{D_o}{D} \exp \int_o^y \frac{v}{D} dy\, dy + K_7 \qquad 7.21$$

K_7 is equal to $\overset{*}{C}_o$ from the boundary condition at y = 0 giving

$$\left(\frac{\overset{*}{C}_o - \overset{*}{C}}{\Delta \overset{*}{C}}\right) = \hat{C} = \frac{1}{\overset{*}{\delta}} \int_o^y \frac{D_o}{D} \exp \int_o^y \frac{v}{D}\, dy\, dy \qquad 7.22$$

Equation 7.22 can be solved to whatever degree of precision as necessary by numerical or graphical methods. Manual calculation is tedius. It involves the following steps:

(1) Choose a constant value of $\overset{*}{D}$ intermediate between D_o and D_{oo}.

(2) Evaluate equation 7.21 assuming $\overset{*}{D}$ to be the value of D for all y.

(3) From the concentration profile obtained determine D as f(y) either numerically or graphically.

(4) Substitute this information into equation 7.22 and evaluate numerically or graphically.

(5) Continue steps 3 and 4 until the concentration profile no longer changes.

This iterative process does not provide a value of an effective diffusion coefficient because the variable diffusivity enters into equation 7.22 and two dissimilar ways. Thus it is necessary to carry out the entire solution for each individual case.

While the uncertainty of diffusion measurements in the selected systems do not justify the effort, equation 7.22 does provide a method of dealing with the problem of variable diffusivity in the boundary layer which though tedius can be utilized to obtain whatever precision is necessary. Hopefully as more detailed and precise information on diffusion coefficients is obtained, this technique for carefully dealing with variable diffusivity will prove valuable.

A more approximate approach is to notice that the forms of equation 7.14 with its boundry conditions is much the same as equation 7.8, the difference being in the righthand side. In the latter case the righthand side involves the first power of the independent variable and in the former, 7.14, the square (since $v \sim y^2$ for small y) of the independent variable. It would be expected that the suggested relation for $\overset{*}{D}$ which has found to be a good approximation in transient diffusion would also be of value here. In view of the low fractional power of D in equation 7.16 this approximation given explicitly in equation 7.10 should be satisfactory

Variable Viscosity

Although the obersvation that the viscosity enters into the expression for effective boundary layer thickness for forced convection only to the one sixth power would suggest that the proper choice of viscosity (i.e. bulk viscosity, mean viscosity, or interface viscosity) has little effect on the result for moderate viscosity distributions. This is not a proper conclusion, however, as the one sixth power results from the quotient of two terms each involving viscosity. If the two terms are affected by viscosity gradients in a different manner, then there is no assurance that dividing one by the other will diminish the variation.

For example consider a case where the ratio of interface to bulk viscosity is four ($\nu_o/\nu_\infty = 4$). Then the one sixth power of the ratio is less than 1.17 suggesting that the maximum error indroduced by the worst possible choice of viscosity is 17%. However, suppose the correct viscosity influence on equation 7.16 is given by $\nu_{oo}^{1/2}\nu_o^{-1/3}$. Then the ratio

$$\left(\frac{\nu_o}{\nu_\infty}\right)^{\frac{1}{2}}\left(\frac{\nu_\infty}{\nu_o}\right)^{-1/3} = \left(\frac{\nu_o}{\nu_\infty}\right)^{2/3}$$

represents the maximum possible deviation from the correct result and for this example a maximum percent error of 50 is

permitted. In general, for a situation of this sort the maximum influence of variable properties is indicated by the absolute sum of the exponents of the viscosity terms i.e. $(\nu_o/\nu_{oo})^{2/3}$ not the algebraic sum i.e. $(\nu_o/\nu_{oo})^{1/6}$.)

It is therefore worthwhile to determine the effect of variable viscosity on forced convection diffusion transfer. Examination of the effect of variable viscosity on Cochran's solution for the rotating disc is beyond the scope of this thesis. It should be possible to gain insight by examining the affect of variable viscosity on the simpler solution for for mass transfer in the case of flow above a flat plate as treated by boundary layer approximations by von Karman*[71] We may presume that such an approach will be fruitful since the form of the solution is the same in each case.

To produce uniform shearing forces in the vicinity of the wall von Karman uses a cubic parabola to represent the velocity.

$$\hat{u} = K_8 \hat{y} + K_9 \hat{y}^3 \qquad 7.23$$

where $\hat{u} = u/u_{oo}$ $\hat{y} = y/\delta_u$ and K_8 and K_9 are constants which can easily be shown to be 3/2 and - 1/2. Differentiating equation 7.23 gives:

---

* especially the treatment given by Echert[72a] p. 66-71, 88-92.

$$\frac{d\hat{u}}{d\hat{y}} = K_8 + 3 K_9 \hat{y}^2 \qquad 7.24$$

fulfilling the requirement when η = constant that the shearing stress,

$$\eta \left(\frac{du}{dy}\right)$$

is virtually constant for small values of y.

To conform to the requirement of uniform shear stress near the wall in the case where viscosity varies, we must rewrite equation 7.24 as

$$\hat{\eta} \frac{d\hat{u}}{d\hat{y}} = K_{10} + 3 K_{11} \hat{y}^2 \qquad 7.25$$

where K_{10} and K_{11} are constants and $\hat{\eta} = \eta / \eta_{oo}$ giving by integration

$$\hat{u} = K_{10} \int_0^{\hat{y}} \frac{1}{\hat{\eta}} d\hat{y} + 3 K_{11} \int_0^{\hat{y}} \frac{1}{\hat{\eta}} \hat{y}^2 d\hat{y} \qquad 7.26$$

with boundary conditions

$\hat{u} = 1$ when $\hat{y} = 1$

$\hat{u} = 0$ when $\hat{y} = 0$

$d\hat{u}/d\hat{y} \neq 0$ when $\hat{y} = 1$.

From equation 7.25 and the final boundary condition:

$$K_{10} + 3 K_{11} = 0 \qquad 7.27$$

Also since the viscosity is constant ($\hat{\eta} = 1$) beyond the concentration boundary layer equation 7.26 can be rewritten

$$\hat{u} = K_{10} \int_0^{\hat{y}} \frac{1}{\hat{\eta}} d\hat{y} + 3 K_{11} \int_0^{\hat{y}} \frac{1}{\hat{\eta}} \hat{y}^2 d\hat{y} \quad \text{for } y \leq \frac{\delta}{\delta_u} = \hat{\delta}$$

$$\hat{u} = K_{10} \int_0^{\hat{\delta}} \frac{1}{\hat{\eta}} d\hat{y} + K_{10} (\hat{y} - \hat{\delta}) + 3 K_{11} \int_0^{\hat{\delta}} \frac{\hat{y}^2}{\hat{\eta}} d\hat{y} + K_{11} (\hat{y}^3 - \hat{\delta}^3) \text{ for } \hat{y} > \hat{\delta} \qquad 7.28$$

when $\hat{\delta} = \frac{\delta}{\delta_u} \ll 1$* and $\hat{y} \gg \hat{\delta}$ the value of the first and third term on the left hand side of equation 7.28 are very small and negligible error is introduced if they are replaced by $K_{10}\,\hat{\delta}$ and $3\,K_{11}\,\hat{\delta}^3$ giving

$$\hat{u}_{(\hat{y} > \hat{\delta})} \approx K_{10}\,\hat{y} + 3\,K_{11}\,\hat{y}^3 \qquad 7.29$$

If the value at $\hat{y} = 1$ is substituted in equation 7.29 the result together with equation 7.27 requires that $K_{10} = 3/2$ and $K_{11} = -1/2$ which are identical to the values of the equivalent constants for the constant viscosity case and introducing these coefficients into equation 7.28

$$\hat{u} = 3/2 \int_0^{\hat{y}} \frac{1 - \hat{y}^2}{\hat{\eta}}\, d\hat{y} \qquad \text{for } \hat{y} \leq \hat{\delta}$$

$$\hat{u} = 3/2 \int_0^{\hat{\delta}} \frac{1 - \hat{y}^2}{\hat{\eta}}\, d\hat{y} + 3/2\,(\hat{y} - \hat{\delta}) - 1/2\,(\hat{y}^3 - \hat{\delta}^3) \qquad \text{for } y > \hat{\delta} \qquad 7.30$$

$$\hat{u} \approx 3/2\,\hat{y} - 1/2\,\hat{y}^3$$

The approach used by von Karman is to balance the momentum loss in the boundary layer with the shear stress at the boundary. The momentum loss, Q, determined in a slice normal to the interface by summing the momentum flux through each of four planes, the interface, a parallel plane a distance δ_u away, two normal planes separated by dx, is

$$Q = \rho \frac{d}{dx} \int_0^{\delta_u} (u_\infty - u)\,(u)\, dy \qquad 7.31$$

or in terms of dimensionless variables

---

* For molten silicates and glycerine $\hat{\delta} = \left(\frac{D}{\nu}\right)^{1/3} < 10^{-2}$

$$\Delta Q = u_{oo}^2 \rho \frac{d}{dx} \int_o^1 \hat{u} - (\hat{u})^2 \, d\hat{y} \qquad 7.32$$

The value of the integral in equation 7.32 depends almost entirely on the higher values of $\hat{u}$ present in the region $\hat{y} > \hat{\delta}$. Thus very little error is introduced by substituting for u the final equation of the set 7.30

$$\int_o^1 (\hat{u} - \hat{u}^2) \, d\hat{y} = 1/2 \int_o^1 (3\hat{y} + 9\hat{y}^2 - \hat{y}^3 - 6\hat{y}^4 + \hat{y}^6) dy \qquad 7.33$$

For the cases of interest where $\hat{\delta} < .01$, the error involved in this assumption is less than the errors involved in the boundary layer approximation themselves.

Evaluation of equation 7.33 and combination with equation 7.32 gives

$$\Delta Q = 39/280 \rho \, u_{oo}^2 \frac{d\delta}{dx} \qquad 7.34$$

The momentum loss is balanced by the shearing stress at the wall $\eta \left(\frac{du}{d\hat{y}}\right)_{\hat{y}} = 0$. From equation 7.25:

$$\hat{\eta} \left(\frac{d\hat{u}}{d\hat{y}}\right)_{\hat{y}=0} = K_{10} = 3/2 \qquad 7.35$$

and substituting to eliminate dimensionless quantities:

$$\hat{\eta} \left(\frac{d\hat{u}}{d\hat{y}}\right)_{\hat{y}=0} = \frac{3/2 \, \eta_{oo} \, u_{oo}}{\delta_u} \qquad + 7.36$$

Equating loss of momentum with shearing stress at the wall, equations 7.34 and 7.36 yield:

$$39/280\ \rho\ u_{oo}^2\ \frac{d\delta_u}{dx} = 3/2\ \eta_{oo}\ \frac{u_{oo}}{\delta_u} \qquad 7.37$$

separating variables

$$\delta_u\ d\delta_u = 140/13\ \frac{\nu_{oo}}{u_{oo}}\ dx \qquad 7.38$$

integrating

$$\delta_u = 4.64\sqrt{\frac{\nu_{oo}\ X}{u_{oo}}} \qquad 7.39$$

Equations 7.38 and 7.39 are identical with those for constant viscosity pointing out the negligible effect of a variable viscosity immediately adjacent to the surface on the velocity boundary layer thickness for flow above a flat plate.

Following the approach of von Karman, it is assumed that the concentration profile also is a cubic parabola, for an entirely equivalent set of reasons as were used to justify the velocity profile

$$\hat{C} = 3/2\ (y/\delta) - 1/2\ (y/\delta)^3 \qquad 7.40$$

Remembering the definition of $\hat{C} = \frac{C_o - C^*}{C_o^* - C_{oo}^*}$ it follows that

$$\left(\frac{dC^*}{dy}\right)_{y=0} = -3/2\ \frac{C_o^* - C_{oo}^*}{\delta} = -\frac{\Delta C^*}{\delta} \qquad 7.41$$

A mass balance within an incremental slice of the diffusion boundary layer gives:

$$dx\ \frac{d}{dx}\int_0^{\hat{\delta}} (C_{oo}^* - C^*)\ u\ dy - dx\ D\left(\frac{dC^*}{dy}\right)_{y=0} = 0 \qquad 7.42$$

converting to dimensionless variables:

$$u_{oo}\,(C_o^* - C_{oo}^*)\,d/dx\,\delta_u \int_o^{\hat{\delta}} (c-1)\,\hat{u}\,d\hat{y} + 3/2\,D\,\frac{C_o^* - C_{oo}^*}{\delta} = 0 \qquad 7.43$$

by simplifying

$$u_{oo}\,\frac{d}{dx}\,\delta_u \int_o^{\hat{\delta}} (1-\hat{c})\,\hat{u}\,d\hat{y} = 3/2\,D/\delta \qquad 7.44$$

call the integral in equation 7.44, I, then substituting for $\hat{u}$ from equation 7.30 c and for $\hat{c}$ from equation 7.40

$$I = 3/2 \int_o^{\hat{\delta}} 1 - 3/2\,\hat{y}/\hat{\delta} + 1/2\,(\hat{y}/\hat{\delta})^3 \; 3/2 \int_o^{\hat{\delta}} \frac{1-y^2}{\hat{\eta}}\,d\hat{y}\,d\hat{y} \qquad 7.45$$

Since the integral is only to be evaluated to $\hat{\delta}$, y^2 is always much less than unity giving

$$I = 3/2 \int_o^{\hat{\delta}} (1 - 3/2(\hat{y}/\hat{\delta})) + 1/2\,(\hat{y}/\hat{\delta})^3) \int_o^{\hat{y}} \frac{d\hat{y}}{d\hat{\eta}}\,d\hat{y} \qquad 7.46$$

The effect of variable viscosity on I can be shown by a correction factor ψ as follows:

$$\psi = \frac{I}{I\,(\hat{\eta}=1)} = \frac{I}{3/20\,\hat{\delta}^2} \qquad 7.47$$

Solution of 7.44 can be achieved by introducing $I = 3/20\,\hat{\delta}^2\psi$:

$$\frac{u_{oo}\psi}{10}\,(\hat{\delta}^3\,\delta_u\,(\frac{d\,\delta_u}{dx}) + 2\,\hat{\delta}^2\,\delta_u^2\,\frac{d\hat{\delta}}{dx} = D \qquad 7.48$$

Substituting for δ_u^2 and $\delta_u d\delta_u$ from equations 7.38 and 7.39 gives:

$$\frac{\nu_{oo}}{D}\,14/13\,(\hat{\delta}^3 + 4.1\,\hat{\delta}^2\,\frac{d\hat{\delta}}{dx}) = \frac{1}{\psi} \qquad 7.49$$

Letting $14/13 \approx 1$ and noting that the ratio $\hat{\delta}$ of concentration boundary layer to the diffusion boundary layer is independent of x:

$$\hat{\delta}^3 = \left(\frac{1}{\psi}\frac{D}{\nu_{oo}}\right) \qquad 7.50$$

$$\delta = \left(\frac{1}{\psi}\frac{D}{\nu_{oo}}\right)^{1/3} \delta_u \qquad 7.51$$

Then substituting for δ and δ_u from equations 7.41 and 7.39 respectively

$$\overset{*}{\delta} = 3.1 \left(\frac{D}{\nu_{oo}\psi}\right)^{1/3} \left(\frac{\nu_{oo} X}{u_{oo}}\right)^{1/2} \qquad \text{(flat plate)} \qquad 7.52$$

This is the expression for the effective boundary layer thickness for flow over a flat plate with the diffusion coefficient constant and the viscosity variable. It is equivalent to the expression for constant viscosity except that the bulk viscosity, ν_{oo}, should be used for the factor involving $\nu^{1/2}$, and a weighted average viscosity ($\nu\psi$) for the factor involving $\nu^{-1/3}$. From equation 7.46, it is apparent that the weighting favors the value of interface viscosity, ν_o, but the entire calculation can be done relatively easily by graphical analysis. It involves determining and plotting ν as a function of $(y/\hat{\delta})$ from the viscosity concentration relationship, and the concentration profile equation 7.40. Then equation 7.47 can be evaluated graphically and the value of ψ determined.

For example, along the $Ca(SiO_3)$-Al_2O_3 binary at 1500^o C with a bulk composition, C_{oo} = 20 weight percent Al_2O_3

$\psi = 1.62$ where $\eta_o = 1.73$

This then is equivalent to

$$\overset{*}{\nu} \equiv \Psi \nu_{oo} = \nu_{oo} + .85 (\nu_o - \nu_{oo}) \qquad 7.53$$

As the viscosity-composition behavior is rather consistent along this binary, this value will be used for all cases in lieu of making the individual calculations for each case.

It should be recognized that the interaction of the case of variable diffusivity and variable viscosity has not been considered but only their independent effects. This is a source of some slight error. To account for the effect of their interaction, equation 7.40 would have to be modified in a like manner to equation 7.23 to take into account variations in diffusivity and preserve a constant diffusion flux near to the surface. This is more difficult in the case of diffusion because the approximations utilized to obtain equation 7.29 etc. are no longer appropriate. Since the flat plate is not the case of particular interest to this work, a detailed approximate solution for this case does not seem justified.

Assuming that the relationships determined for variable viscosity for flow above a flat plate are transferrable to rotating disc flow, and introducing the effective diffusion coefficient $\overset{*}{D}$ defined by equation 7.10, one obtains:

$$\overset{*}{\delta}^2 = 1.61 \left(\frac{\overset{*}{D}}{\overset{*}{\nu}}\right)^{1/3} \left(\frac{\nu_{oo}}{\omega}\right)^{1/2} \qquad \text{(rotating disc)} \qquad 7.54$$

$$\overset{*}{J}_2 = .62 \, D_o \left(\frac{\overset{*}{\nu}}{\overset{*}{D}}\right)^{1/3} \left(\frac{\omega}{\nu_{oo}}\right)^{1/2} \Delta \overset{*}{C} \quad \text{(rotating disc)} \qquad 7.55$$

$$\dot{M} = .62 \, D_o \left(\frac{\overset{*}{\nu}}{\overset{*}{D}}\right)^{1/3} \left(\frac{\omega}{\nu_{oo}}\right)^{1/2} \Delta \overset{*}{C}_t \quad \text{(rotating disc)} \qquad 7.56$$

It is evident that the flux, $\overset{*}{J}_2$, and total corrosion, M_2, are independent of radius. This is one of the special conveniences of using the rotating disc for solution experiments. They all depend, however, on Cochran's solution for flow to a rotating disc. This assumes a disc of infinite diameter and therefore takes no account of edge effects. When the boundary layer thickness is of the same order as the radius, the edge effects can become important. For most of these experiments, the velocity boundary layer is larger than the radius, but the concentration boundary layer is vastly smaller. It is, therefore, advisable to measure the change of length as near as possible to the centerline.

The velocity boundary layer is often of the same order of size as the distance between the bottom of the sample and the bottom of the crucible. This conceivably could interfere with the flow behavior and might be expected to also influence the diffusion flux from the sample.

Free Convection

The solution for free convection transfer for vertical cylinders has been solved by Ellenbaas[113]. His approach was to take the solution for the vertical plate, equation 4.8, which has been verified experimentally and assume, following Langmuir that the boundary layer thickness about a vertical cylinder is independent of the cylinder radius. With this assumption, he shows that it is possible by a very simple transformation to take account of the effect of the radius. His expression is

$$Nu_{(do)} \exp\left(-2/(Nu)_{dm}\right) = 0.6(Gr\ Pr)_{xo}^{1/4} \frac{d}{x} \qquad 7.57$$

The subscripts refer to whether the diameter, d, or the distance from the leading edge, x, is selected as the characteristic length, and the property values are selected for conditions at the interface, o, or the mean value for the entire boundary layer, m.

Nu, is the Nusselt number which is a dimensionless group that indicates the rate of heat transfer for a given value of conductivity. For purposes of mass transfer, it can be expressed as the ratio of a characteristic length to the effective boundary layer thickness, i.e.

$$Nu_{do} = \frac{d}{\delta^*} \qquad 7.58$$

$$Nu_{dm} = \frac{d + \delta^*/2}{\delta^*}$$

Pr is the Prandtl number which is an entirely analagous concept to the Schmidt number except that it is the ratio of thermal diffusivity rather than mass diffusivity to kinematic viscosity.

The constant in equation 7.57 was obtained empirically by several investigations, for example, Pohlausen, Schmidt and Beckmann[114] for heat transfer from a flat plate to gases. Since the Schmidt number for viscous liquids is many orders of magnitude higher than the Prandtl number for gases, it follows from the approximate analysis of Echert[72a] that a lower value for the constant will be required. This is confirmed by Wagner's[74] solution studies of NaCl in water where 0.545 was the constant. In case of very viscous liquids, a value of 0.510 comes out of Echert's analysis.

It is evident from equation 7.57 that so long as $Nu \gg 2$ the correction for the sample being cylindrical rather than plane is slight.

Physically, this can be visualized because a thin ring can very nearly be unrolled into a flat plate.

With the definition of Nu and the change of constant

$$\overset{*}{\delta}_3 = 1.96\,(Gr\ Sc)^{-1/4}\ X\ \exp\left(\frac{2\overset{*}{\delta}}{d + 1/2\ \overset{*}{\delta}}\right) \qquad 7.59$$

$$\overset{*}{\delta}_3 = 1.96\left(\frac{D_o \nu_o X}{g\Delta\rho}\right)^{1/4}\lambda$$

where λ is a correction factor similar to $\mathcal{B}$ to convert the flat plate solution to a solution valid for the cylinder, $\lambda = \exp - (2\overset{*}{\delta}/(d + \frac{1}{2}\overset{*}{\delta}))$. Except for λ equation 7.59 is identical with equation 4.8.

The effect of variable properties is implicitly taken care of by equation 7.59 as it specified that both the viscosity and the diffusivity are to be the values at the interface. While this is probably not rigorously true, most solutions for the free convection equation are approximate. The product of viscosity and diffusivity is often very nearly constant. (Equation 17 in the Appendix). All the reasons make the use of equation 7.59 as it stands practical.

The relation describing the total amount of solution from free convection is readily deduced from equation 7.59. It is

$$M_3 = .510\,\lambda^{-1}\,(D_o^{3/4}\,\nu_o^{-1/4}\,g^{+1/4}\,\Delta\rho^{+1/4}\,x^{-1/4}\,\overset{*}{\Delta C}\,t \qquad 7.60$$

Interaction of Transient Convection with Steady State Convection

In all types of solution experiments, there is a period, however, short, when the boundary layer thickness for free diffusion is less than that

for the steady state solution. The initial time period indicated by the relation $t < t'$; in other words $t = t'$ when $\overset{*}{\delta}_{trans} = \overset{*}{\delta}_{steady}$.

It seems reasonable to presume that so long as the boundary layer thickness for free diffusion is least, the solution rate will be governed by free diffusion and for all times after $\overset{*}{\delta}_{trans} = \overset{*}{\delta}_{steady}$, the rate will be governed by steady state kinetics. This is equivalent to the assumption that the convection does not interfere with free diffusion, a premise that has not rigorously been tested.

By differentiating equation 7.13, the effective boundary layer thickness for transient free diffusion from a cylindrical surface is

$$\overset{*}{\delta}_{transient} = \frac{(\pi \overset{*}{D} t)^{1/2}}{\beta + d\beta/dt} \qquad 7.61$$

The value of $\beta + d\beta/dt$ can be determined from Figure 7.1 by converting from dimensionless to absolute values. Since this is just another correction factor, it will be designated as $\Omega = \beta + d\beta/dt$, giving

$$\overset{*}{\delta}_{transient} = \frac{(\pi \overset{*}{D} t)^{1/2}}{\Omega} \qquad 7.62$$

For a plane surface, the correction factor is extraneous and equation 4.11 applies.

For forced convection, equations 4.11 and 7.54 lead to

$$t_2' = .825 \overset{*}{\nu}^{-2/3} \overset{*}{D}^{-1/3} \nu_{oo}^{-1} \omega \qquad 7.63$$

To avoid confusion with M, a new symbol, L, is utilized here to represent the total amount of solution when steady and transient processes combine.

For $t < t'_2$

$$L_2 = M_1 = \frac{2}{\sqrt{\pi}} (\Delta C^*) \; D_o (t/D^*)^{1/2}$$

For $t > t'_2$

$$L_2 = M_{1(t')} + .62 \, D_o (\nu^*/D^*)^{1/3} \, (\omega/\nu_{oo})^{1/2} \, (t - t') \, \Delta C^* \qquad 7.64$$

$$L_2 = M_{1(t')} + M_2 \left(\frac{t - t'}{t}\right)$$

For free convection from equation 7.59 and 7.62

$$t'_3 = 1.25 \, \frac{\zeta^2 \Omega^2}{D^*} \left(\frac{D_o \nu_o}{g \Delta \rho}\right)^{1/2} x^{1/2} \qquad 7.65$$

An interesting feature of this relationship is that t' is a function of x. The time until steady state dominates is shorter the closer the distance from the leading edge.

The overall expression governing the total amount of solution at distance x from the leading edge can be expressed by the following set of equations:

for $t < t'_3$

$$L_3 = M_1 = \frac{2}{\sqrt{\pi}} \beta_{(t)} \; (\Delta C^*) \; D_o \; (t/D^*)^{1/2}$$

for $t > t'_3$

$$L_3 = M_{1(t')} + .510 \, \zeta^{-1} \, D_o^{3/4} \nu_o^{-1/4} g^{1/4} \Delta\rho^{1/4} x^{-1/4} (t - t') \Delta C^*$$

$$L_3 = M_{1(t')} + M_3 \left(\frac{t - t'}{t}\right) \qquad 7.66$$

Then the set of equations 7.64 and 7.66 summarize the results of this section by giving the relationship between total amount of solution and pertinent parameters for both the free convection and the forced convection case.

VIII. RESULTS AND DISCUSSION OF SODIUM CHLORIDE-GLYCERINE EXPERIMENTS

Property Measurements

In order to clarify and expand the data on the pertinent property values, several measurements were necessary.

Measured values of the dynamic viscosity of glycerine from 0° C to 50° C agreed well with the results of Sheeley.[95] Dividing this viscosity value by the density gives the kinematic viscosity. As discussed in Section V, page 50, dividing the viscosity into 6.5×10^{-7} gives a reasonable estimate of the sodium chloride diffusion coefficient in pure glycerine. The kinematic viscosity and diffusivity calculated from the measured dynamic viscosity are shown in Figure 8.1.

It is also necessary to know the variation of properties with concentration. Measured values corrected to constant temperature of the variation of specific conductivity and viscosity with sodium chloride concentration are shown in Figure 8.2. While the variation in conductivity may be primarily connected more with the mobility of the chloride ion than in the sodium ion[115] and the diffusion coefficient involves their joint migration, since they have nearly the same mobility, it seems reasonable to presume that the Nernst- Einstein equation applies and $\frac{D}{D_{oo}} = \frac{\sigma/C}{(\sigma/C_{oo})}$ where σ is the conductivity expressed in arbitrary units. Figures 8.1 and 8.2 permit the value for the interface diffusion coefficient, D_o, and the interface viscosity, ν_o, to be obtained directly. The effective diffusion coefficient can be obtained by making use of equation 7.11 of page 84.

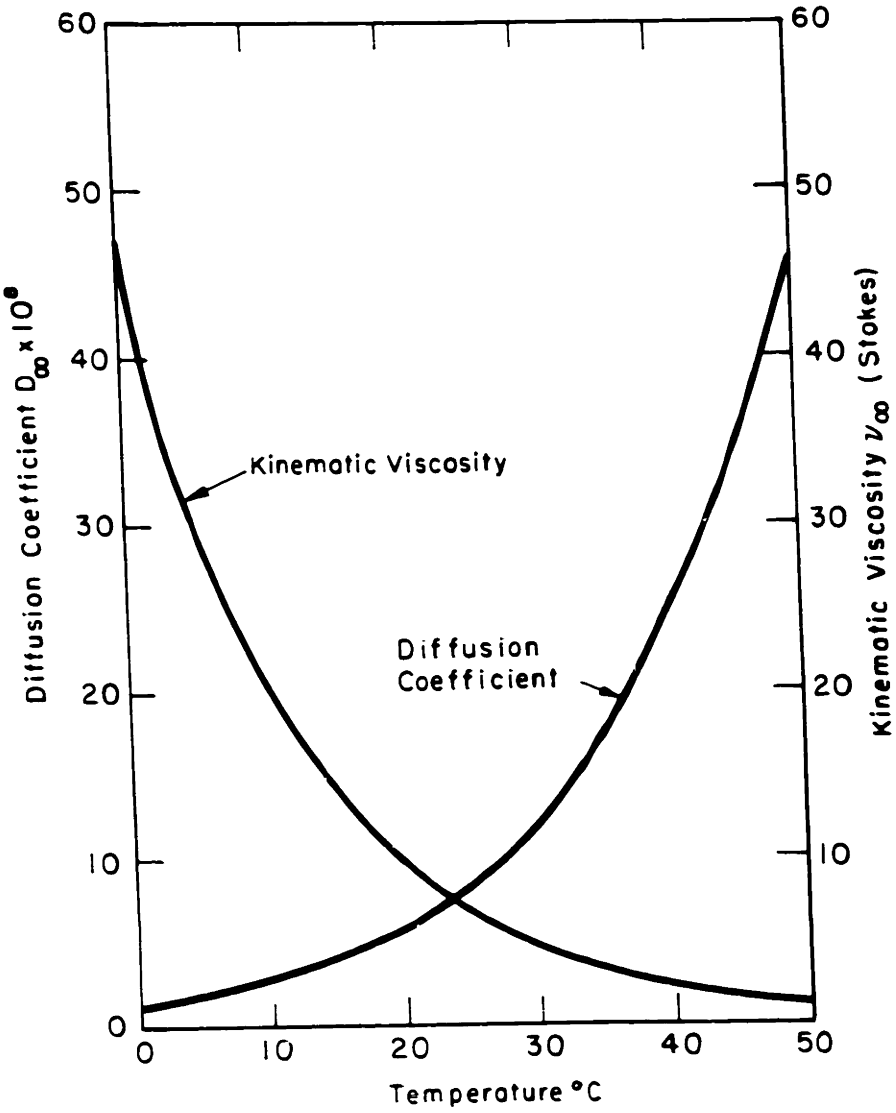

FIGURE 8.1 VARIATION OF DIFFUSION COEFFICIENT OF SODIUM CHLORIDE IN GLYCERINE AND KINEMATIC VISCOSITY OF GLYCERINE WITH TEMPERATURE

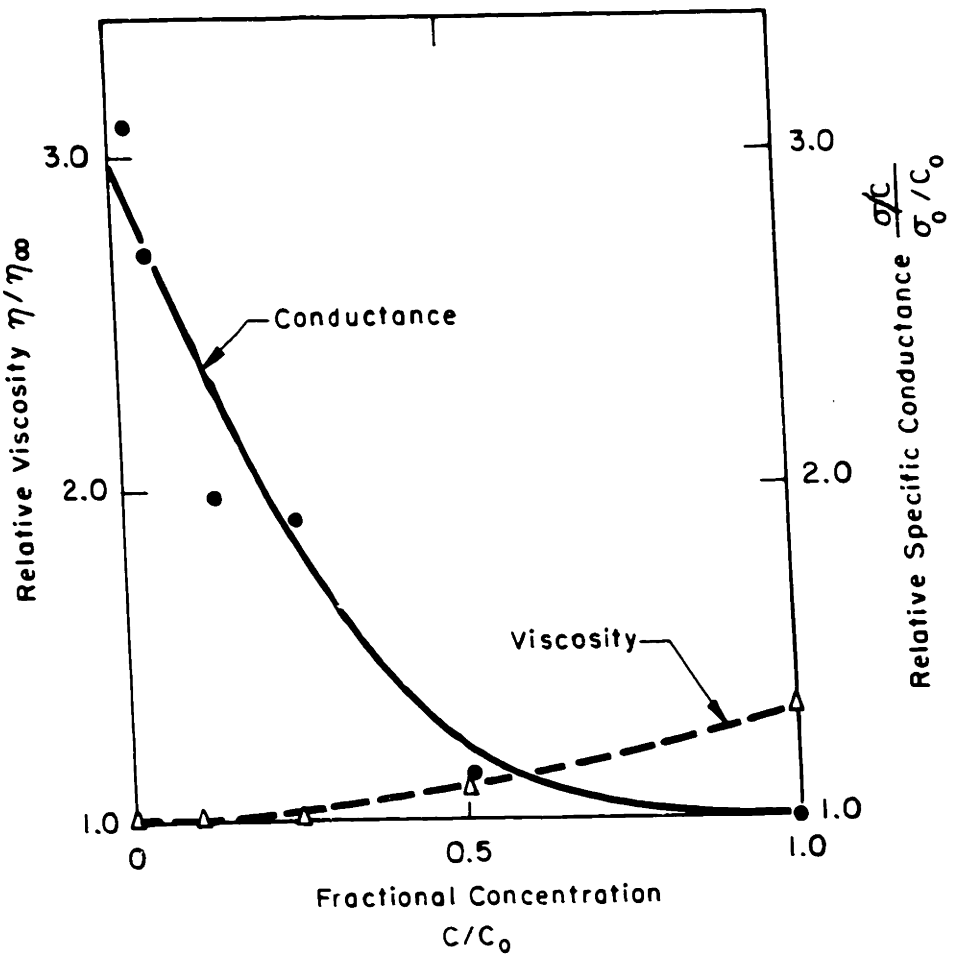

FIGURE 8.2 DEPENDENCE OF SPECIFIC CONDUCTANCE AND VISCOSITY ON SODIUM CHLORIDE CONCENTRATION

$$\overset{*}{D} = \frac{2}{\Delta \overset{*}{C}} \int_{\overset{*}{C}_{oo}}^{\overset{*}{C}_{o}} D \left(\overset{*}{C} - \overset{*}{C}_{oo}\right) d\overset{*}{C} \qquad 8.1$$

and solving from Figure 8.2 graphically. For the effective viscosity, $\overset{*}{\nu}$ equation 7.53 on page 97 is utilized

$$\overset{*}{\nu} = \nu_{oo} + .85 \left(\nu_{o} - \nu_{oo}\right) \qquad 8.$$

and the value of $\overset{*}{\nu}$ is obtained from Figure 8.2. These calculations lead to the following relations

$$D_{o} = .33\, D_{oo}; \quad \overset{*}{D} = .4\, D_{oo}$$

$$\nu_{o} = 1.33\, \nu_{oo}; \quad \overset{*}{\nu} = 1.28\, \nu_{oo} \qquad 8.$$

which along with Figure 8.1 summarizes the viscosity and diffusion data. Solubility, $\Delta \overset{*}{C}$, and the density differential, $\Delta\rho$, are the other necessary information.

The solubility of sodium chloride in glycerine was measured at -18° C, 25° C and 55° C. The value agreed well with Herz and Knoch's[94] result at 25° C. Table VIII-1 gives the measured sodium chloride solubility at different temperatures

TABLE VIII-1

Solubility of Sodium Chloride in Glycerine

Temperature	solubility cc NaCl/cc glyc.
-18° C	4.4×10^{-2}
25° C	4.45×10^{-2}
55° C	4.38×10^{-2}

There is no indication of a significant change in solubility with temperature and the value of 4.4×10^{-2} cm^3/cm^3 is used in all calculations.

A density differential, $\Delta\rho$, of 0.029 determined at 25^{o} C will be assumed to be appropriate at all temperatures (see page 50).

Effect of Inherent Variations in Experiments

One of the advantages of model experiments is that variations which are difficult to analyze can be examined in the model system.

The effect of eccentricity of rotation on transport to a rotating disc has not been studied previously. Two experiments encompassing the anticipated range of eccentricity were conducted with sodium chloride in glycerine using totally immersed samples. The results given in Table VIII-2 show that for eccentricities up to 0.030 inch or more than one-tenth the diameter, eccentricity has a negligible influence on solution rate.

TABLE VIII-2

Effect of Eccentricity of Rotation on Corrosion of Sodium Chloride

Eccentricity	Corrosion Rate 1/2 loss in length	Loss in Weight
.003"	5.5×10^{-6} cm/sec	93.2 mg/hr
.033" to .037"	5.9×10^{-6} cm/sec	90 mg/hr

Table VIII-3 shows that within the range of variation anticipated in these experiments, the container diameter has a negligible effect on solution rates.

TABLE VIII-3

Effect of Container Diameter on Corrosion Rate
of Sodium Chloride-Glycerine at 25° C

Diameter	Corrosion Rate 1/2 loss of length	loss of weight
3 11/32	1.53×10^{-6} cm/sec	21.1 mg/hr
3 3/32	$1,57 \times 10^{-6}$ cm/sec	20.9 mg/hr

When forced convection samples were totally immersed, the depth of immersion was an unavoidable variable. Table VIII-4 shows the negligible effect of this variable.

TABLE VIII-4

Effect of Depth of Immersion of Forced Convection Samples

Depth of NaCl top disc beneath surface	Corrosion Rate 1/2 loss of length corrected to 41° C and 0 NaCl
1/2 "	5.5×10^{-6} cm/sec
3/4 "	5.6×10^{-6} cm/sec
1 1/16 "	5.7×10^{-6} cm/sec

A similar test at a different temperature revealed that loss of length of totally immersed samples was twice that of those in which only a single disc face was exposed.

The distance between the container bottom and the rotating disc face may be less than the velocity boundary layer thickness of some experiments. It is important to check the effect both from practical and basic consideration. The velocity boundary layer thickness can be calculated according to equation 4.3 and Figure 8.3 shows the effect on corrosion rate of the ratio of velocity boundary layer thickness to the gap between disc face and bottom.

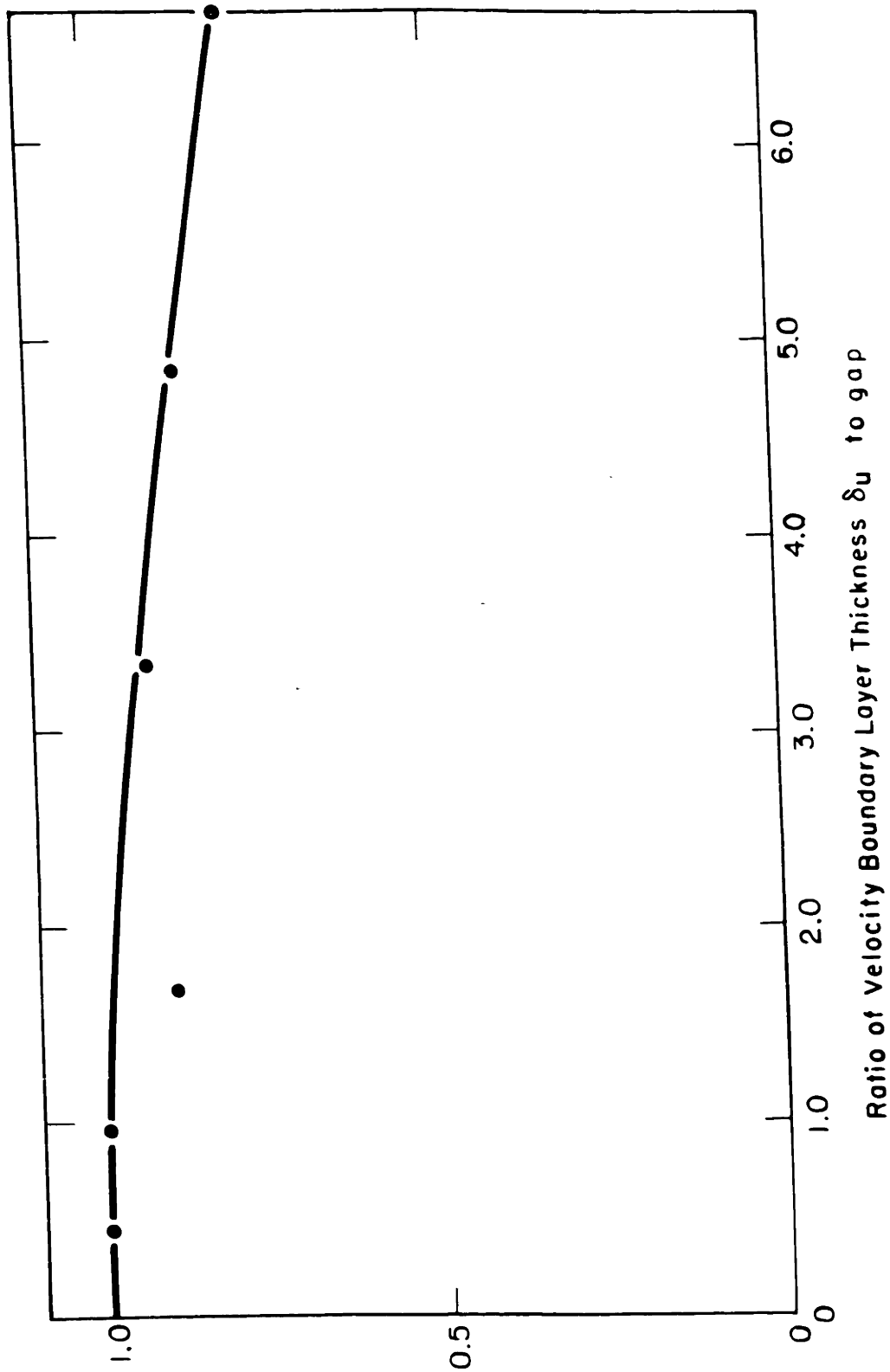

FIGURE 8.3 EFFECT ON FORCED CONVECTION CORROSION OF THE RATIO OF VELOCITY BOUNDARY LAYER APPROACHING AND EXCEEDING THE GAP BETWEEN DISC FACE AND CONTAINER BOTTOM

The deviations are barely within the precision of experiments, but since the runs were conducted consecutively, the trend is probably valid. In any event,, up to velocity boundary layer thickness several times the gap distance, the effect on corrosion rate is negligible.

A large number of experiments have been directed at determining the effect of time on corrosion rate for forced convection. A typical result for forced convection is shown in Figure 8.4 which gives measurements of total amounts of corrosion versus time for solution at 10° C. This and all other such experiments indicate that apparent initial corrosion rates are faster than the eventual equilibrium rates.

It is possible that this is due to transient diffusion dominating at the early stage of the solution process. Calculations of t'_2 from equation 7.63 show that the time during which free diffusion dominates is seven seconds. The corrosion during this period, $L_{2(t = t')}$, according to equation 7.64 is equal to 1.0×10^{-5} cm which is hardly enough to account for the correction of about 10^{-3} cm.

Another possibility is that the initial surface is rough. Micrometer measurements read the upper peaks of this rough surface. There is, therefore, less sodium chloride to be dissolved to obtain a given change in dimensions than would be the case for corrosion of a perfectly smooth surface. Some support for this premise is found in the observations that the pock marks on disc surfaces disappear at about the same time as corrosion rate becomes stable. To compensate for rough surfaces, 1×10^{-3} cm has been subtracted from each measurement of forced convection corrosion.

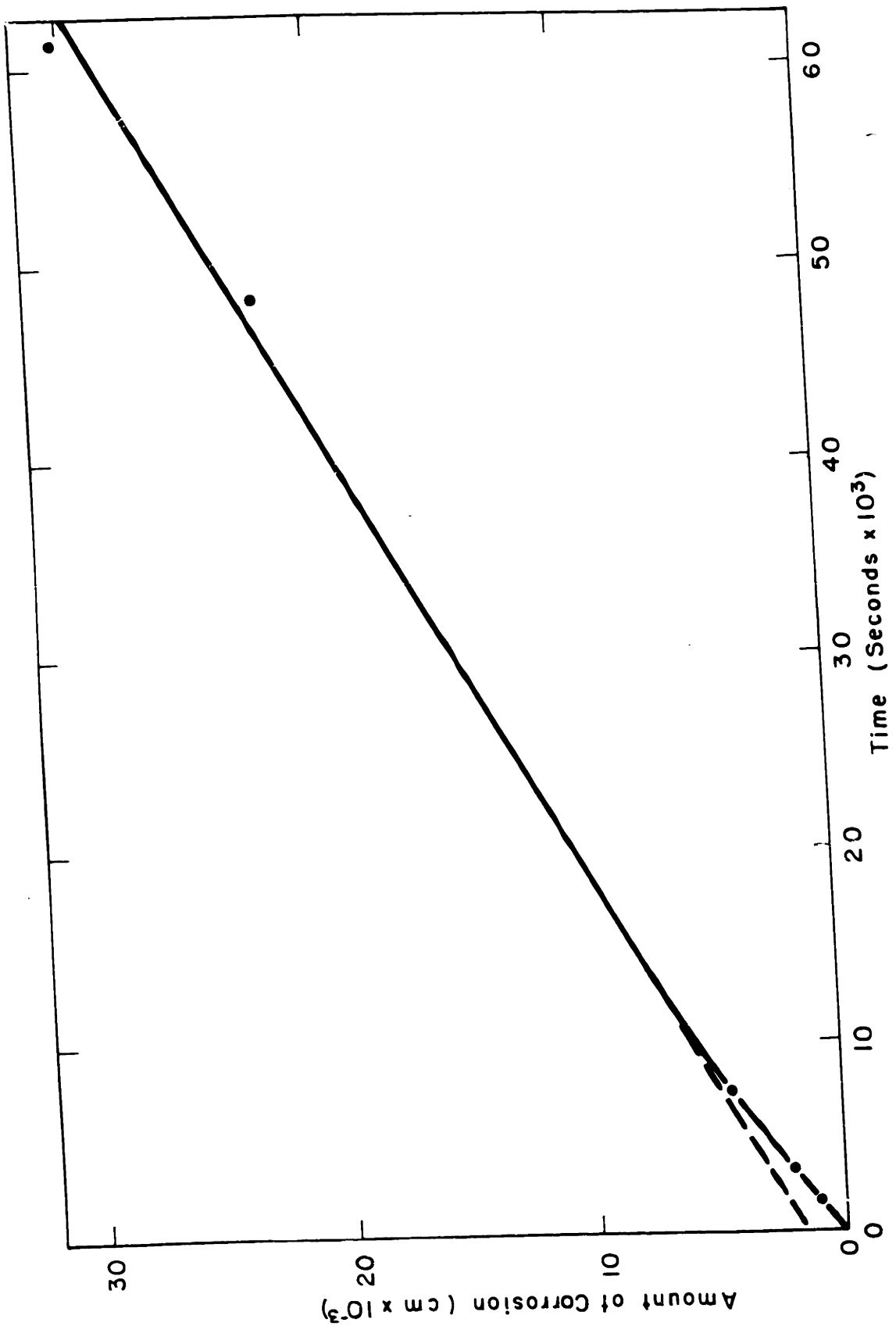

FIGURE 8.4 EFFECT OF TIME ON CORROSION OF A ROTATING (1200 RPM) DISC

Forced Convection

A concise quantitative method to show whether solution rates are determined by diffusion in the liquid without evaluating pertinent physical properties is to vary the angular velocity, ω, of a rotating disc. The results of such an experiment at 41° C are shown in Figure 8.5. It is clear from this plot that the dependence of sodium chloride solution rate is directly proportional to the square root of the angular velocity as required by equation 7.55.

A tracing of the contour of a highly corroded forced convection sample is reproduced ias Figure 8.6 with the broken lines indicating the original size. It is clear that corrosion is greatest at the leading edge and also that in a band near to the middle marked A A' on Figure 8.6, a region of abnormally low corrosion is present. It is believed that this is caused by the laminar intersection of the flow stream from the top and bottom disc faces creating a region of virtual stagnance.

The flow along the cylindrical surfaces of the sample resembles flow along a flat plate, that is the axial flow generated by the rotating disc faces continues along the sides of the cylindrical surface. In the same way that Ellenbaas obtained the free convection solution for a cylinder from that of a flat plate, it could be shown that axial forced convection flow along a cylinder should have the same form as flow along a flat plate and hence the corrosion rate should be proportional to the reciprocal square root of distance from the leading edge.

Figure 8.7 shows the dependence of corrosion on distance from the leading edge for an experiment conducted at 41° C. While the excellent agreement with the predicted square root relationship is partly fortuitous

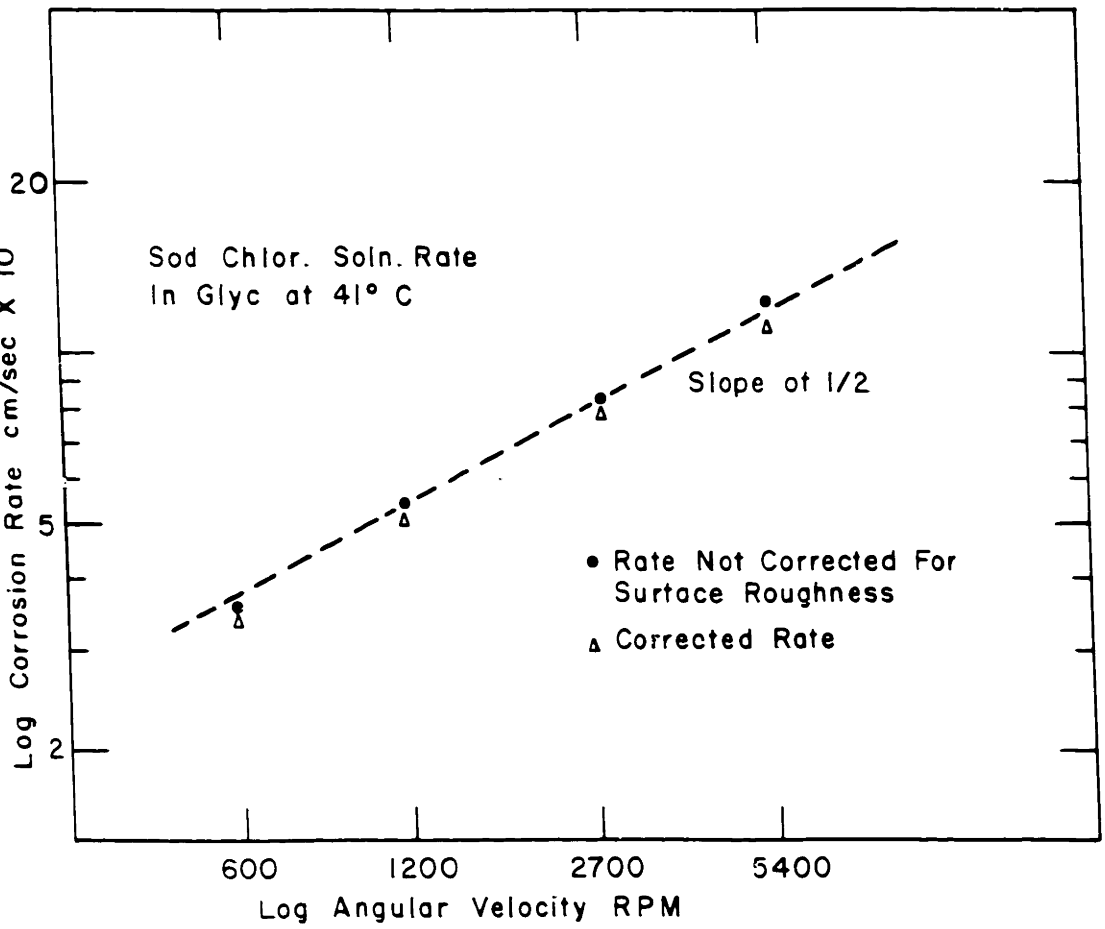

FIGURE 8.5 EFFECT OF ANGULAR VELOCITY ON CORROSION RATE FOR A ROTATING SODIUM CHLORIDE DISC

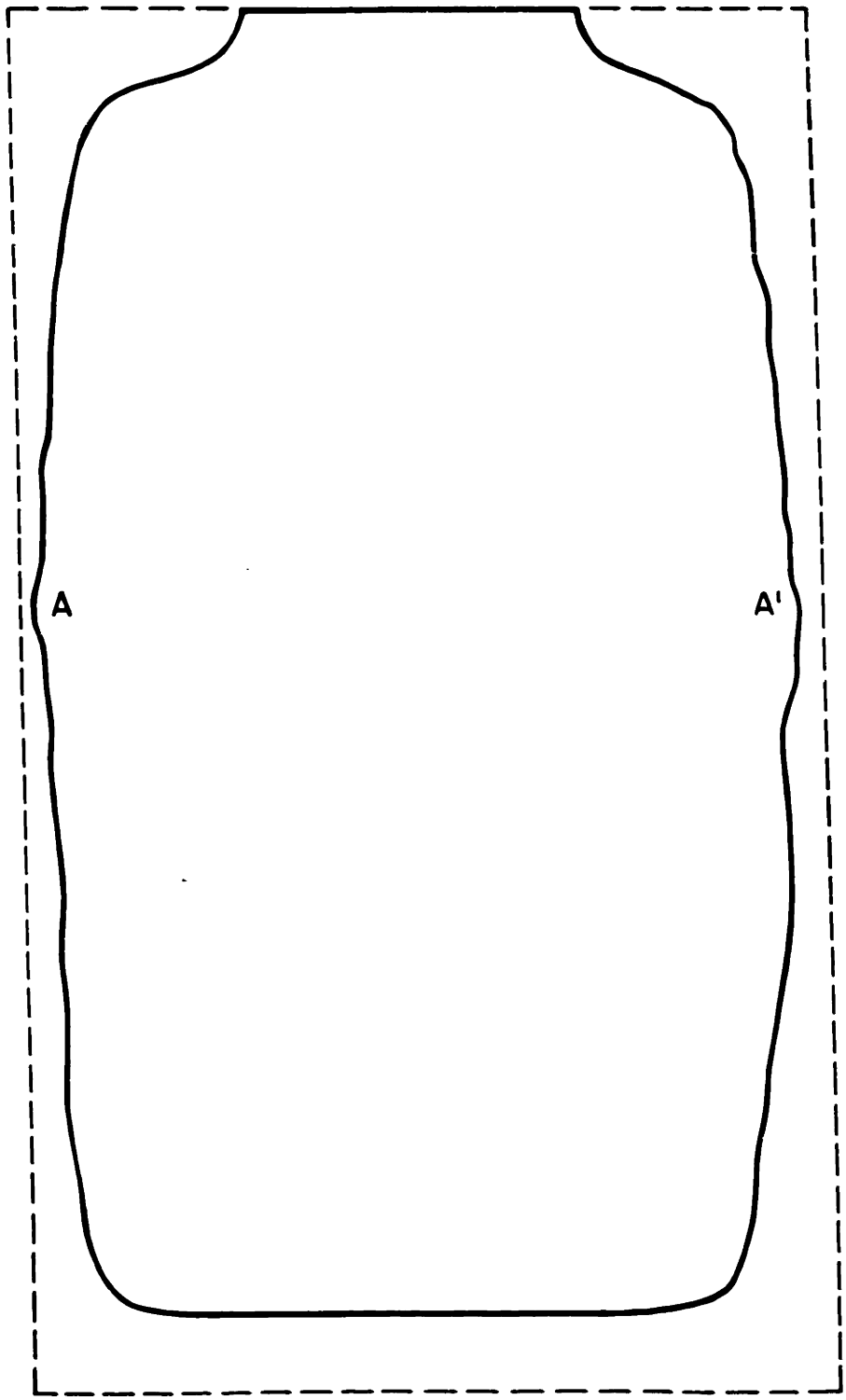

FIGURE 8.6 CONTOUR OF TOTALLY IMMERSED FORCED CONVECTION SODIUM CHLORIDE SAMPLE (BROKEN LINE REPRESENTS ORIGINAL SIZE)

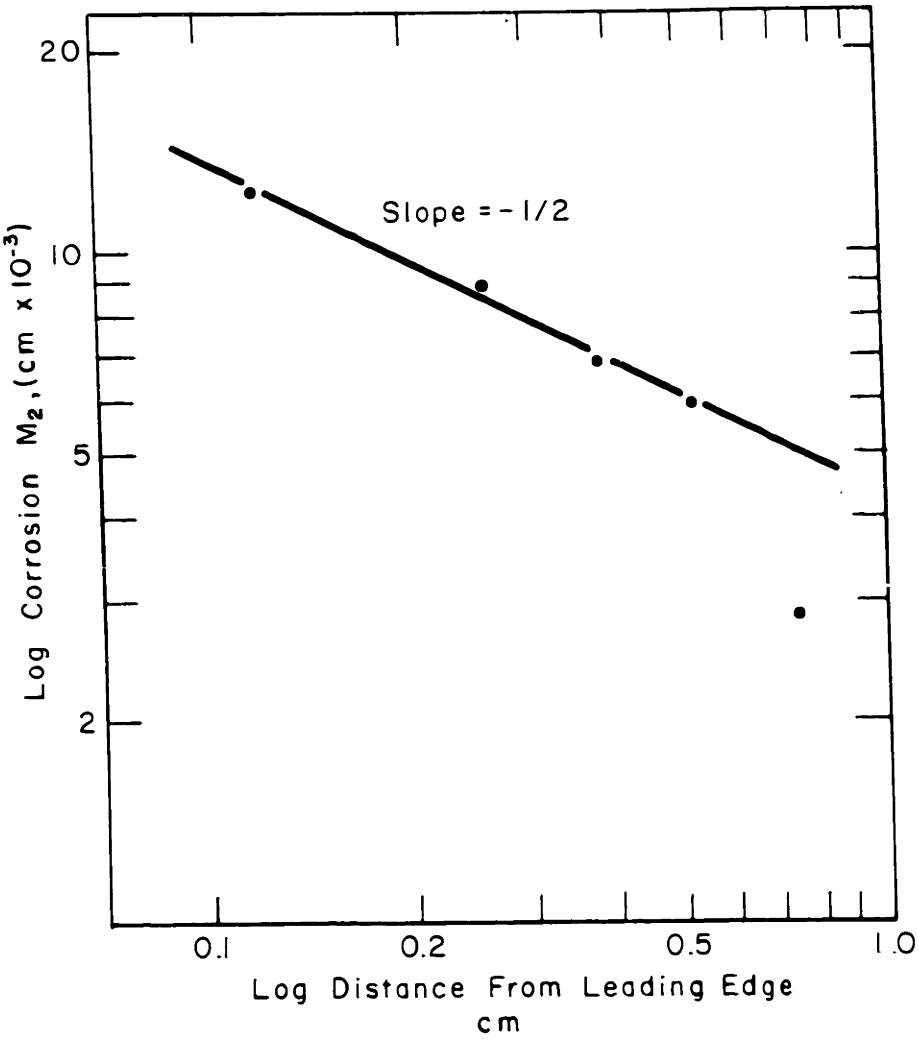

FIGURE 8.7 EFFECT OF DISTANCE FROM LEADING EDGE ON CORROSION OF SODIUM CHLORIDE BY FORCED CONVECTION

considering the irregular contour shown on Figure 8.6, all samples clearly revealed this general pattern including the unusually low corrosion near the intersection of flow streams (approximately 0.6 cm. from leading edge on Figure 8.7.)

A summary of the forced convection results from 10° C to 50° C are shown in Figure 8.8 where corrosion rate is plotted versus temperature. Also shown in the line calculated from equation 7.55 and the data from Figures 8.1 and 8.2:

$$\overset{*}{J} = 0.62\ D\ \left(\frac{\overset{*}{\nu}}{\overset{*}{D}}\right)^{1/3} \left(\frac{\nu}{\omega}\right)^{1/2}\ \Delta\overset{*}{C} \qquad 8.4$$

Because of the negligible effect of free diffusion, it is not necessary to use the more involved expression, equation 7.64.

The agreement between predicted experimental results is satisfying at temperatures of 30° C and higher. At 10° C the experimental results are about 70% of the calculated values.

In most forced convection experiments, the cylindrical surfaces persisted with circular perimeters even after corrosion. Although, the diameter changed markedly during corrosion, each radial section remained circular. Not so in the forced convection experiments conducted in the vicinity of 10° C. These developed eight facets along the originally cylindrical surface.

The circular cross section transformed to octagonal shape. This is illustrated in a photograph, Figure 8.9, looking at the disc face of a high temperature and low temperature forced convection sample. The octagonal outlines are visible on the low temperature sample.

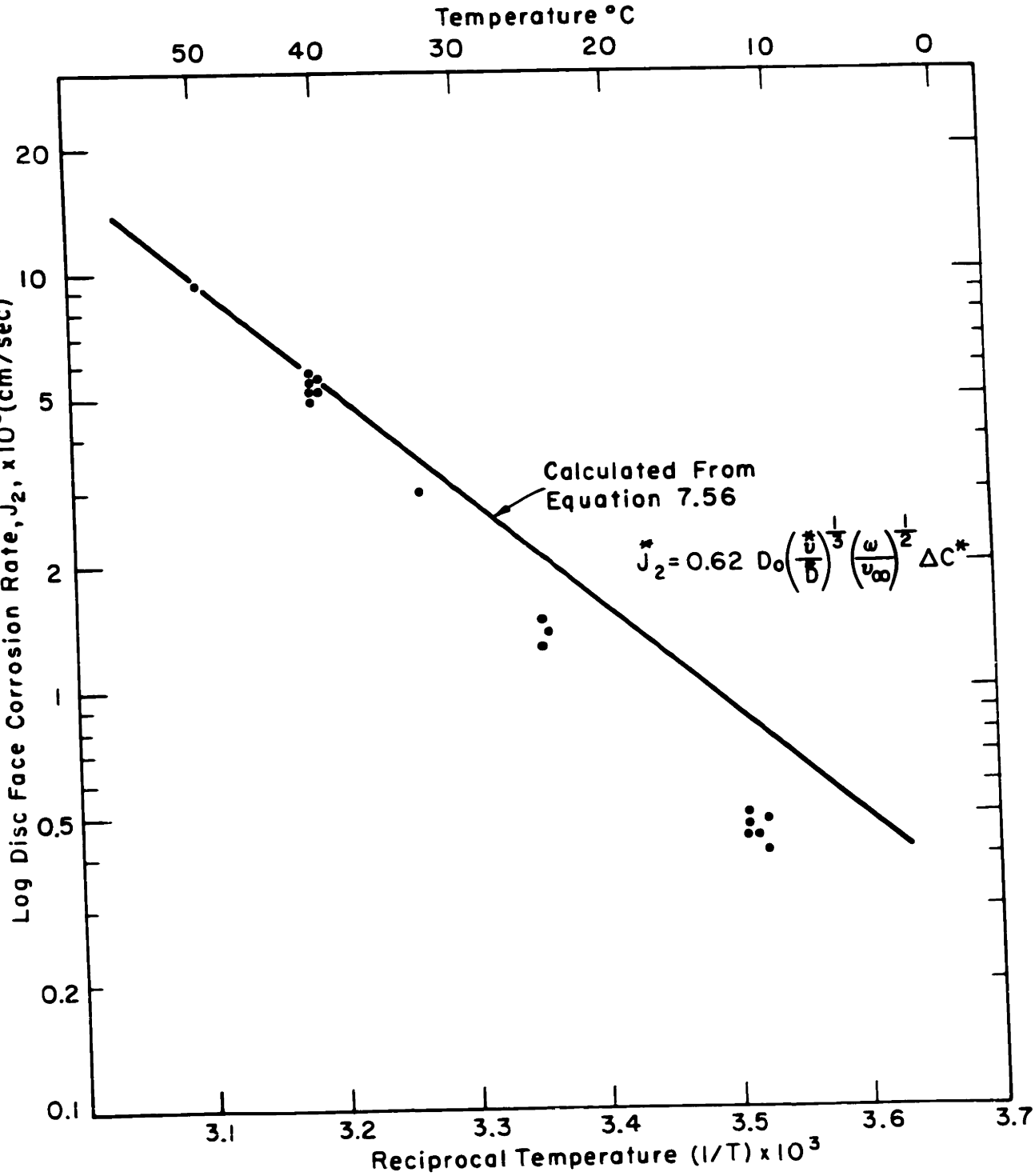

FIGURE 8.8 TEMPERATURE DEPENDENCE OF FORCED CONVECTION CORROSION RATE OF SODIUM CHLORIDE

FIGURE 8.9 VIEW OF DISC FACE OF SODIUM CHLORIDE FORCED CONVECTION SAMPLES (LEFT 10°C - RIGHT 40°C)

The regularity of the facets suggested that their origin is related to crystal symmetry. The sodium chloride cylinders have one cubic axis as the cylinder axis. Accidental cleavage cracks in the crystals are always parallel to a pair of facets.

An additional second order effect is the appearance of screw markings on the cylindrical surfaces. A slight additional amount of corrosion occurred along a helix. This is the reason for the irregularities of profile on Figure 8.6. The pitch of the helix depended upon the speed of rotation and the viscosity. It apparently is caused by there being a certain spot on the perimeter of the disc face where the convection first starts up the cylindrical surface.

Free Convection

Totally immersed samples and those with the liquid surface intersecting the sample had a negligible difference in corrosion rate. This is illustrated by Figure 8.10 which shows a magnified tracing of two samples corroded at 41° C for 12 hours. Except for the edge effect causing a rounding of the corner in the totally immersed sample, the contours and corrosion rates are nearly identical.

It is clear from Figure 8.10 that the corrosion decreases with distance from the leading edge. Measurements for a typical sample are shown in Figure 8.11. According to equation 7.60, the corrosion should be proportional to $x^{-1/4}$. A reasonable agreement with this premise is found in Figure 8.11.

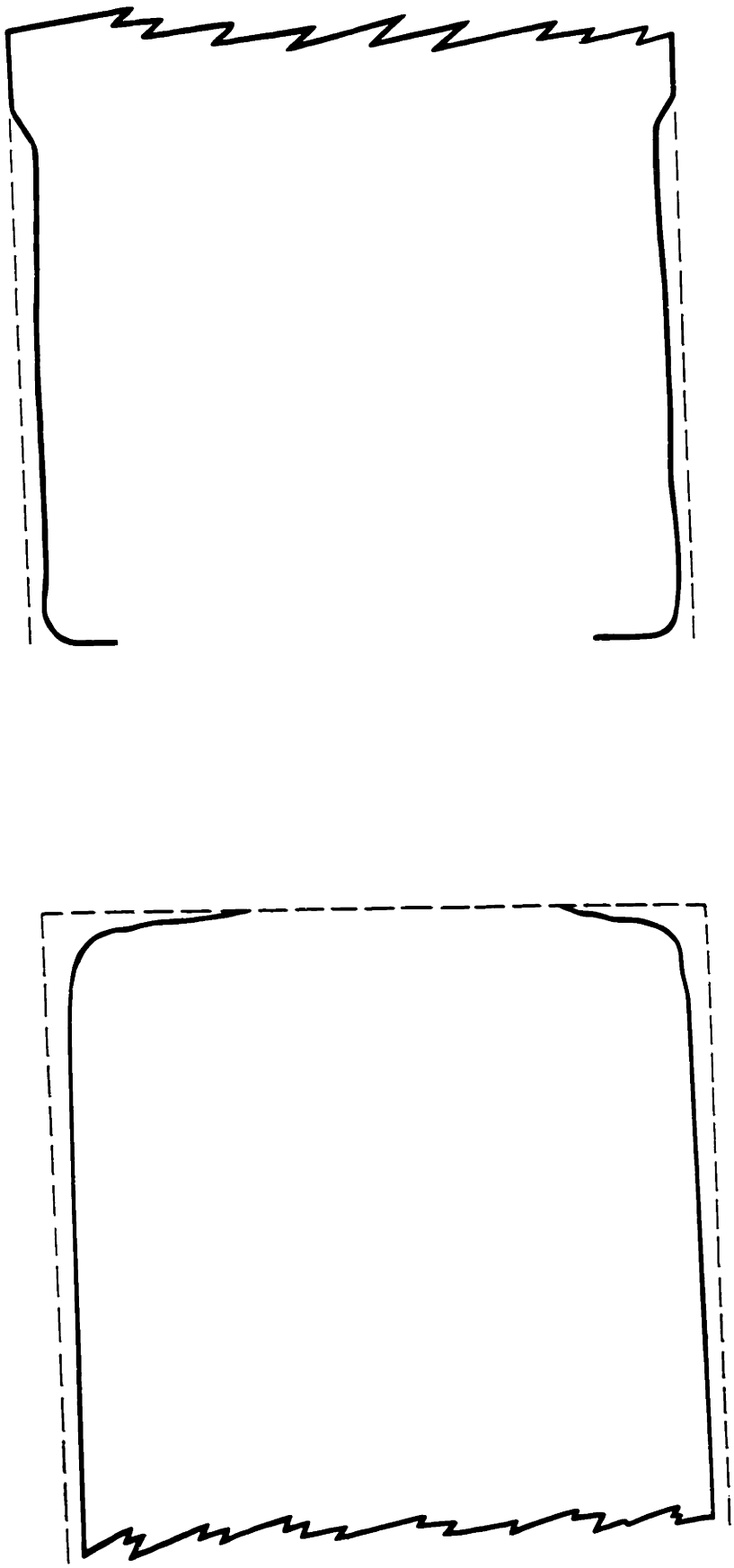

FIGURE 8.10 CONTOUR OF SODIUM CHLORIDE FREE CONVECTION SAMPLES, UPPER PARTIALLY IMMERSED, LOWER TOTALLY IMMERSED (BROKEN LINE REPRESENTS ORIGINAL SIZE)

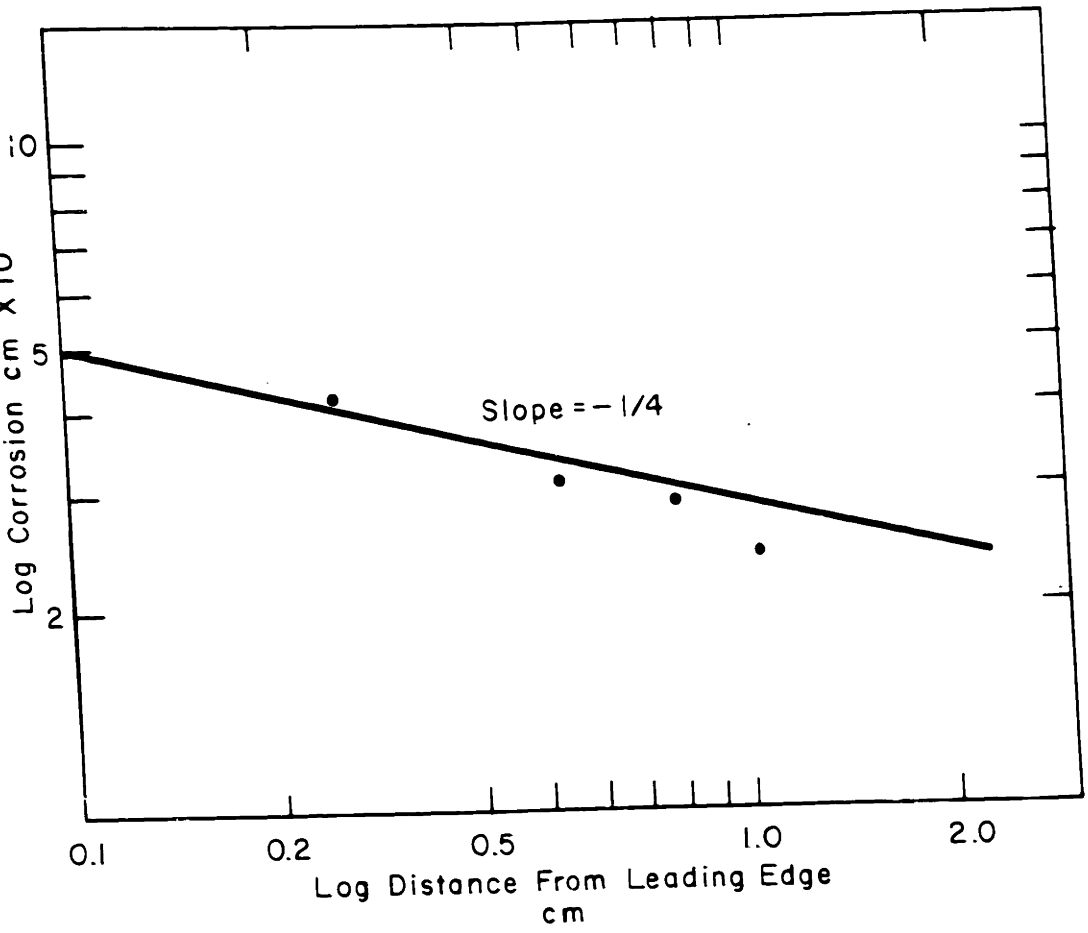

FIGURE 8.11 EFFECT OF DISTANCE FROM LEADING EDGE ON FREE CONVECTION CORROSION OF SODIUM CHLORIDE CYLINDERS

Transient or free diffusion plays a more important part in free convection than in forced convection. Enumeration of equation 7.65 predicts the time, t'_3 during which transient diffusion dominates. It varies from 4400 sec. at 10° C to 310 sec. at 40° C. However, the amount of corrosion from transient diffusion predicted by equation 7.66 is virtually constant at 2.3×10^{-4} cm. About one half of this or 1.2×10^{-4} cm is in excess over that which would occur in the same time from free convection. This difference is barely perceptible by micrometer measurements and hence will be ignored.

Surface roughness, on the other hand, would be expected to give erroneous high readings of corrosion. Based on the forced convection results, a correction of 0.001 cm was subtracted from the diameter differential to counteract the surface roughness.

The data for solution rate 0.1 inches beneath the leading edge in free convection over temperatures ranges 0° C to 50° C, is summarized in Figure 8.12. The results predicted by Ellenbaas' expression for free convection, equation 7.60, are also shown:

$$\overset{*}{J}_3 = .510\, \lambda^{-1}\, D_o^{3/4} \left(\frac{g\Delta}{\nu_o X}\right)^{1/4} \Delta \overset{*}{C} \qquad 8.5$$

In general the experimental results are higher than predicted, but hardly by more than the spread of the data itself.

Compared with forced convection to a rotating disc at 1200 RPM, the free convection corrosion rates are an order of magnitude lower throughout the range of measurements.

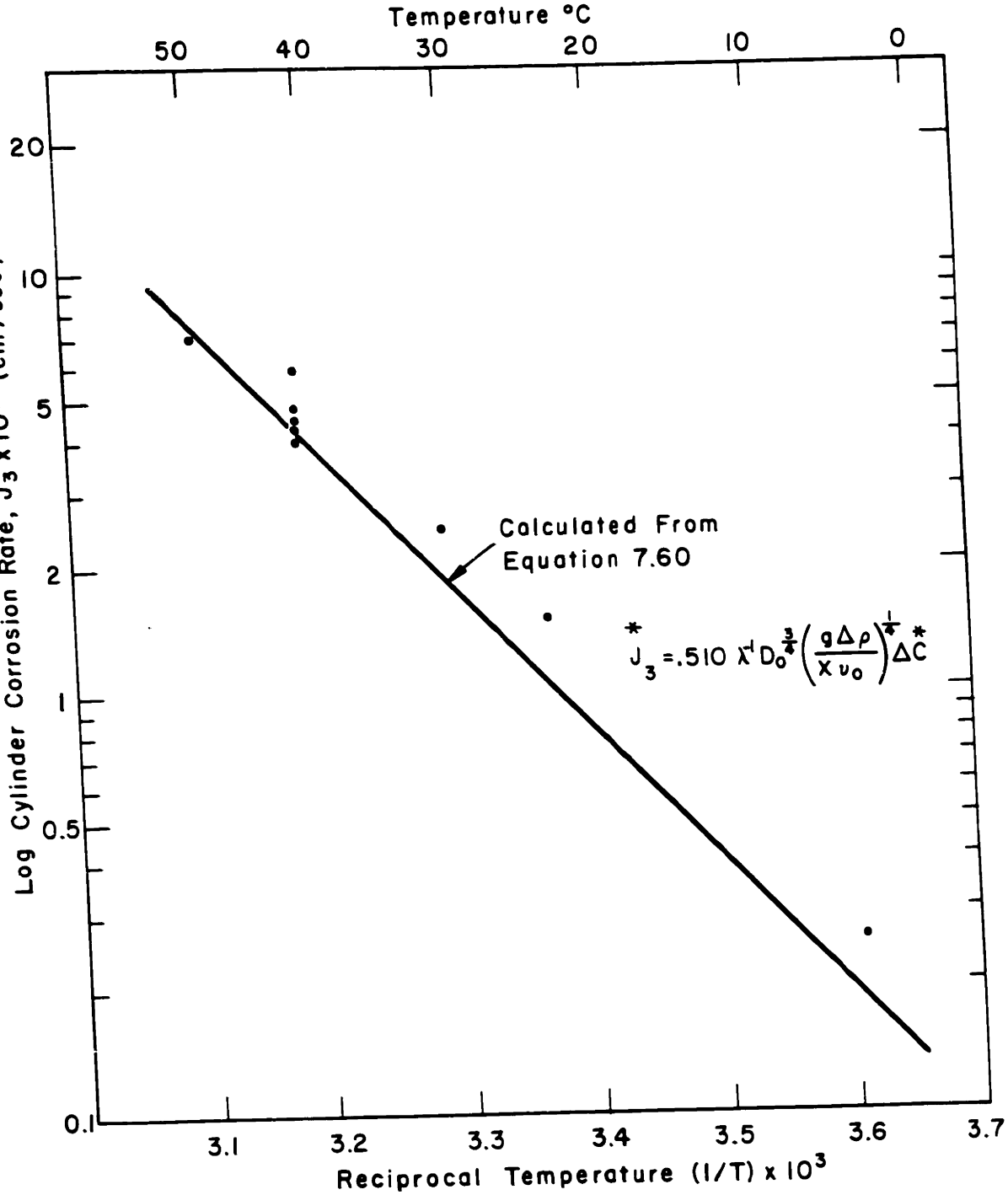

FIGURE 8.12 TEMPERATURE DEPENDENCE OF FREE CONVECTION CORROSION RATE OF SODIUM CHLORIDE CYLINDER

Discussion

There can be no doubt that solution kinetics of sodium chloride dissolving in glycerine are controlled by diffusion in the liquid. Nor is there any doubt that the quantitative relations for free and forced convection adequately describe results in most cases although minor discrepancies are noted.

The faceting of cylindrical surfaces at low temperatures is evidence that an interface reaction is beginning to play a role. In this case, equation 3.3 describes the kinetics. Both an interface reaction and a diffusion process would govern the process until one became markedly slower. If two processes have different activation energies, the dominant process can change with temperature as shown schematically in Figure 8.13.

Such a reason can explain the lower than predicted results at low temperatures for forced convection. It is clear that the diffusion process still plays the major role at 10° C because forced convection samples still corrode much more rapidly than free convection samples. It is also clear that the reason for noticing the effects of interface reaction only in the forced convection experiments relates to the fact that forced convection enhances diffusion in the liquid and thus makes interface control more probable.

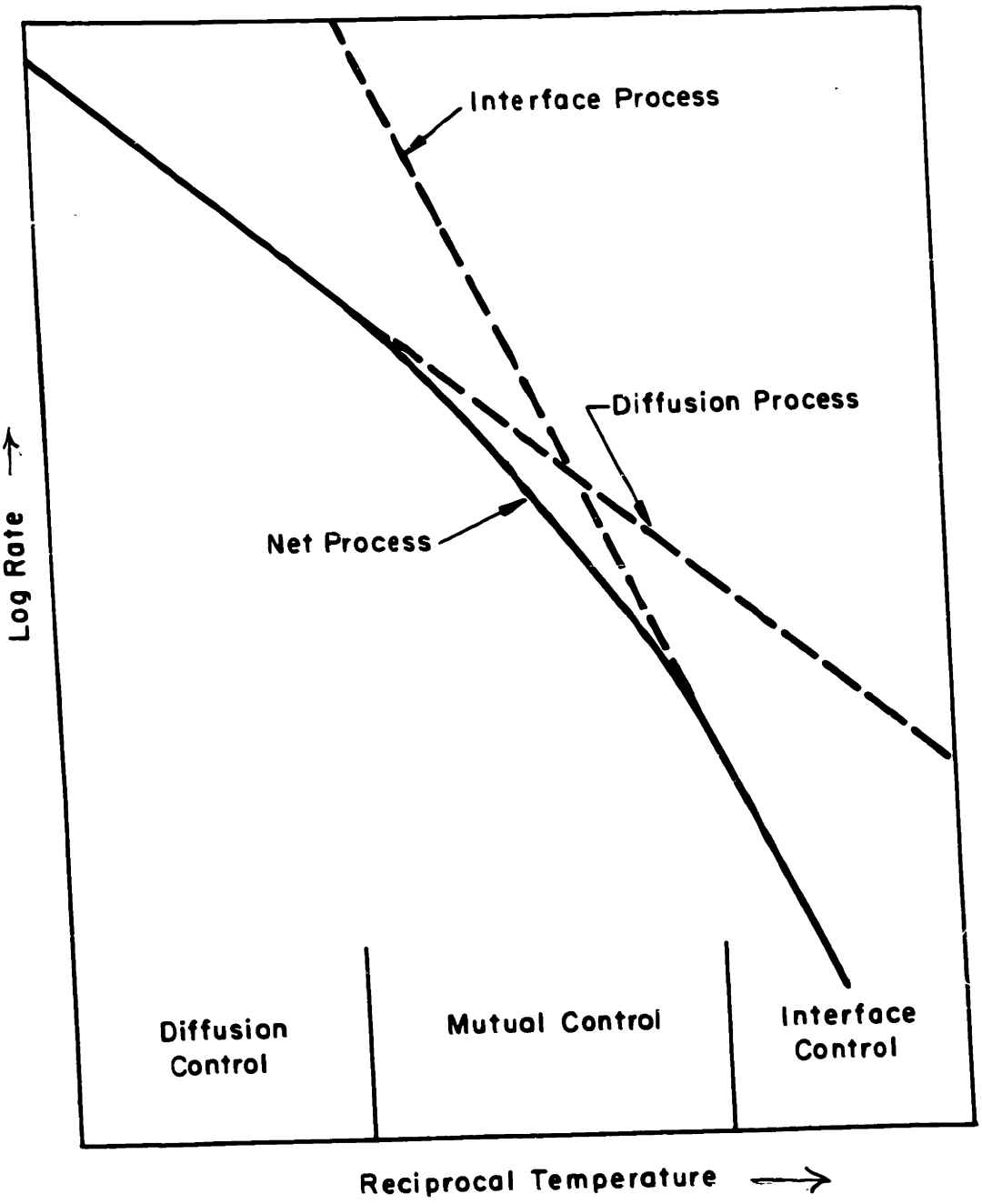

FIGURE 8.13 SCHEMATIC DIAGRAM OF CHANGE WITH TEMPERATURE FROM INTERFACE CONTROL TO BOUNDARY LAYER CONTROL

IX. RESULTS AND DISCUSSION OF SAPPHIRE-SLAG EXPERIMENTS

Comparison with Sodium Chloride Glycerine

The pattern of the high temperature corrosion experiments followed that of the glycerine-sodium chloride model system. This is illustrated by Figure 9.1 showing the similarity of the corrosion profiles for the slag-sapphire and glycerine-sodium chloride results. In addition, time scales covered the same range in both series of experiments. A major difference between the systems was the lower density differential, $\Delta \rho = (\rho_o - \rho_{oo})$, in the high temperature system. This permits transient diffusion control of solution to be examined for the sapphire-slag system.

Precision

Determinations of changes in length or diameter require two measurements of which the change is a relatively small portion of the total, and in the early technique (using totally immersed forced convection samples) the contours of the surfaces made for poor reproducibility of measurements. It is estimated that a possible error of $\pm$ 15% exists in these early determinations of change of linear dimensions. Improved techniques mentioned in the discussion of experimental methods reduced the variation of the absolute error considerably, but a major share of this improvement was utilized to extend experiments into regions of less total corrosion.

FIGURE 9.1 PHOTOGRAPH COMPARING THE CORROSION PROFILES OF (CLOCKWISE FROM UPPER LEFT: POLYCRYSTALLINE ALUMINA, SODIUM CHLORIDE TOTALLY IMMERSED, SODIUM CHLORIDE PARTIALLY IMMERSED, AND SAPPHIRE)

Temperatures have shown variations of up to $\pm$ 5° C during an experiment and comparison of the control couple with a standard couple reveal similar deviations.

Composition has varied during experimental series from two causes. There have been occasions when samples, pieces of muffle tube, or piece of the thermocouple protection tube have fallen into the melt. Periodic analyses have been made to keep track of such variations. Results are reported without correction from compositions showing no more than $\pm$ 1% variation from the nominal alumina content. Results are corrected to take into account changes in solubility resulting from variations of $\pm$ (1% - 3%) in Al_2O_3 content; no larger deviations were observed. Also, analyses have indicated a selective volatilization of calcium from the melts causing a progressive change from 1.0 to 0.8 of (Ca/Si) during a series of experiments. There is no obvious basis for correction for this change, and therefore it represents a source of loss of precision.

Transient Diffusion Studies

It became evident in free convection experiments that at early stages, the corrosion was not a linear function of time. Investigation of this initial transient stage of the solution process revealed the results summarized in Figures 9.2, 9.3 and 9.4 for the corrosion of a 0.5 cm. diameter sapphire cylinder in slag, containing 7, 15 and 21 weight percent Al_2O_3. The corrosion, M_1, was obtained directly from the change in radius, ΔR. (see page 37)

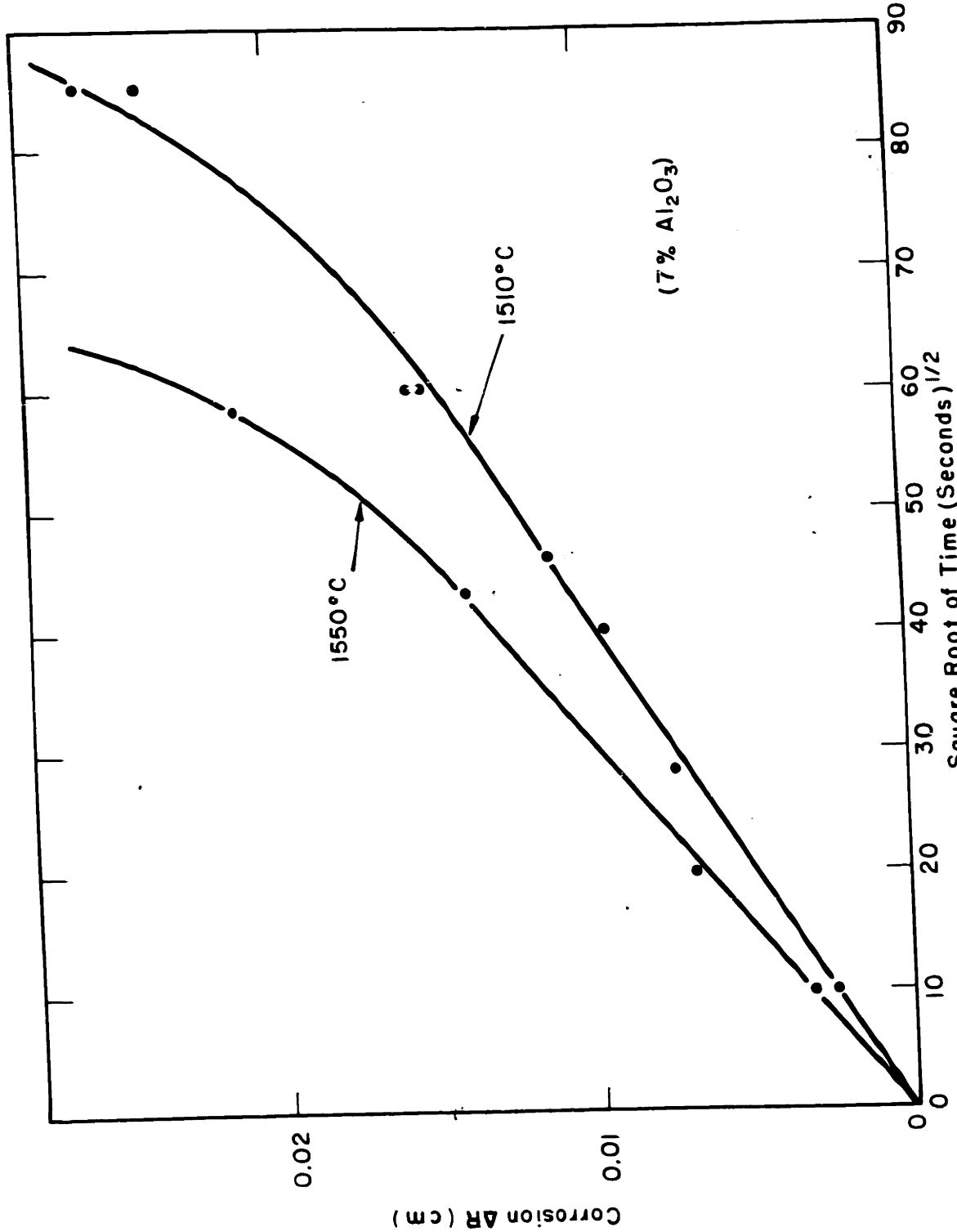

FIGURE 9.2 TRANSIENT CORROSION OF SAPPHIRE CYLINDER IN $CaO-SiO_2-Al_2O_3$ WITH 7 WT% Al_2O_3

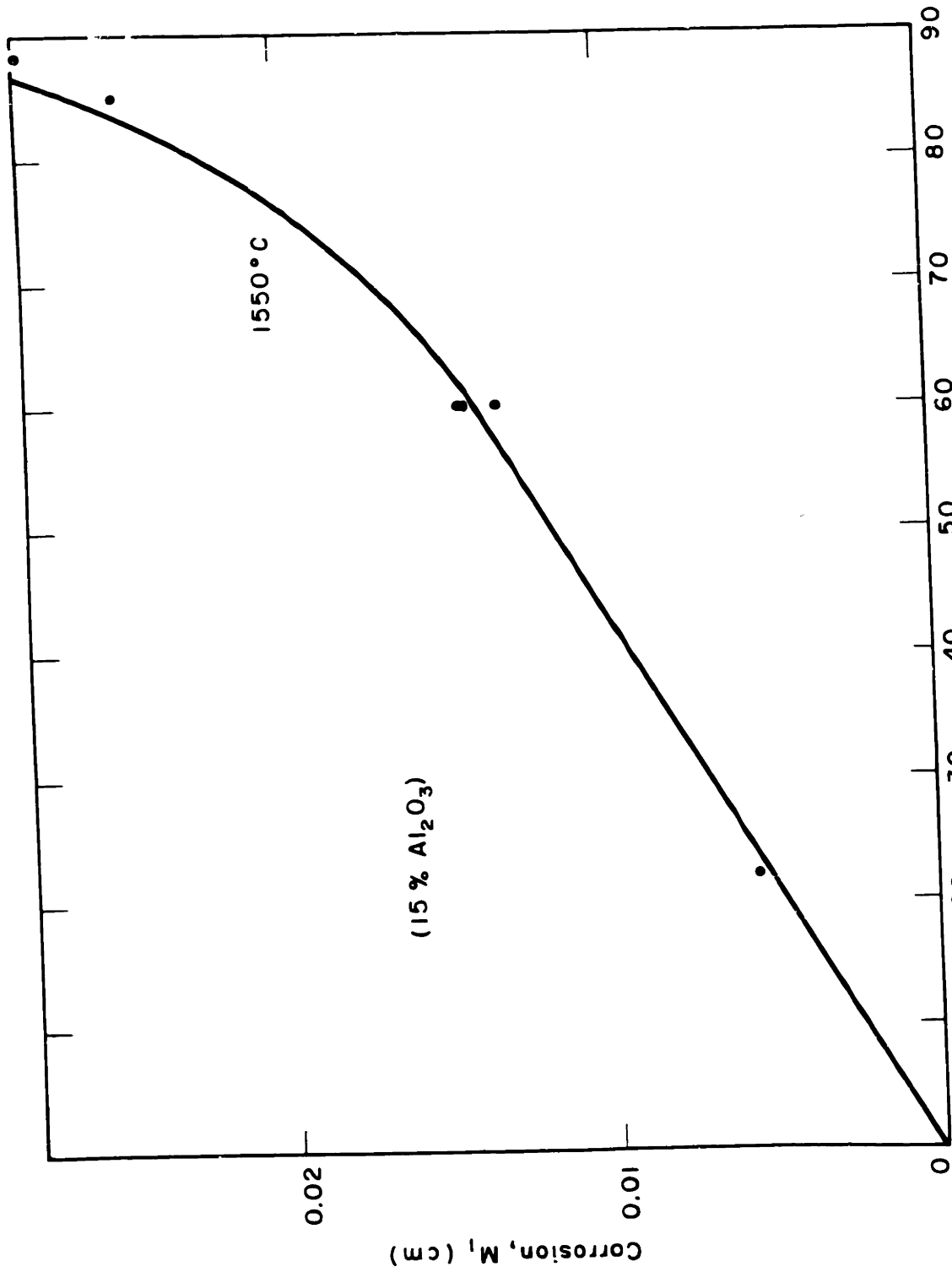

FIGURE 9.3 TRANSIENT CORROSION OF SAPPHIRE CYLINDER IN $CaO-SiO_2-Al_2O_3$ WITH 15 WT% Al_2O_3

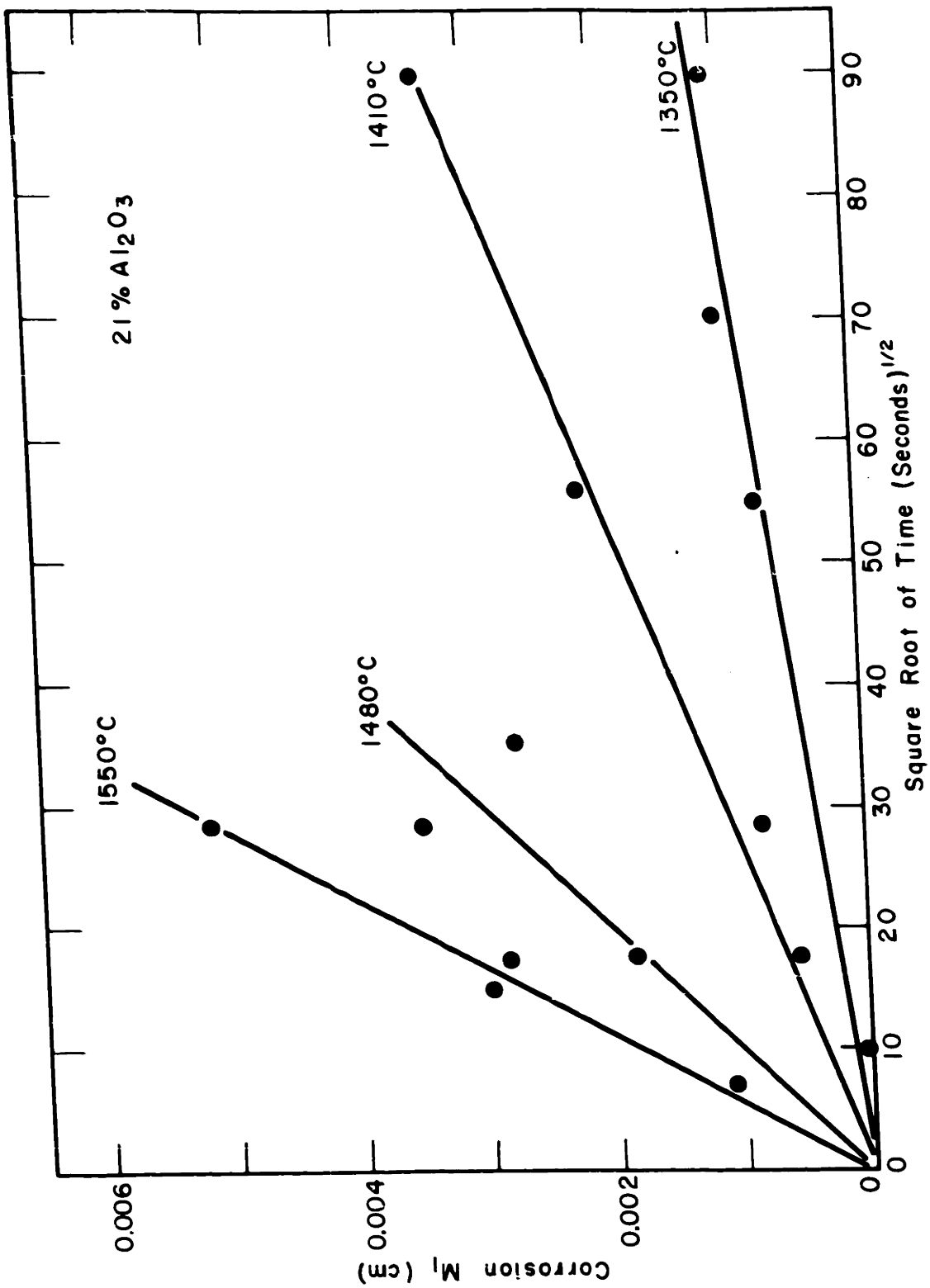

FIGURE 9.4 TRANSIENT CORROSION OF SAPPHIRE CYLINDER IN $CaO-SiO_2-Al_2O_3$ WITH 21 WT% Al_2O_3

The corrosion, directly proportional to the square root of time at corrosion values less than 0.01 cm., as predicted by equation 7.13, is:

$$M_1 = 1.13 \beta_t D_o \left(\frac{t}{\overset{*}{D}}\right)^{1/2} \Delta \overset{*}{C} \qquad 9.1$$

On further corrosion, the square root relationship breaks down for two reasons. First, the value of the correction factor, β_t, increases as the cylindrical surface cannot be approximated by a plane one when the boundary layer becomes thick and secondly, and generally, more important, the steady state free convection process begins to dominate. Both of these increase the value of $\frac{dM_1}{d(t)^{1/2}}$.

In addition to the proportionality of corrosion with the square root of time, examination of Figures 9.2 to 9.4 reveals the effect of solubility $\Delta \overset{*}{C}$ and temperature, T, on corrosion rate.

Provided a value can be selected for the ratio of interface diffusion coefficient and effective diffusion coefficient, $\frac{D_o}{\overset{*}{D}}$, the results summarized in Figures 9.2 to 9.4 along with the solubility $\Delta \overset{*}{C}$ from Figure 5.2 can be utilized in the evaluation of equation 7.13 to yield a value for the interface diffusion coefficient, D_o. The discussion on diffusion coefficient in the material properties section revealed that with the present limited data in the $CaO-Al_2O_3-SiO_2$ system, it is impossible to take account of anything other than viscosity variation in extrapolating diffusion data. Equation 17 in the Appendix leads directly to the following proportionality

$$\frac{D_o}{\overset{*}{D}} = \frac{\overset{*}{\nu}}{\nu_o} \equiv \frac{1}{\alpha} \qquad 9.2$$

where α is a dimensionless number defined by equation 9.2. The value of $\nu^* N_o$ is obtained from equation 7.43 and Figure 5.7, from which one obtains the values of α shown in Table IX-1.

TABLE IX-1

Ratio (α) of Effective Diffusion Coefficient to Interface Diffusion Coefficient Along Al_2O_3-$CaSiO_3$ Binary

Temp.	Wt. % Al_2O_3 7	15	21
1350			1.07
1400	1.08	1.07	1.07
1450	1.12	1.10	1.08
1500	1.11	1.11	1.07
1550	1.11	1.09	1.05

From the definition of α, equation 7.13 is simplified to

$$M_1 = 1.13 \beta \left(\frac{D_o}{\alpha}\right)^{1/2} t^{1/2} \Delta C^* \qquad 9.3$$

As shown by Figure 7.1 provided $\hat{t} = \left(\frac{t D_o}{R^2}\right) < 10^{-2}$, the correction coefficient is near enough to unity to be ignored. Then

$$D_o = .8 \frac{\alpha M_1^2}{t \Delta C^{*2}} \qquad 9.4$$

so that the interface diffusion coefficient can be calculated from information available from Figures 9.2 to 9.4, Table IX-1 and Figure 5.2.

The results of such calculations have been plotted on Figure 9.5 by showing the relation between log interface diffusion coefficient and reciprocal temperature. If the assumption of proportionality between

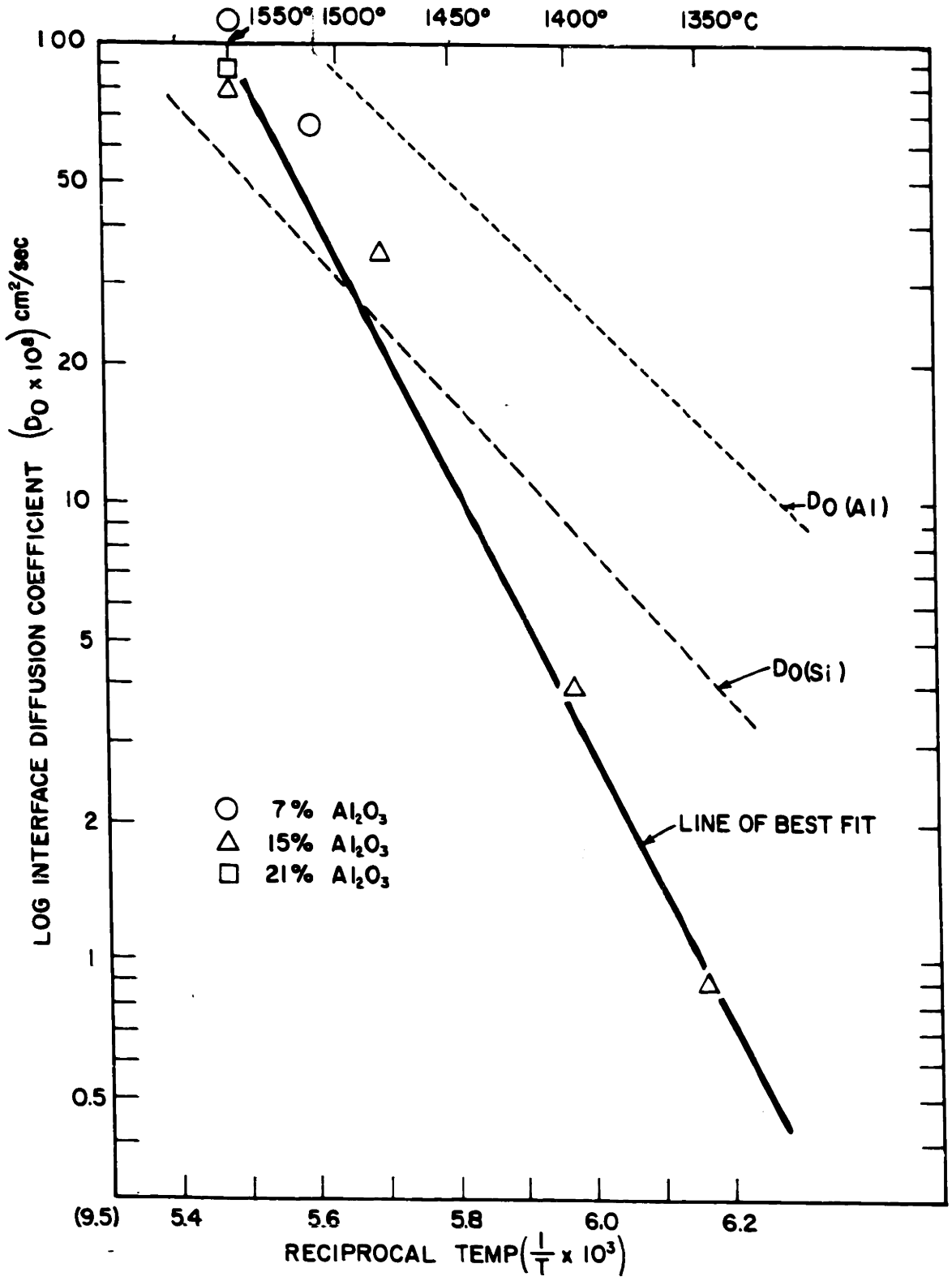

FIGURE 9.5 VALUES OF THE LOG INTERFACE DIFFUSION COEFFICIENT, CALCULATED FROM TRANSIENT CORROSION DATA, VERSUS RECIPROCAL TEMPERATURE

fluidity ($\frac{1}{\nu}$) and diffusivity is correct, the calculated values for interface diffusion coefficient should be independent of the composition used to conduct the experiments. While the results obtained do not show unqualified support of this premise, the discrepancy is small enough to suggest that it could be eliminated by a minor correction.

Also shown on Figure 9.5 are the diffusion coefficients at the interface composition for silicon and aluminum. These values were taken from Table V.-1 . They result from the extrapolation both in composition and temperature of tracer diffusion results corrected for tracer correlation (equation 5.8).

It is seen that a large share of the values of the interface diffusion coefficient calculated from transient diffusion studies fall within the extrapolated values for D_{Al} and D_{Si}. At the lower temperatures, however, the diffusion coefficient appropriate to describe experimental results is significantly lower than D_{Si} or D_{Al}. For this reason the line of best fit, determined visually, has a much steeper slope than the activation energy for D_{Si} or D_{Al} would predict.

Figure 9.5 along with the ratios of Table IX-1 and equation 9.4 provide a compact means of summarizing all the results of the transient diffusion experiments.

Forced Convection

Figure 9.6 shows the dependence of the measured rate of corrosion of a sapphire rotating disc face on angular velocity. The corrosion rate is proportional to the square root of angular velocity as predicted by equation 7.55. Bulk composition for this set of results was CaO - 32.5 %, Al_2O_3 - 25 %, SiO_2 - 42.5 % and the temperature was 1440° C.

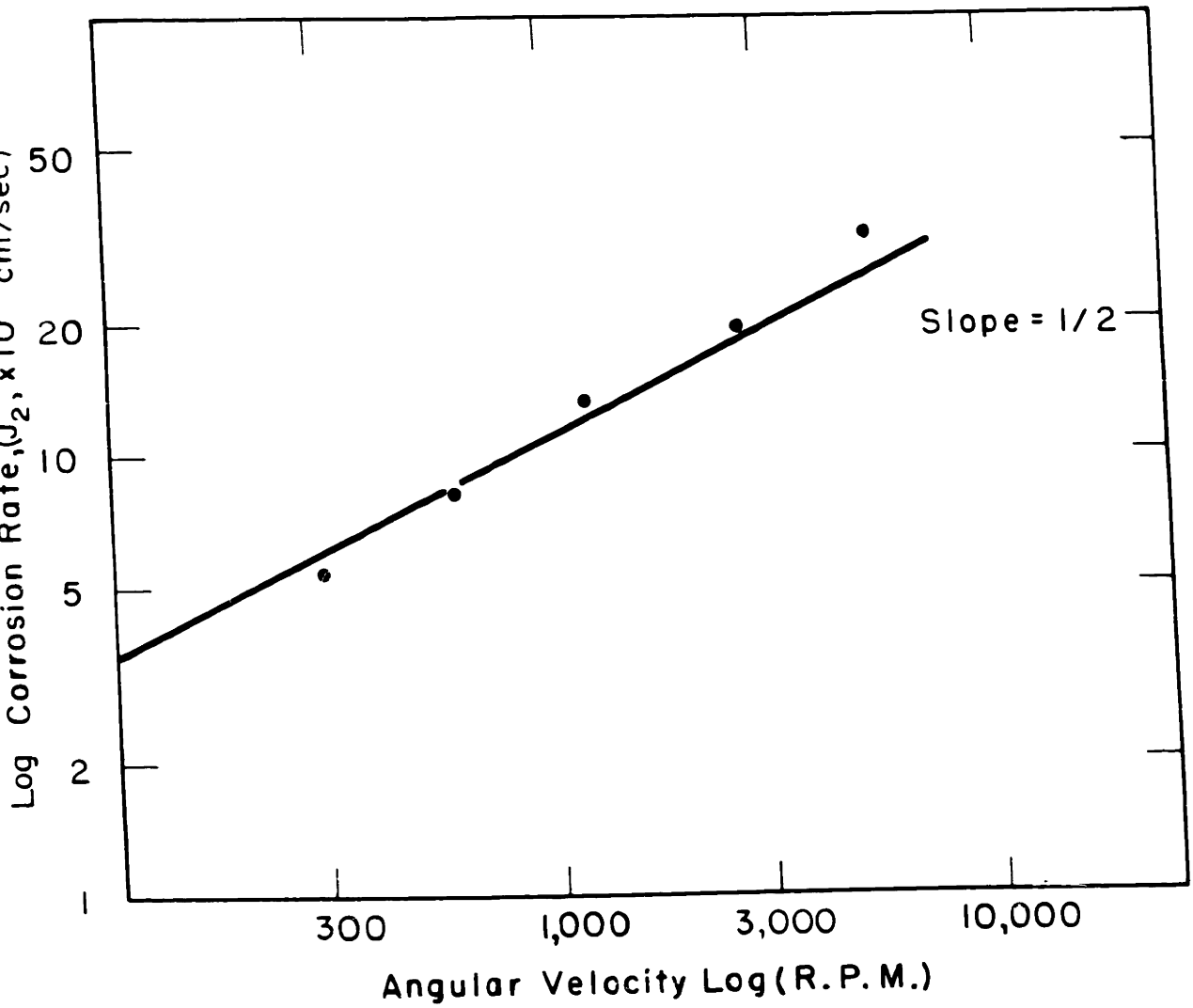

FIGURE 9.6 DEPENDENCE OF CORROSION RATE OF SAPPHIRE ROTATING DISC ON ANGULAR VELOCITY

A further manifestation of diffusion control is seen in Figure 9.7, where the corrosion profiles at 2700 RPM and 5400 RPM are compared. The 2700 RPM sample shows the center region of abnormally low corrosion previously noted on Figure 8.9 and explained by the laminar intersection of the streams from the upper and lower disc faces causing a region of near stagnation. When the streams intersect at sufficient velocity, rather than stagnation, a turbulent effect is obtained. Turbulence causes an enhancement of the rate of solution which explains the considerably more rapid corrosion noted in the 5400 RPM sample. A schematic diagram illustrating these effects is shown in Figure 9.8.

Results from the forced convection experiments (rotating disc 1200 RPM) are given in Figures 9.9, 9.10 and 9.11 representing sapphire solution in slags containing nominally 7, 15 and 21 weight percent Al_2O_3. The general pattern of the effect of temperature and solubility on solution rates is apparent from these plots.

For careful analysis of forced convection rates, it is necessary to examine the influence of the initial transient diffusion on corrosion of a rotating disc face. This is achieved by determining from equation 7.63, the period $t_{\frac{1}{2}}'$ when transient diffusion dominates. This time proves to be negligibly small varying from less than 0.1 sec. at high temperatures 1550° C to about 0.2 sec. at 1350° C.

The line of best fit for the interface diffusion coefficients of Figure 9.5, the kinematic viscosity from Figure 5.7 and the solubility inferred by Figure 5.2 can be utilized to predict the temperature dependence of the corrosion rate for forced convection according to equation 7.55.

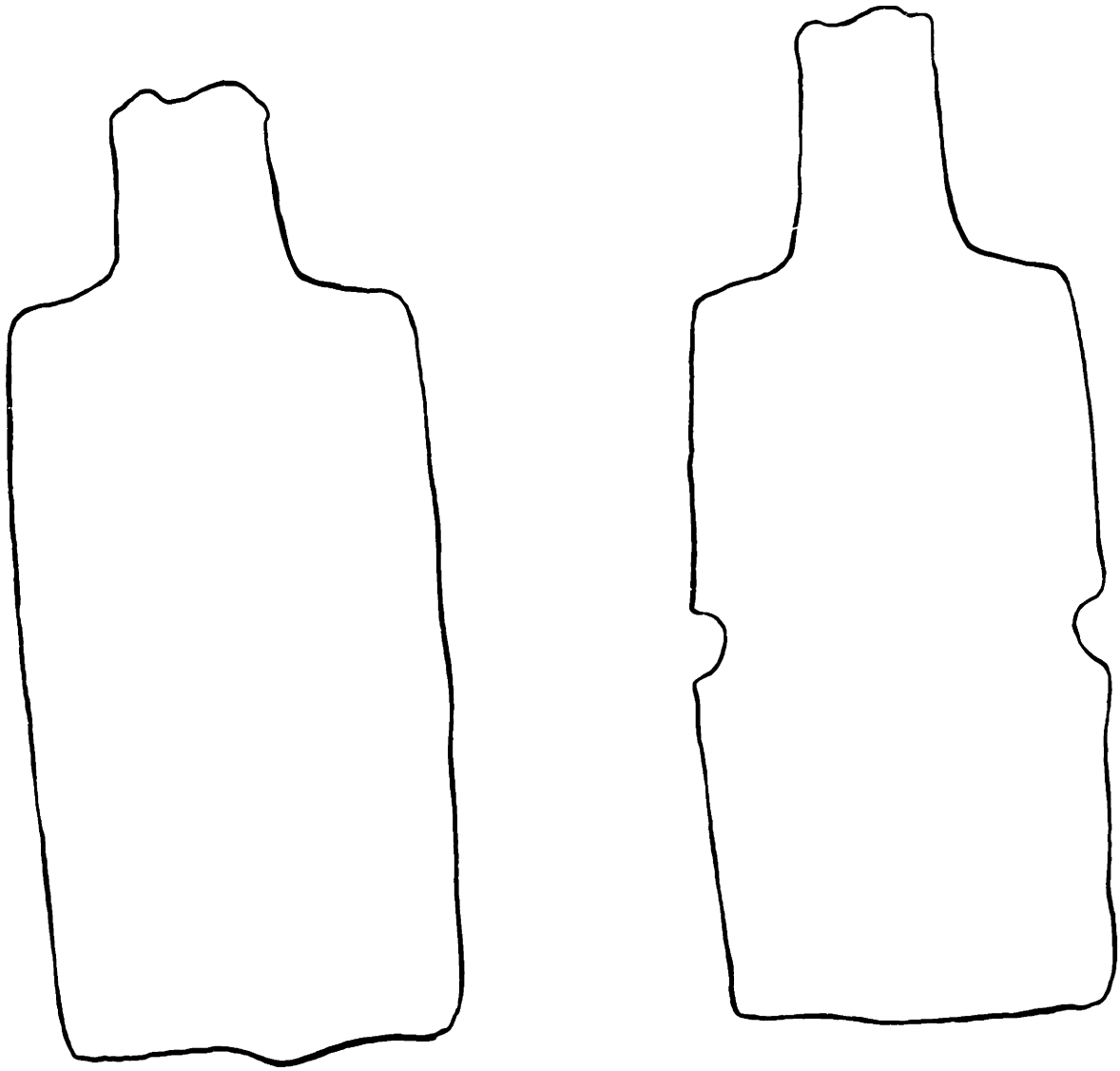

FIGURE 9.7 COMPARISON OF CORROSION PROFILES OF SAPPHIRE SAMPLES AT 2700 AND 5400 RPM

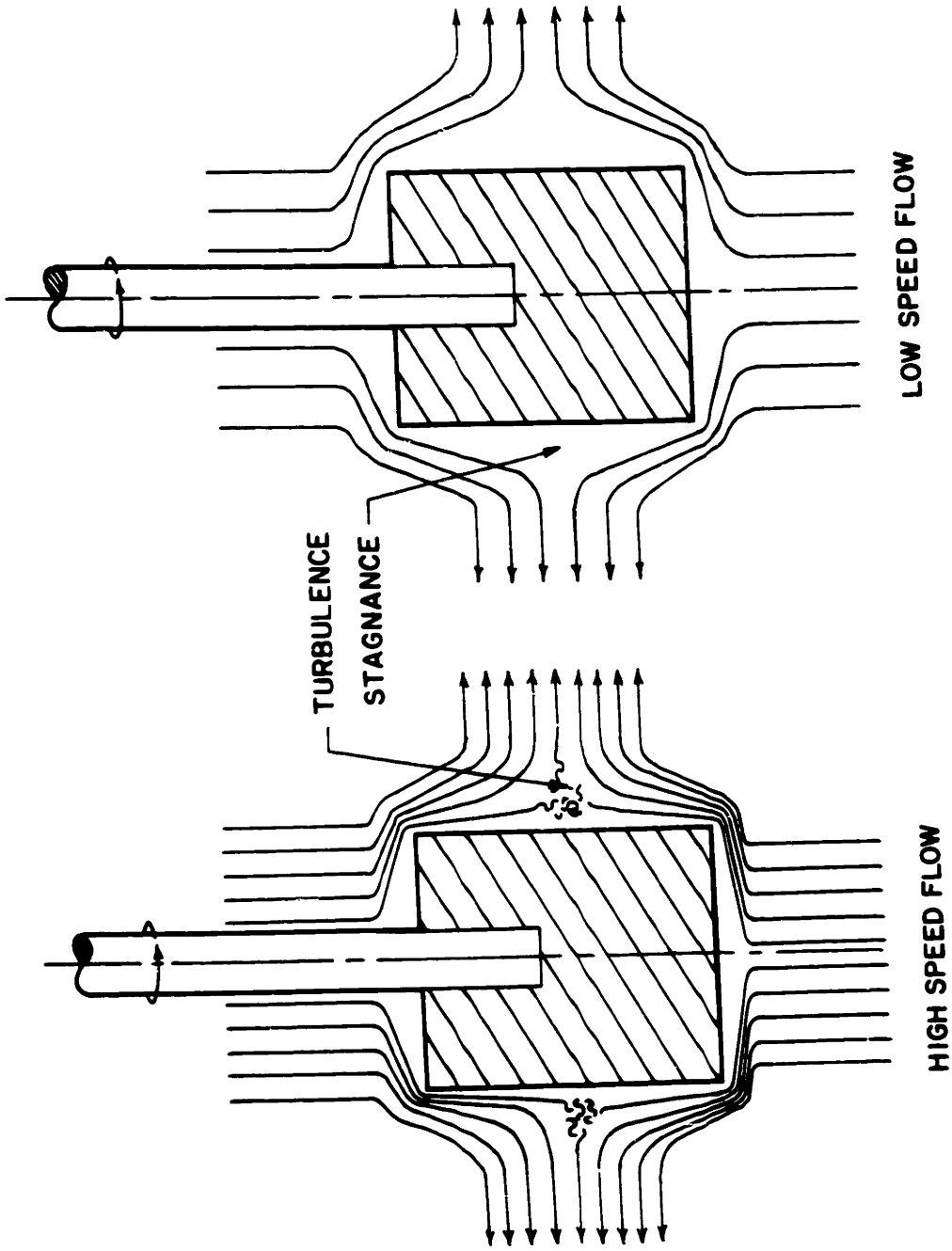

FIGURE 9.8 SCHEMATIC COMPARISON OF DIFFERENT FLOW BEHAVIOR AT LOW SPEED AND HIGH SPEED ROTATION

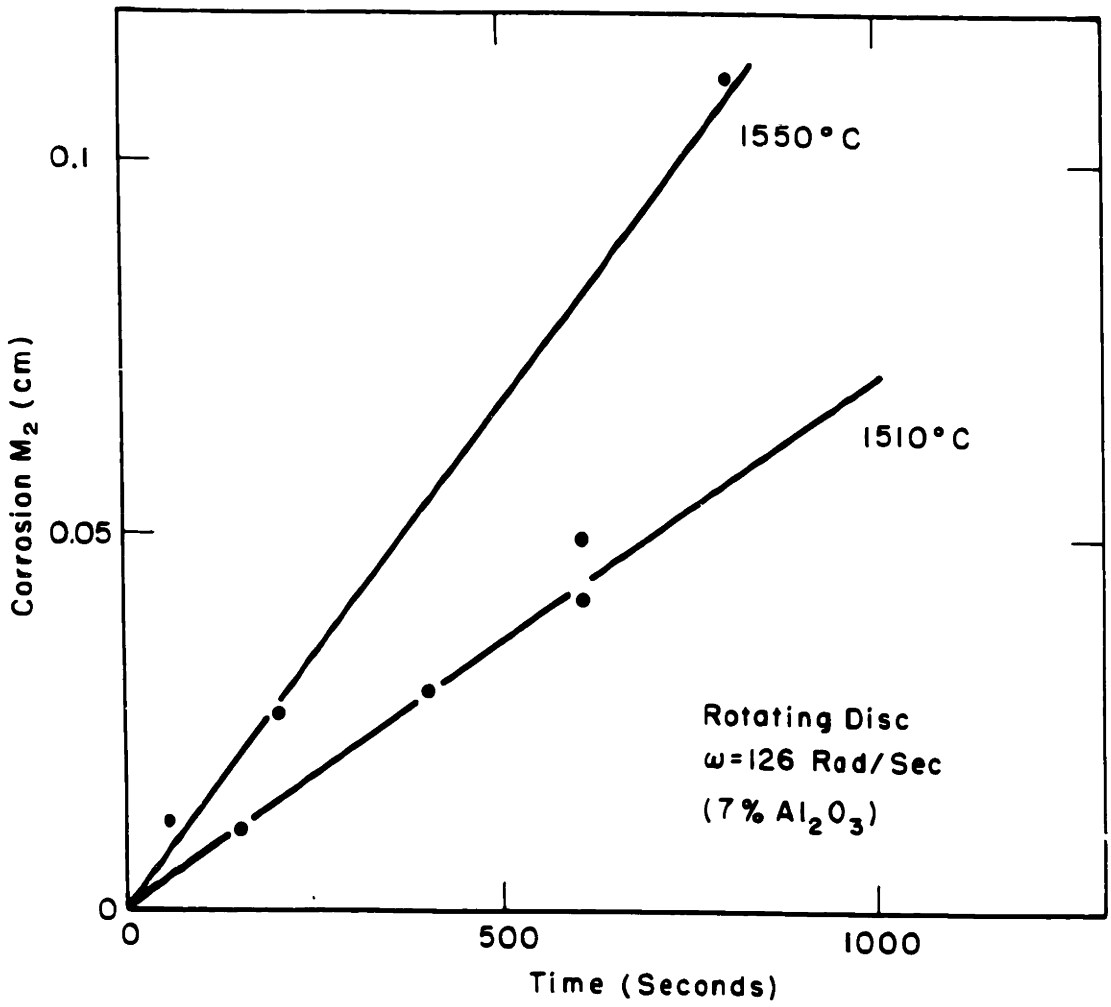

FIGURE 9.9 FORCED CONVECTION CORROSION OF SAPPHIRE DISC FACE IN $CaO-SiO_2-Al_2O_3$ WITH 7 WEIGHT PERCENT Al_2O_3

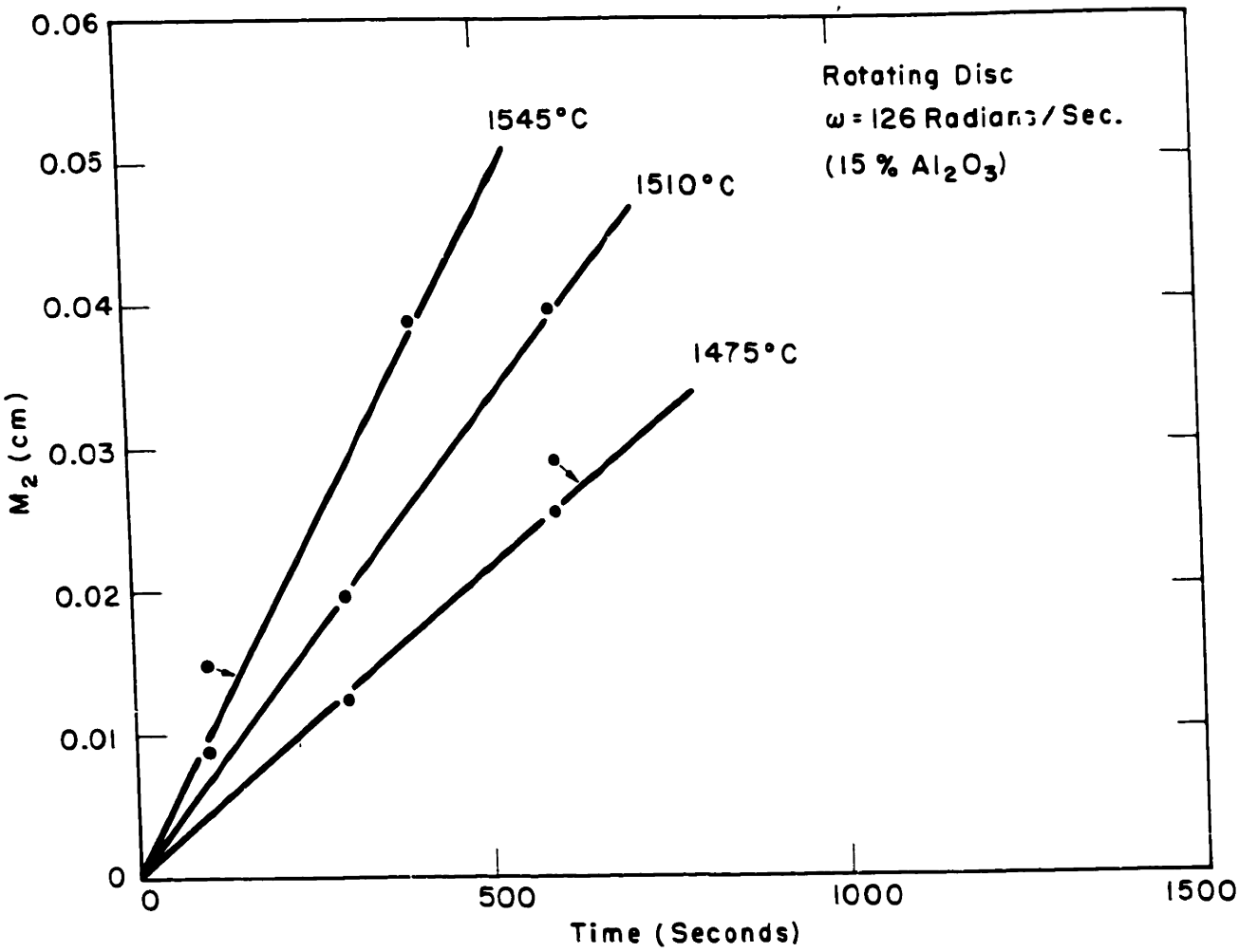

FIGURE 9.10 FORCED CONVECTION CORROSION OF SAPPHIRE DISC FACE IN $CaO-SiO_2-Al_2O_3$ WITH 15 WEIGHT PERCENT Al_2O_3

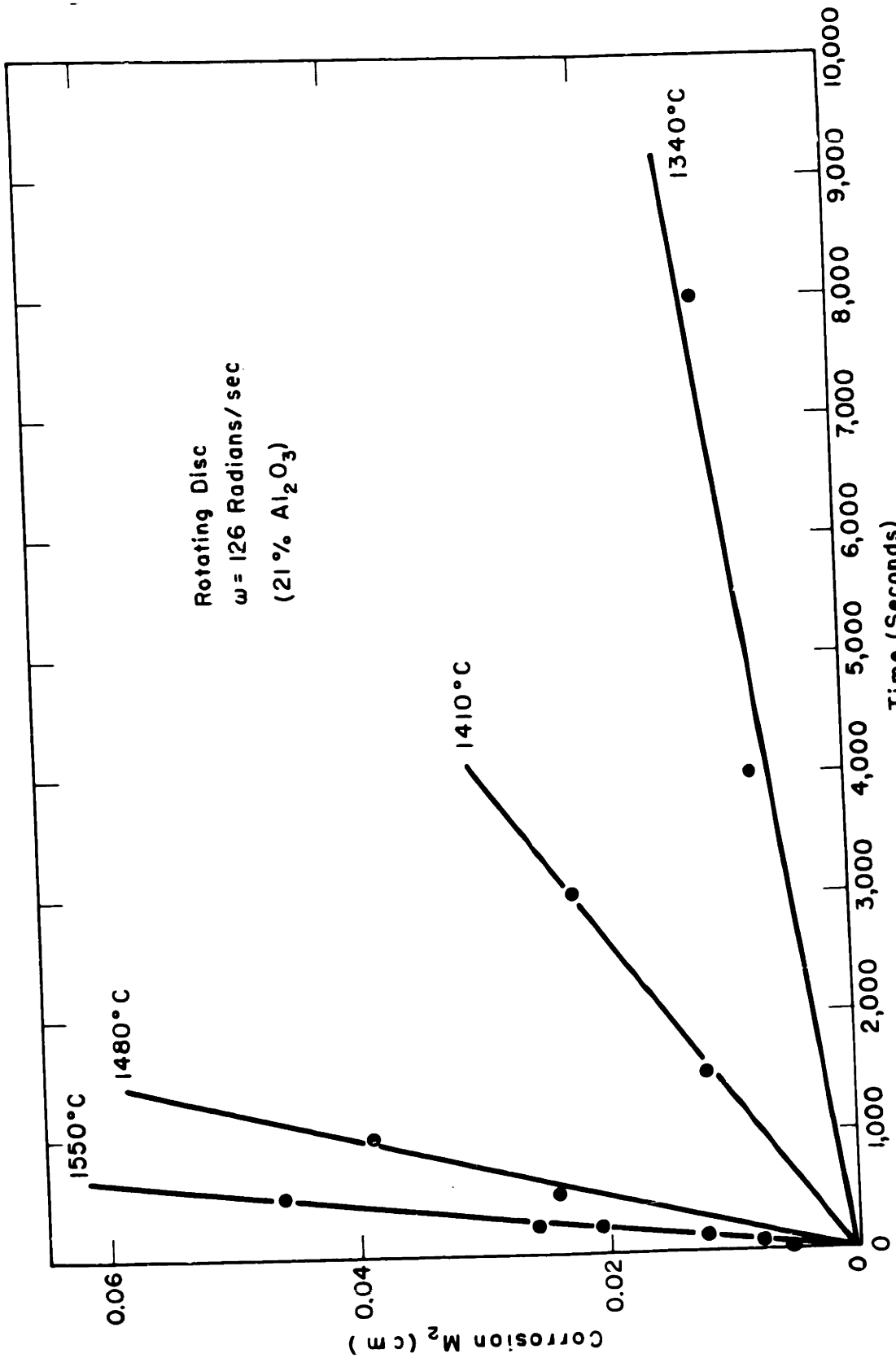

FIGURE 9.11 FORCED CONVECTION CORROSION OF SAPPHIRE DISC FACE IN $CaO-SiO_2-Al_2O_3$ WITH 21 WEIGHT PERCENT Al_2O_3

The relationship given in equation 9.2 yields a slight simplification of equation 7.55 as

$$\overset{*}{J}_2 = .62\ D_o^{2/3} \nu_o^{1/3} \left(\frac{\omega}{\nu_{oo}}\right)^{1/2} \Delta \overset{*}{C} \qquad 9.5$$

In Figure 9.12, the measured corrosion rates in a bulk composition of 21 weight percent Al_2O_3 are compared with the predictions of equation 9.5.

The agreement of the predicted with the actual results is satisfactory. The log predicted rate on Figure 9.12 does not have a constant slope with reciprocal temperature, but has a slightly negative curvature, because of the increased solubility, $\Delta \overset{*}{C}$, at high temperature. The corrosion rate data are not precise enough to confirm or refute this tendency.

Equation 9.5 can likewise be applied to all the forced convection data to calculate the interface diffusion coefficient, D_o. The value of log D_o obtained in this manner is plotted against reciprocal temperature in Figure 9.13. Included again are D_{Si}, D_{Al} and the line of best fit from Figure 9.5. This comparison shows that the value of D_o obtained from forced convection measurements to be in reasonable agreement with D_o obtained from transient diffusion.

Free Convection

Otherwise identical tests at 1500° C and 21 weight percent Al_2O_3 comparing completely immersed samples with those with the surface exposed as described by Figure 6.3 showed corrosion rate to be markedly higher at the melt surface than at the upper edge of immersed samples. This is

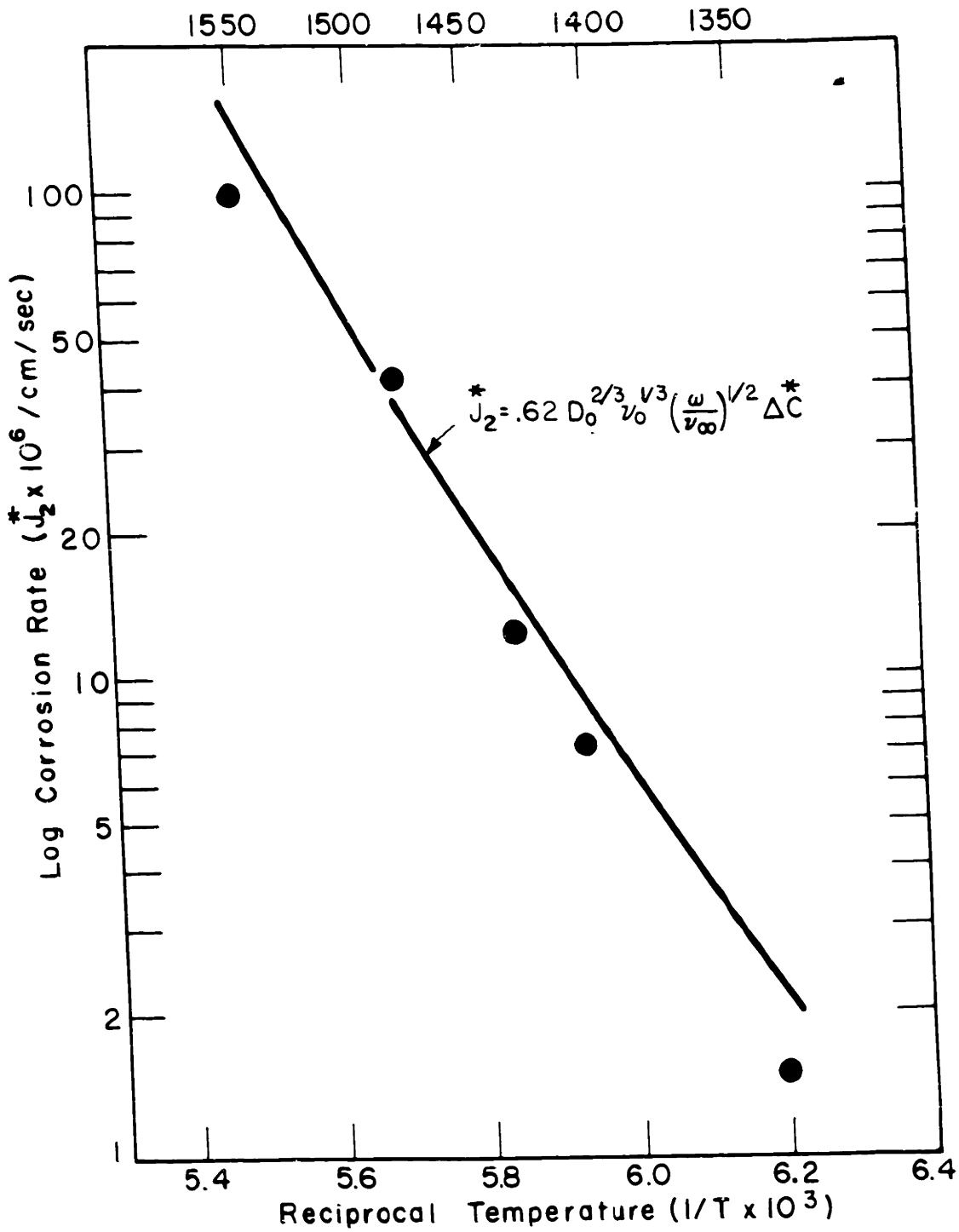

FIGURE 9.12 COMPARISON OF PREDICTED TEMPERATURE DEPENDENCE OF FORCED CONVECTION WITH MEASURED VALUES (21 WEIGHT PERCENT Al_2O_3)

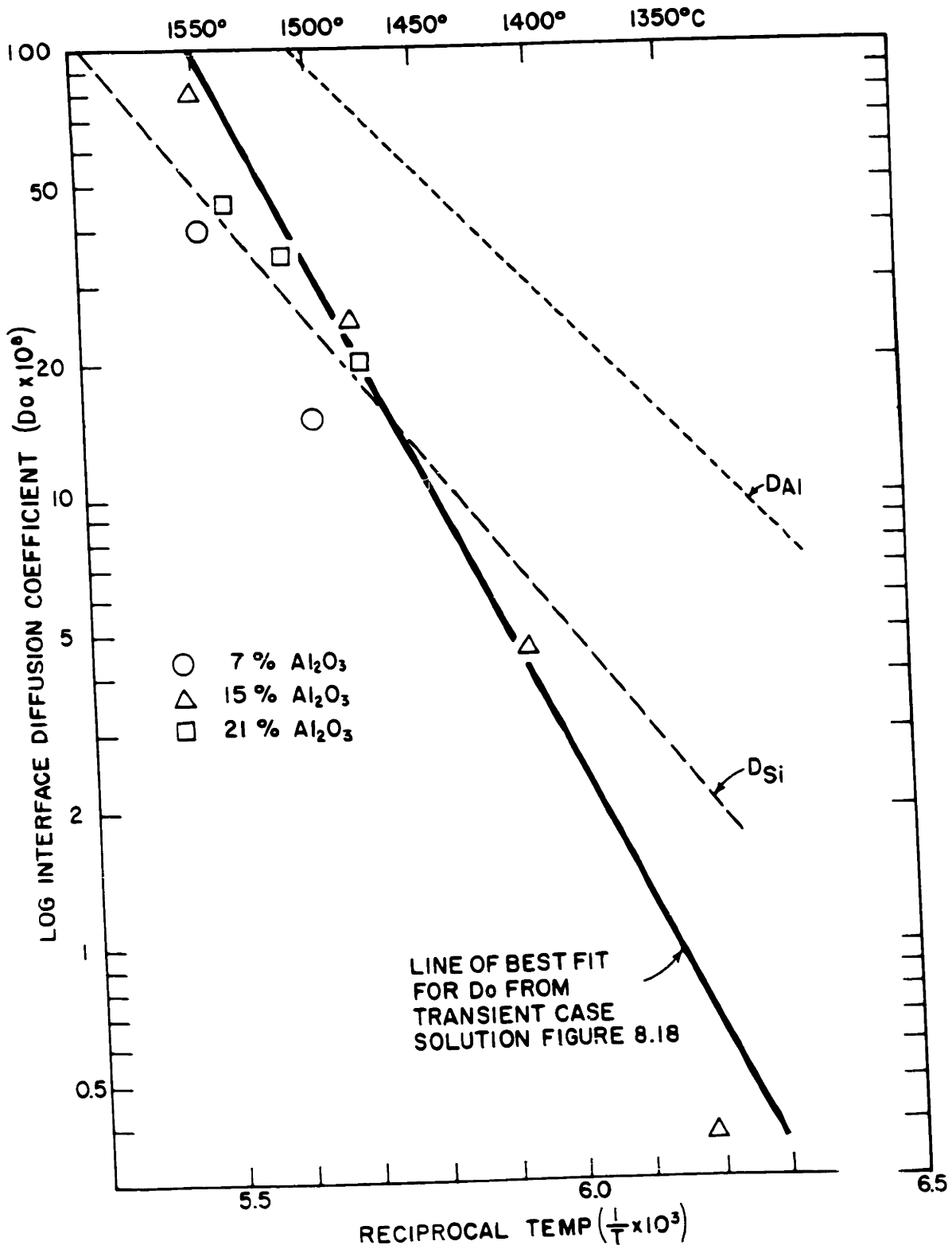

FIGURE 9.13 VALUES OF THE LOG INTERFACE DIFFUSION COEFFICIENT (CALCULATED FROM FORCED CONVECTION CORROSION DATA) VERSUS RECIPROCAL TEMPERATURE

illustrated by the magnified profile of the two samples on Figure 9.14. It suggests the existence of a driving force for free convection flow in addition to the density difference between saturated and bulk solution. For this reason, the driving force for free convection flow will be given the general designation for a pressure gradient $\frac{dP}{dx}$ rather than the specific pressure gradient for a density diffusion $g \Delta \rho$.

The free convection results for 7 weight percent and 21 weight percent Al_2O_3 are summarized in Figures 9.15 and 9.16. The initial enhanced corrosion rate associated with transient diffusion is evident on both of these plots. Experimental times in the vicinity of several days are necessary to attain steady state free convection at temperatures below 1450° C.

The apparent steady state slope of the data in Figures 9.15 and 9.16 can be utilized to determine the driving force for the free convection flow according to the following relation obtained from equation 7.60

$$\frac{dP}{dx} = \frac{16\,(J_3)^4\,\lambda^4}{D_o^3\,\Delta\,\hat{C}^{*4}} \times \nu_o \qquad 9.6$$

The value for the time t'_3 during which the transient process is dominant can then be obtained from equation 7.65 rewritten to include α.

$$t'_3 = \frac{\lambda^2\,\Omega^2}{\alpha}\left(\frac{x\,\nu_o}{\frac{dP}{dx}\,D_o}\right)^{1/2} \qquad 9.7$$

The values for the transition time t'_3 and the driving force $(\frac{dP}{dx})$ obtained from these calculations are shown in Table IX-2.

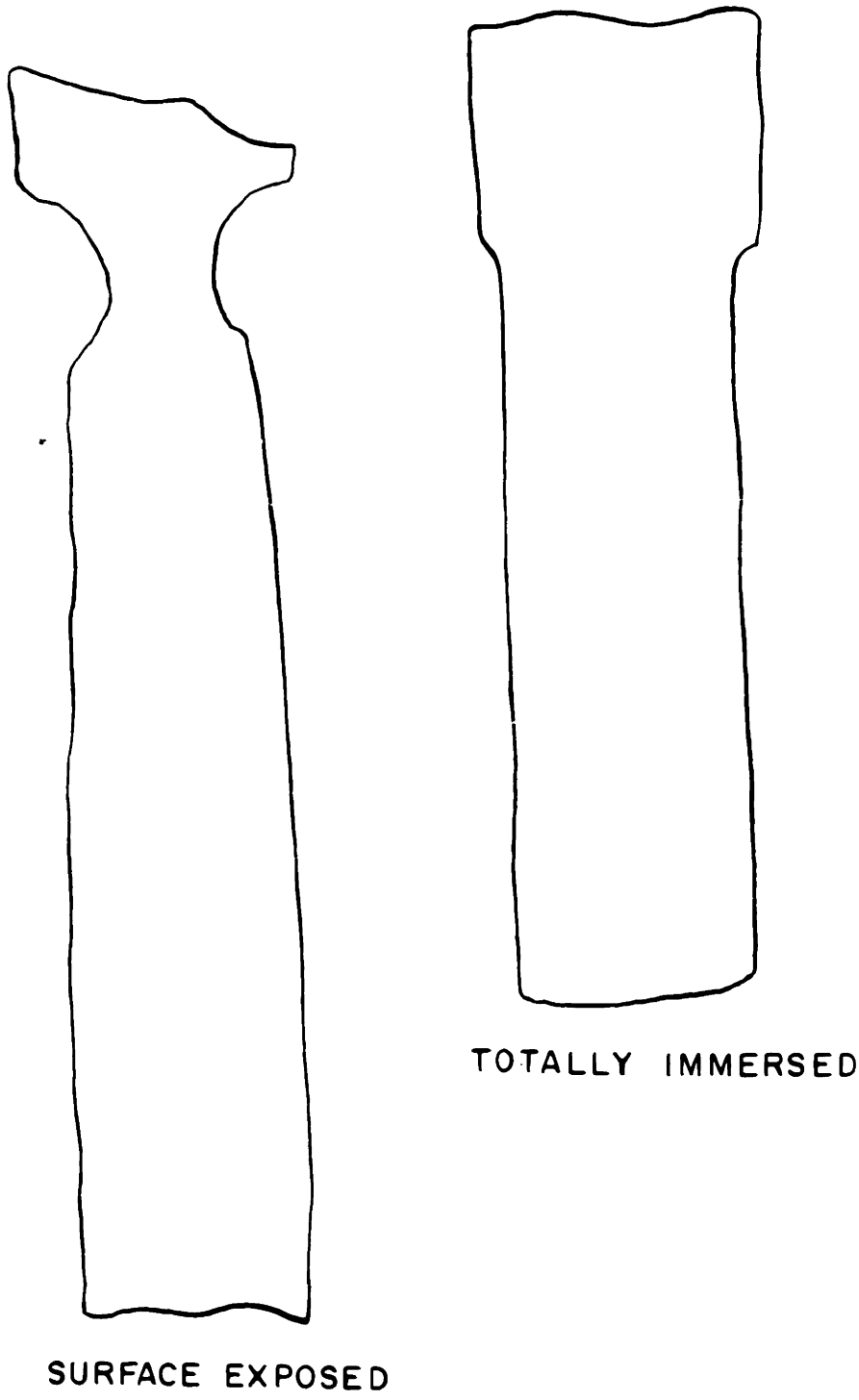

FIGURE 9.14 COMPARISON OF PROFILES OF TOTALLY IMMERSED AND PARTIALLY IMMERSED SAPPHIRE SAMPLES AFTER 12,000 SECOND CORROSION AT 1560° C IN MELT WITH 21 WEIGHT PERCENT Al_2O_3.

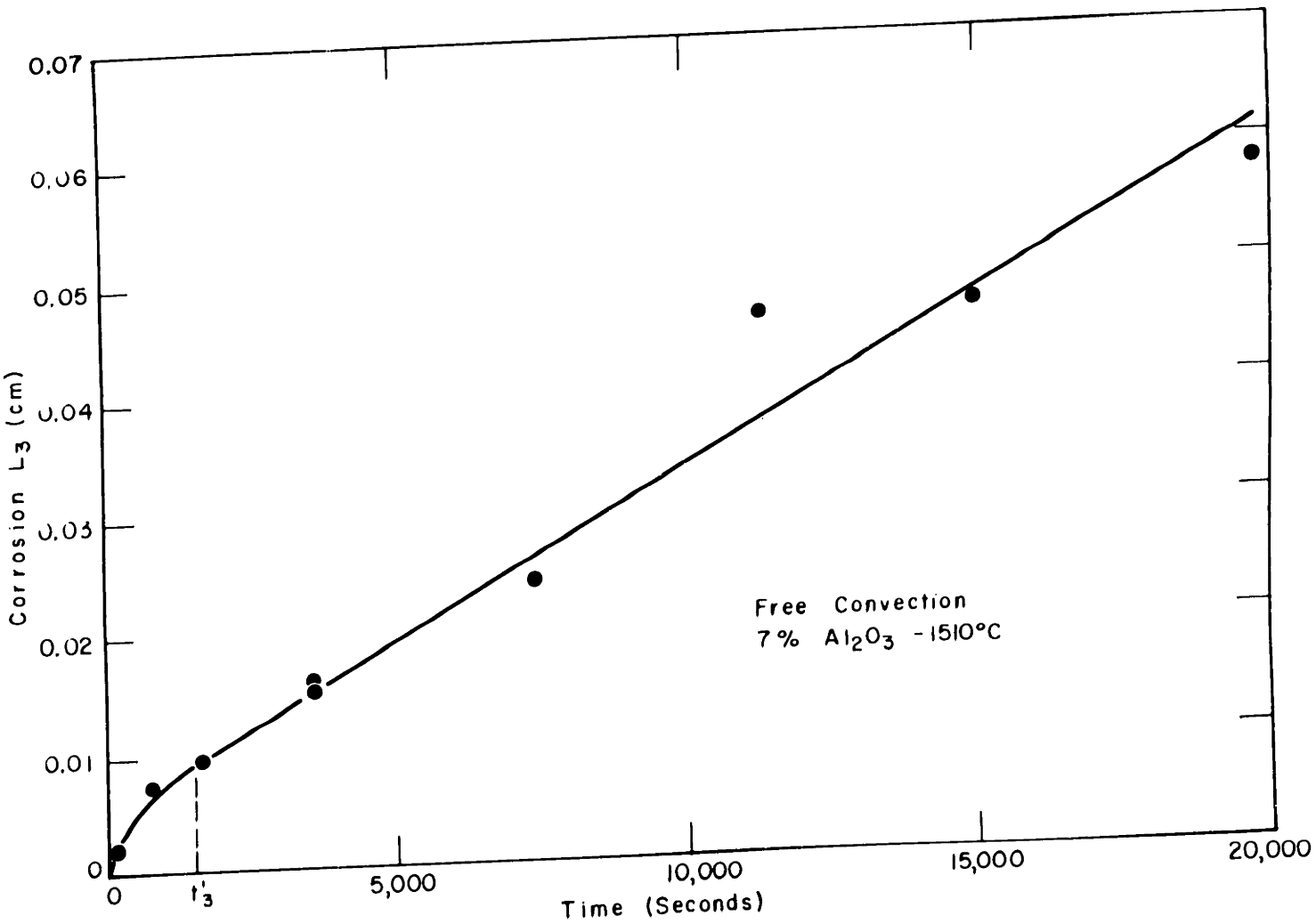

FIGURE 9.15 FREE CONVECTION CORROSION OF SAPPHIRE CYLINDERS IN CaO-Al_2O_3-SiO
7 WEIGHT PERCENT Al_2O_3 (SLOPE OF LINE AT TIMES GREATER THAN
TRANSITION TIME ($t > t'$) DETERMINED FROM EXPERIMENTAL POINTS
POSITION OF LINE DETERMINED FROM SET OF EQUATIONS 7.66

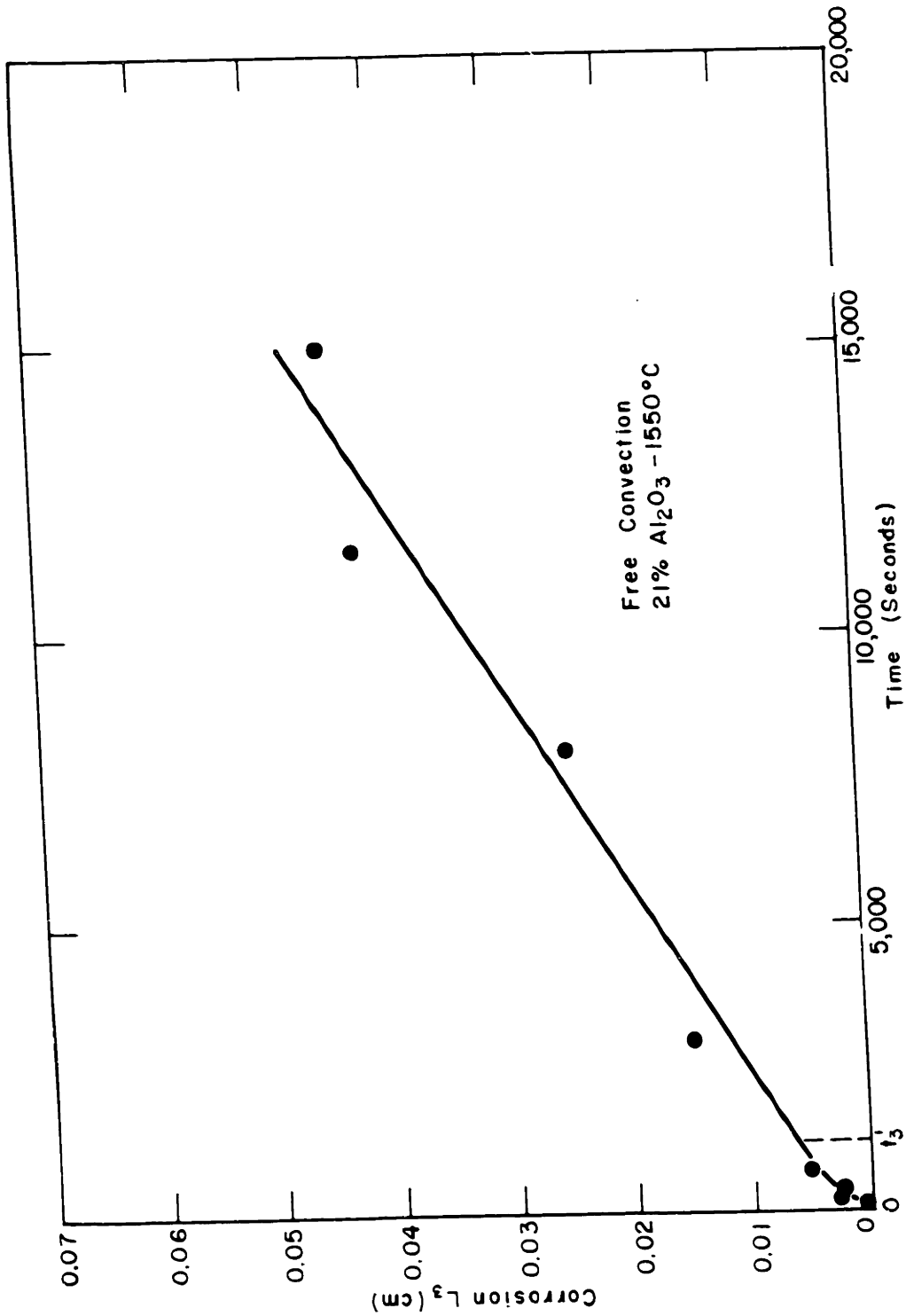

FIGURE 9.16 FREE CONVECTION CORROSION OF SAPPHIRE CYLINDERS IN CaO-Al_2O_3-SiO_2 21 WEIGHT PERCENT Al_2O_3 (SLOPE OF LINE AT TIMES GREATER THAN TRANSITION TIME ($t > t_3'$) DETERMINED FROM EXPERIMENTAL POINTS POSITION OF LINE DETERMINED FROM SET OF EQUATIONS 7.66

TABLE IX-2

Values of Transition Time t'_3 and Driving Force
Obtained from Figures 9.15 and 9.16

	Driving Force $(\frac{dP}{dx})$ dynes/cm^3	Transition Time t'_3 seconds
1510° C 7 % Al_2O_3	3.5	1500
1550° C 21 % Al_2O_3	1.3	1200

The quantitative effect of surface tension forces on the driving force are not established and thus it is presently impossible to compare the driving force inferred by the free convection results with surface energy difference between saturated and bulk solutions suggested by the measurements of Barrett and Thomas[85]. Qualitatively, however, the results in Table IX-2 are understandable since the surface tension difference between saturated and bulk solutions is greater for the 7 than the 21 weight percent Al_2O_3 melt[85]. The transition times t'_3 are in reasonable agreement with the times indicated independently by the loss of linearity between total solution and square root of time in transient diffusion studies, Figures 9.2 and 9.4.

Composition of Boundary Layer at 1500° C

Two experiments were conducted in which a sapphire sample was carefully made concentric with a diamond cutting tool. Then it was immersed into the melt for about two hours. After removal from the melt, cylindrical layers of glass were carefully cut off the sample with the diamond tool.

Unfortunately, the concentricity was not always maintained and the layers were not perfectly concentric with the sample. The results from chemical analyses of these layers are shown in Table IX-3. For convenience in designation, the layer with the highest Al_2O_3 content is considered to be the interface though it is obvious in one case that the eccentricity of the sample caused an enrichment of the innermost layers with Al_2O_3 from the sapphire itself.

TABLE IX-3

Variation of Composition with Distance from the Interface

Time and Temp.	distance from interface mils.	weight percent CaO	SiO_2	Al_2O_3	molar ratio Ca/Si
2 hrs. at 1495° C	0	10	15	73	.71
	2 - 4	22	20	64	1.17
	4 - 8	26	23	53	1.15
	oo	36.2	44	18.3	.88
2 hrs. at 1475° C	0 - 2	28	26	46	1.15
	3 5	34	29	40	1.25
	7 9	33	35	32	1.01
	10 17	34	35	29	1.03
	oo	33	42	24	.78

The results of Table IX-3 are not of high precision because sample size for analysis is small (approximately 20 mg.). They are subject to possible error of $\pm$ 3 % for each constituent.

Even with this lack of reliability a change in Ca/Si ratio from the bulk to the interface is probable with higher values for (Ca/Si) being encountered near the interface. The trend, however, is not drastic and an average value of the (Ca/Si) ratio within the boundary layer is not significantly different from unity.

Second Order Effects

While the profiles of the samples follow that expected for diffusion control in the liquid, two deviations from smooth surfaces occur on the lower disc face of free convection samples.

Figure 9.17 is a photograph of this face of both a sodium chloride and a sapphire sample revealing similar intersecting grooves less than a tenth of a millimeter deep on each sample. These grooves in the surface are only rarely found in rock salt, but in sapphire, they seem to be typical unless there is some other exaggerated corrosion pattern.

Figure 9.18 illustrates the exaggerated corrosion on both polycrystalline alumina and single crystal sapphire. The pock-marked surface is typical of many samples. The cavities range from 0.1 to 1.0 mm. in diameter and often are about half as deep as wide. On the smaller diameter (0.5 cm.) sapphire samples, usually only a single cavity develops. Such a cavity which is nearly 2 mm. deep is seen on the sample with the smallest diameter in Figure 9.18.

FIGURE 9.17 COMPARISON OF GROOVES ON DISC FACE OF SODIUM CHLORIDE (LEFT) AND SAPPHIRE FREE CONVECTION SAMPLES

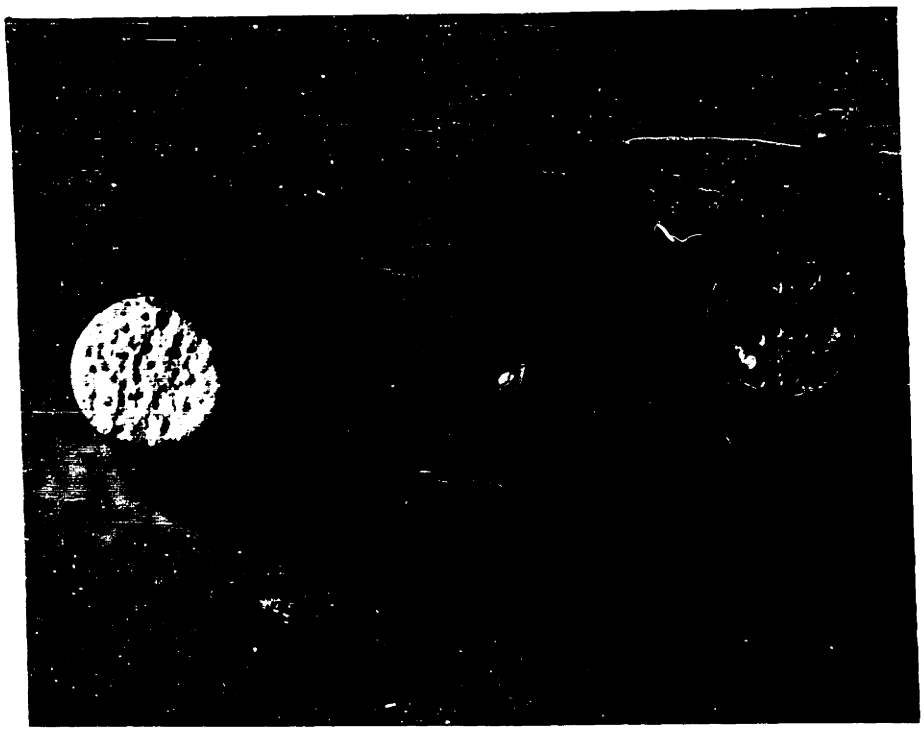

FIGURE 9. 18 POCK MARKS AND CAVITIES ON DISC FACE OF POLYCRYSTALLINE ALUMINA (LEFT) AND SAPPHIRE SAMPLES

Discussion

The data presented in Figures 9.2 to 9.16 are all consistent with diffusion in the liquid as the rate controlling mechanism for solution of sapphire single crystals in $CaO-Al_2O_3-SiO_2$ slag. The results are an example of how the three separate cases, transient, forced convection, and free convection can be utilized to experimentally examine solution kinetics.

They have been shown to be quantitatively self consistent; the diffusion coefficient calculated from forced convection studies is, within the scatter of results, identical with the diffusion coefficient calculated from transient diffusion studies, as shown by Figure 9.13. This value is also consistent with the free convection results as shown by the calculated value of the transition time, t'_3 agreeing with the observed time when corrosion became directly proportional to time.

As there is no published data for diffusion coefficients in the composition region near the alumina liquidus, nor sufficient, reliable activity data to permit confident extrapolation of the available diffusion data, all that can be expected from this study is the internal self consistency already demonstrated.

It is tempting to speculate, however, regarding the coarse agreement of the calculated interface diffusion coefficients with the diffusion coefficients for the silicon ion extrapolated to the liquidus.

To rigorously evaluate a diffusion flux in a multi-compoenet system, the relations taken from Onsager[116] and summarized in Appendix A are required. The lack of reliable, consistent information in the system $CaO-Al_2O_3-SiO_2$ makes utilization of these relations impossible.

In a more approximate evaluation of diffusion flux in a four component system, it should be required that the build-up of space charge be prohibited and volume be conserved within the boundary layer. Then the diffusion process can be considered as two consecutive steps, (1) diffusion of reactants to the interface and (2) diffusion of products from the interface (this assumes the interface reaction is rapid, which has been shown to be the case.) Whichever of these steps is slower will govern the rate.

Measurements of diffusion coefficients show that $O^{=}$, Ca^{++} and Al^{+++} in that order are the fastest diffusing species. Then the two steps could be: (1) diffusion of CaO to interface and (2) diffusion of Al_2O_3 away. No space charge would build up because Ca^{++}, $O^{=}$ and Al^{+++} could migrate to preserve electrical neutrality and it would appear from a molecular viewpoint that CaO was diffusing to the boundary and Al_2O_3 away. The solution rate would be approximately governed by the diffusion of the slowest of these components; i.e., Al^{+++}. Silicon, the least mobile species, would remain immobile in this arrangement and the diffusion path would be that shown as $\overline{AB}$ on the section of the CaO–Al_2O_3–SiO_2 diagram shown as Figure 9.19. This requires existence of a metastable equilibrium of Al_2O_3 with liquid out to composition B. Neither data for diffusion coefficient value nor the composition variation of the interface support this premise.

A second alternative would be to have the liquidus project only as far as the phase boundary between anorthite and alumina because crystallization of anorthite prevents the existence of the metastable alumina liquidus. In this case the diffusion path would be that indicated by $\overline{AC}$ on Figure 9.19.

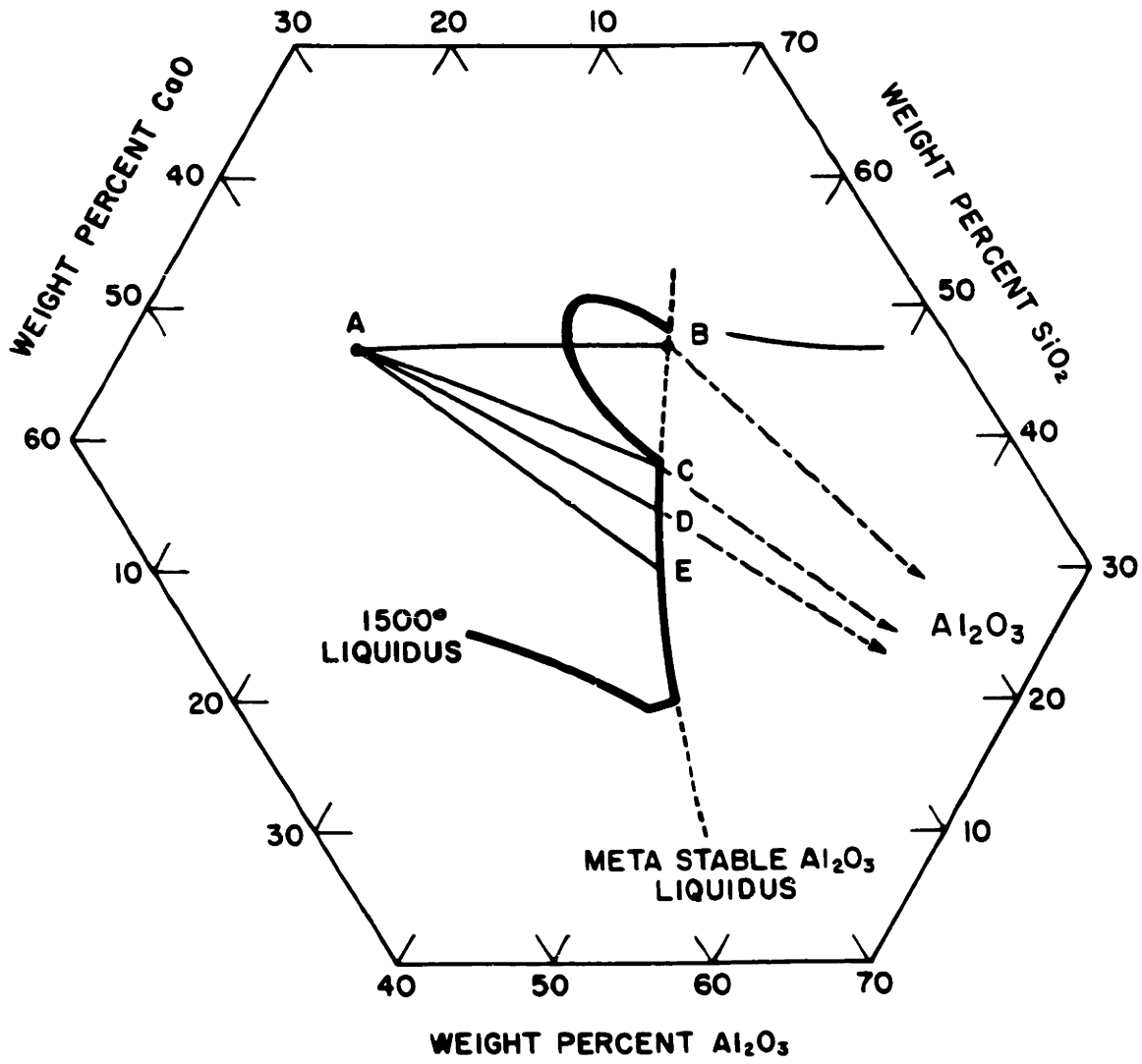

FIGURE 9.19 PORTION OF $CaO-Al_2O_3-SiO_2$ EQUILIBRIUM DIAGRAM SHOWING 1500° C LIQUIDUS AND POSSIBLE DIFFUSION PATHS

Even though silicon is the least mobile species, its migration is required along the path $\overline{AC}$, and silicon diffusion would most likely control the overall process. If, contrary to the published diffusion data, oxygen is the least mobile species and it is essentially immobile, then the flux of Ca^{++} and Si^{++++} moving toward the boundary will balance the flux Al^{+++} moving away from the boundary. This gives the diffusion path $\overline{AD}$. The best approximation of the chemical analyses of boundary layer gives the path $\overline{AE}$.

For the paths $\overline{AC}$ or $\overline{AD}$ the rate controlling diffusion species would most likely be Si^{++++}. This is in best agreement with the kinetic studies and it is not outside the possible error of the chemical analyses of the boundary layer, (Table IX-3). Along the path, $\overline{AD}$, the flux density of silicon is written

$$J_{Si} = - D_{Si} \left(\frac{d C_{Si}}{dy}\right) \qquad 9.8$$

and according to the assumption that oxygen is immobile (path $\overline{AD}$)

$$J_{Al_2O_3} = - \left(\frac{Al_2O_3}{Si}\right) J_{Si} \qquad 9.9$$

because one silicon ion and one calcium ion must migrate jointly to balance the opposite migration of two aluminum ions. However, the concentration gradients for alumina and silicon must be similarly correlated

$$\frac{d C_{Si}}{dy} = - \frac{Si}{Al_2O_3} \frac{d C_{Al_2O_3}}{dy} \qquad 9.10$$

Therefore, from equations 9.8, 9.9 and 9.10 in the simplest case:

$$J_{Al_2O_3} = - D_{Si} \frac{d C_{Al_2O_3}}{dy} \qquad 9.11$$

and when it is desirable to express the flux density as the change of dimensions of sapphire normal to the interface

$$\overset{*}{J}_{Al_2O_3} = - D_{Si} \left(\frac{d \overset{*}{C}_{Al_2O_3}}{dy}\right) \qquad 9.12$$

This reveals that if the diffusion coefficient for silicon were rate controlling, D_{Si} can be substituted for the previously undesignated diffusion coefficient, D, i.e.

$$D_o = D_{o\ Si}$$

$$\overset{*}{D} = \overset{*}{D}_{Si} \qquad 9.13$$

While the premise cannot be rigorously demonstrated by the results of this work, indications, both from the analyses of the boundary layer glass and from the calculated values of the interface diffusion coefficient, D_o, are that the solution rate is governed by silicon diffusion in the liquid. It is proposed, therefore, that the relations presented in equation 9.13 are approximately correct for solution of sapphire by slag.

There is too much scatter in the results shown in Figure 9.12 to seriously test the premise regarding the treatment of variable viscosity presented in section VII, page 89. (There it was derived, following von Karman's approximate treatment, that the bulk viscosity determines the velocity boundary layer thickness and that the bulk viscosity is the most appropriate value for the factor involving the square root of viscosity in the equation for diffusion transfer in forced

convection flow over a flat plate. It was then assumed, since the form of the equations was similar, that an equivalent use of the bulk velocity would be appropriate in the equation for diffusion transfer to a rotating disc.)

Figure 9.12 shows that the derived relationship gives a reasonable fit to the results over a wide temperature range. However, in this case, the ratio $(\frac{\nu_o}{\nu_{oo}})^{1/2}$ is only about 1.35 and introducing this factor into the expression for predicted rate of solution does not significantly alter the "goodness" of the fit of the predicted to the measured results. These experiments, therefore, are not sufficiently sensitive to elucidate the detailed influence of variable viscosity.

Primarily, because of the change of solubility with temperature the logarithm of the predicted rate of solution has a slight negative curvature when plotted versus reciprocal temperature shown in Figure 9.12. Since this curvature is slight, it explains why the results of refractory corrosion experiments[54,55] often show very nearly an Arrhenius relationship with temperature.

The decidedly different contours shown in Figure 9.14 for the partially immersed and totally immersed samples suggest that surface forces mentioned by Tress[47] are effective in causing flow at the melt surface thereby increasing solution rates in this vicinity.

Surface forces can also be invoked for an explanation of the pitting of the lower surface of the free convection samples. Gas bubbles on this surface could cause accelerated corrosion if steeper diffusion gradients were induced by surface active constituents of the melt as first discussed by Preston and Turnbull.[49] These bubbles could

result from adsorbed gases on sapphire surface, exolved gas, or bubbles in the melt. No evidence is available to support this premise, but it should be possible to locate these bubbles in future tests, by microscopic examination of the surface before removal of the glass.

An interesting result from section VII is the prediction of the corrosion when both unsteady and steady state processes are influential in determining the total amount of solution. Such a situation occurs in the free convection experiments. When the driving force, for free convection, $(\frac{dP}{dx})$, is determined from the steady state slope of the free convection experiments, the value for the transition time, t'_3 is established. Its agreement with the beginning of a linear relationship between corrosion and time and the agreement of the predicted and the measured amount of corrosion at t'_3 confirm the inclusive relationships for solution developed in the set of equations 7.66.

X. FUTURE WORK

A variety of lines of work are suggested by this thesis. These include:

(1) Measure diffusivity and viscosity as a function of composition in alkali halide-glycerine systems. For the system showing maximum composition dependence on properties perform the three cases of solution experiments and determine experimentally the validity of equations 7.64 and 7.66.

(2) Explore kinetics of sodium chloride solution in glycerine at lower temperatures until the process becomes completely interface reaction controlled.

(3) Determine the quantitative relation between surface forces and free convection and check with solution experiments.

(4) Examine in a model system (sodium chloride-glycerine) or in a refractory oxide molten silicate system, the effect of ceramic properties, grain size porosity and microstructure on corrosion behavior.

(5) In a given system, perhaps $CaO-Al_2O_3-SiO_2$, study solution kinetics of each end member.

APPENDIX A

DIFFUSION IN LIQUIDS

Introduction

It is possible for well-designed experiments to determine when solution is a diffusion controlled process and in addition to determine the value of an effective diffusion coefficient. The effective diffusion coefficient provides a convenient way to catalogue the experimental results in a way which is useful for calculation of the anticipated rate of solution under a variety of possible conditions.

It is also necessary to ascertain that convection conditions in effect in a particular experiment or application and determine the other pertinent physical properties, kinematic viscosity, density difference, and solubility and use relationships of the sort given in the sets of equations 4.12 and 4.13 to predict the rate of solution. While precise information about the other properties may be lacking and the convection may be difficult to characterize, in principle, there is no deterrent to this sort of calculation.

It may also be possible to calculate an activation energy for the effective diffusion coefficient and thus express the value of the effective diffusion coefficient as a function of temperature. Knowing the temperature dependence of the other physical properties including solubility, the temperature dependence of the solution process is predictable.

While cataloging results in a useful and concise way and accurately predicting rates of solution under a variety of conditions are desirable ends in themselves, it is of basic importance to understand the details that underlie the "effective diffusion coefficient." Is it governed by the migration of a single species or the interaction of several species? Understanding at this level markedly increases the possibility of affecting the rate of solution.

Diffusion in Multi-Component Systems

The question of diffusion in multi-component systems has been treated thoroughly by Onsager[116] and reviewed by Bosworth.[117] The following utilizes their treatments, particularly that of Onsager. The simplest statement of diffusion flux of component i is Fick's law which was utilized by Nernst for equation 2.2. It takes no cognizance of the fact that the gradients of other species may affect the flux of a given species. If it is assumed with Onsager that the relative velocities of the components will be linear combinations of the concentration gradients, Fick's law can be generalized as

$$J_i = \sum_{k=1}^{s} D_{ik} \nabla C_k \qquad (1)$$

where s is the number of species participating in the diffusion. Since interest will, in general, be confined to cases where the concentration gradient is unidimensional, $\nabla C_k = i \frac{\partial C_k}{\partial x} + j \frac{\partial C_k}{\partial y} k \frac{\partial C_k}{\partial z}$ is replaced by $\frac{dc}{dy}$, where the direction of y is normal to equal concentration surfaces.

Either of two convections for the flux of i, can be adopted. It can refer to the flux velocity of a species relative to a fixed point or the flux velocity of a species relative to the remainder of the solution. Onsager utilizes the second convention, and this seems most appropriate for the examination of solution kinetics.

In application of diffusion coefficients, it is important to recognize which of these conventions was utilized for the original measurements of diffusion coefficient. In general, when dealing with dilute solution, there is little difference in the values obtained from the different conventions.

The first restriction applied by Onsager is that the diffusion causes no bulk motion of the liquid. Call $\bar{V}_i$ the partial volume of i, i.e., $\frac{\partial V}{\partial W_i}$ where W_i is the weight of component i. Th.. .f the bulk flow from diffusion u_D is required to vanish

$$u_D = \sum_i \bar{V}_i J_i = 0 \qquad (2)$$

Using equation (1) it can be readily shown that one set of conditicns which will assure no bulk flow from diffusion is

$$\sum_i \bar{V}_i D_{ik} = 0 \qquad (3)$$

for all k.

This gives s restrictions on the s^2 diffusion coefficients D_{ik}.

The condition that the product of pressure and volume is constant at constant temperature is given by the following equation

$$K\Delta P = \sum_i \bar{V}_i D_{ik} C_i = 0 \qquad (4)$$

where κ is the compressibility.

If pressure P is constant,

$$\sum_i \bar{V}_i \; C_i = 0 \tag{5}$$

According to Onsager, the set

$$\sum_k D_{ik} \; C_k = 0 \tag{6}$$

satisfies the requirement.

Thus s additional restrictions are placed on the diffusion coefficients. The 2s restrictions placed on the diffusion coefficients of equation (2) from equations (3) and (6) are not independent because they both imply

$$\sum_{ik} \bar{V}_i \; D_{ik} \; C_i = 0 \tag{7}$$

Thus this gives (2s - 1) restrictions or $(s - 1)^2$ independent diffusion coefficients.

According to these relations, for a system in which there are three components, there are four independent diffusion coefficients, one more than the self diffusion coefficients (diagonal terms) usually measured. This makes utilization of equation (2) with (s - 1) restrictions impractical for a system of three or more compoennts unless there is some information on the cross diffusion terms (D_{ik} $K \neq i$) as well as the diagonal terms.

Useful to further reduce the number of independent coefficients are Onsager's reciprocal relations[118] derived from the principle of microscopic reversibility which states that the probability of an equilibrium system changing from a state j to i in a time t is the same as the probability of changing from i to j in the same interval. This means that equilibrium can only be maintained by equal and opposite flow processes and never by a cyclic change.

Onsager and Machlup[119] have shown, that provided the transport equations are written so that the potential (driving force) is the rate of change of entropy with respect to displacement (flux), the conductance matrix is symmetric in the absence of internal fields. These are the reciprocal relations and are expressed explicitly in the following equations.

Defining b_i as the displacement of quantity with units (gm cm)* and S as the entropy, the transport equation showing the proportionality between flux and potential is written

$$\frac{d\, b_i}{dt} = \dot{b}_i \sim \frac{\partial Si}{\partial b_i} \tag{8}$$

or in more general form, allowing for the interaction of transport processes,

$$\dot{b}_i = \sum_j G_{ij} \frac{\partial S}{\partial b_j} \tag{9}$$

where G is the proportionality constant called conductance.

---

* This quantity can be any extensive thermodynamic property: mass, volume, heat, charge and thus the validity of the reciprocal relations extends into fields other than mass transfer.

The time derivative of the displacement $\dot{b}_i$ is equivalent to a flux times a volume factor.

The Onsager reciprocal relations state that the conductance coefficients are symmetric, i.e.

$$G_{ij} = G_{ji}$$
$$G = G_{(tr)} \tag{10}$$

Although it is inferred by Bosworth[117], Darken[120] and Bardeen and Herring[91] that the reciprocal relations imply a symmetry of the diffusion matrix, that this is not so, is demonstrated by the fact that the diffusion coefficients obtained by Baldwin, Dunlop and Gosting[121] and Fuhita and Gosting[122] for aqueous systems NaCl-LiCl and KCl-LiCl do not form a symmetric matrix. Also, the enforcement of conditions of no bulk velocity, and constant volume (equations (3) - (6)) plus reciprocal relations of the diffusion coefficients, leads to the relation for a two-component system that

$$\bar{V}_1 \; C_2 = \bar{V}_2 \; C_1 \tag{11}$$

which need not be valid.

By using an alternate form of the transport equation involving a dissipation function, F

$$2F\,(J,J) = \sum_{ik} W_{ik} \; (J_i \cdot J_k) \tag{12}$$

in which the reciprocal relation applies to the coefficients W_{ik}.

Onsager shows the effect that the reciprocal relations have on the diffusion coefficients. The dependence is

$$\sum_j \left(\frac{\partial \mu_i}{\partial C_j}\right)_P D_{jk} = \sum_j \left(\frac{\partial \mu_k}{\partial C_j}\right)_P D_{ji} \qquad (13)$$

Provided the chemical potentials, μ, are known, these equations give a total of 1/2 s(s-1) restrictions on the coefficients of diffusion.

In combination with equation (3) this gives a total of $1/2(s^2+s)$ restrictions leaving only 1/2 s(s-1) independent diffusion coefficients. Thus, for a system of three components there are only three independent diffusion coefficients making possible calculations of flux of any component from knowledge of the three self diffusion coefficients and the chemical potentials.

The treatment has thus far ignored the effect of charges on the diffusing species. This adds a further restriction, which states that most simply there be no build up of space charge.

Variable Diffusivity

In most liquid systems the diffusion coefficient is function of composition. To understand the basis for this variation it is advisable to write the diffusion equation so that the driving force is the gradient of chemical potential as first suggested by Nernst.

$$J_i = - B_i \frac{d\mu_i}{dy} \qquad (14)$$

The relation between the diffusion coefficient, D, and the mobility, B, is obtained by the following thermodynamic identity:

$$\mu_i = \overset{o}{\mu}_i + RT \ln a_i \tag{15}$$

where $\overset{o}{\mu}_i$ is the chemical potential of i in a standard state and a_i is the activity of i.

From this it follows that

$$\frac{d\mu_i}{dy} = RT \left(\frac{d \ln a_i}{d C_i}\right)\left(\frac{d C_i}{dy}\right) \tag{15a}$$

and

$$J_i = - B_i \, RT \left(\frac{d \ln a_i}{d C_i}\right)\left(\frac{d C_i}{dy}\right) \tag{15b}$$

but the definition of D from Eick's first law is:

$$D = - J_i \left(\frac{d C_i}{dy}\right)^{-1} \tag{15c}$$

so

$$D = B_i RT \frac{d \ln a_i}{d C_i} = \frac{B_i RT}{C_i} \frac{d \ln a_i}{d \ln C_i} \tag{16}$$

This is analogous to the expression derived by Hartley[124].

When the solution is ideal $\frac{d \ln a_i}{d \ln C_i} = 1$

and hence

$$D_i = \frac{B_i RT}{C_i} \tag{17}$$

which is the equation used by Bardeen and Herring.[91] It seems of no value to use equation (14) when the solution is ideal since the simple expression of Fick's first law is equally valid. When the solution is not ideal, and only equation (16) is appropriate, the value of expressions such as equation (17) is small.

The coefficient of mobility, B_i/C_i is of greater constancy than the diffusion coefficient D_i.[125] Knowledge of the variation of activity with composition then is the first requirement for extrapolation of diffusion data.

For systems in which changes in viscosity occur over the region of interest, it is also necessary to take into account changes of mobility of the diffusing species. Diffusivity is inversely proportional to the viscosity of ideal solutions, that is

$$D_i = K_3 (1/\eta) \qquad (18)$$

where K_3 is a constant and, η, the dynamic viscosity. For the Stokes-Einstein relation, the constant $K_3 = \frac{kT}{6\pi r}$ where r is the radius of the diffusing species. In any event, K_3 is a constant which is related to the shape and size of the diffusion species.

In non-ideal cases, rather than diffusivity itself, it would be expected that the mobility $\frac{B_i}{C_i}$ bears the inverse relation to viscosity. This permits proper account to be taken of both viscosity and the activity in determining D. Defining a new constant K_4 that still contains the shape factor, one obtains

$$\frac{RT\ B_i}{C_i} = K_4/\eta \qquad (19)$$

Substituting equation (15) and lumping the constants together

$$D_i = \frac{K_5}{\eta} \frac{d \ln a_i}{d \ln C_i} \qquad (20)$$

which permits extrapolation of diffusion data when the diffusion coefficient is known at one composition, the variation of activity and viscosity with composition are known and the character of the diffusing species does not change. Equation (19) is entirely equivalent to the one derived more rigorously by Hartley and Crank.(126)

It has been found to apply in several instances(127) and its failures(128) occured when the size of the diffusing complex may have changed with change in composition.

BIOGRAPHICAL SKETCH

Alfred R. Cooper, Jr., was born in New York City on January 1, 1924. He was educated in the public schools of White Plains, New York, and did undergraduate work in glass technology at Alfred University, Alfred, New York, and received the degree of Bachelor of Science in 1948. During World War II, which interrupted his education at Alfred University, he served in the United States Navy.

After graduation from Alfred, he was employed by the Radio Corporation of America for four years in a cathode ray tube plant where he directed a group of production engineers dealing with glass fabrication and breakage problems. He was employed as a glass technologist and manager of Customer Service Laboratory for the Hartford Empire Division of the Emhart Manufacturing Company for four years. His work included consultation with and visits to glass manufacturing companies.

In 1956, Mr. Cooper started graduate work in the Ceramics Department at M.I.T. as an Aluminum Company of America fellow. In 1958 he was appointed Instructor in the Ceramics Department, and in 1959 served as an Assistant Professor.

Mr. Cooper's interests have been in the area of understanding the fundamentals of ceramic processes, particularly continuous glass melting, and he has published two papers analyzing flow and mixing in glass tanks.

In 1948 he wed the former Jacqueline F. Kennedy of Quincy, Massachusetts. Their children are Thomas Micheal, Stephen Wright, Abigail Grace, Karl Kennedy and Amy Lisa.

BIBLIOGRAPHY

1. E. A. Moelwyn Hughes, The KINETICS OF REACTIONS IN SOLUTION, Chapter XII, Clarendon Press, Oxford, 1947.

2. L. Bircumshaw and A. Riddiford, Transport Controlled Processes, Quarterly Reviews, 6, 157 (1952).

3. A. A. Noyes and W. R. Whitney, Z. Physichal Chem., 23, 689 (1897).

4. W. Nernst, Z. Physichal Chem., 47, 52 (1904).

5. P. G. von Name and G. Edgar, J. Amer. Chem. Soc., 38, 253 (1916).

6. C. Wilke, M. Eisenberg and C. Tobias, Free Convection Mass Transfer at Vertical Plates, Chem. Eng. Progress, 49, 663 (1953).

7. B. Roald and W. Beck, The Dissolution of Magnesium in Hydrochloric Acid, J. Elect. Chem. Soc., 98, 277 (1951).

8. M. Eisenberg, C. Tobias and C. Wilke, Ionic Transfer and Concentration Polarization at Rotating Electrodes, J. Elect. Chem. Soc., 101, 306 (1954).

9. L. L. Bircumshaw and M. H. Everdell, Trans. Chem. Soc., 8, 595 (1942).

10. R. Linnell and H. M. Haendler, Beryllium Fluoride in Water and Ethanol Solutions, J. Phys. Chem., 52, 819 (1948).

11. M. J. Prior and U. R. Evans, Passivity of Metals, Part X, J. Chem. Soc., 3330 (1949).

12. A. Berthoud, J. Chem. Phys., 10, 633 (1912).

13. REFRACTORIES BIBLIOGRAPHY (1928-1947) and (1947-1956), Norman University of Oklahoma Press. There are numerous abstracts on this subject under such headings as glass tank refractories, corrosion of, glass attack, slag, corrosion of, etc.

14. R. Sosman, Some Fundamental Principles Govering the Corrosion of Fire Clay Refractories by Glass, J. Am. Ceram. Soc., 8, 191 (1925).

15. N. McCallum and L. R. Barrett, Some Aspects of the Corrosion of Refractories, Trans. Brit. Cer. Soc., 51, 523 (1952).

16. J. Wiegman, On the Solution Velocity of Clay in Glass, Z. Phys. Che., 204, 286 (1955).

17. G. V. McCauley, Symposium on Glass Industry's Refractories, Bull. Am. Cer. Soc., 4, 605 (1925).

18. W. K. Brownlee, Insulation of Glass Tanks, J. Amer. Ceram. Soc., 7, 457 (1924).

19. F. C. Flint, A. R. Payne, Tank Block Corrosion by Shelving, J. Amer. Ceram. Soc., 9, 613-617 (1926).

20. T. S. Busby and J. H. Partridge, Improved Materials for Tank Blocks, J. Soc. Glass Tech., 36, 131 (1952).

21. J. Loffler, Reaction between Glass and Refractory Walls II, Relation of the Density of Cords from Refractories Wall to that of the Glass at High Temperature, Glas. tech. Ber., 27, 392-393,

22. L. Reed and L. R. Barrett, The Slagging of Refractories I. Trans. Brit. Ceram. Soc., 54, 671 (1955).

23. H. R. Moore and R. Heeley, An Experimental Investigation of Alumino Silicate Refractories of High Purity for use in Glass Melting, J. Soc. Glass Tech., 34, 274 (1950).

24. K. Endell, R. Fehling and R. Kley, Influence of Hydrodynamic Characteristics and Solvent Action of Slag on the Destruction of Refractories at High Temperatures, J. Amer. Ceram. Soc., 22, 105 (1939).

26. N. V. Solomin, The Nature of the Corrosion Process in Glass Tanks, Steklo i Keram, 6, 13 (1949).

27. A. R. Cooper, (a) Mixing and Flow in Glass Tanks, J. Amer. Ceram. Soc., 41, 93 (1959), (b) Effect of Aspect Ratio and Viscosity Gradients in Flow Through Open Channels, ibid, 42 (1960).

28. J. Loffler, Reactions between Glass and Refractory Walls I, Fire Clay Walls and Soda Lime Glass, Glas. tech. Ber., 25, 405-11 (1953).

29. E. Steinhoff, Solution Process of Sidewall Blocks, Glas. tech. Ber., 27, 309 (1954).

30. K. Konopicky, On the Changes in Fire Clay Brick in Use, Glas. tech. Ber., 27, 9, 319-31 (1954).

31. G. R. Rigby, Mechanism of Bursting Expansion of Chrome Magnesite, Brick, Trans. Brit. Ceramic Soc., 55, 22-35 (1956).

32. J. L. Lambert, Private communication.

33. E. Plumat, Study of Contact Phenomena between Glass and Oxide at High Temperature by Measurement of Electrical Potentials, Silicates Ind., 19, 141 (1954).

34. P. LeClerc and I. Peyches, Behavior of Refractories in Molten Electrolytes such as Fused Silicates, Trans. Intern. Ceramic Congr., 217-222 (1952).

35. J. F. Hyslop, R. Gumm, and H. C. Biggs, Some Corrosion and Erosion Phenomena and their Bearing on the Macrostructure of Refractories, J. Soc. Glass Tech., 10, 405 (1926).

36. J. D. Harrison and C. Wagner, The Attack of Solid Alloys by Liquid metals and Salt Melts, Acta Metallurgica, 7, 722 (1959).

37. J. H. Part ridge, C. F. Adams and J. R. Lait, Clay Mixtures for Glass Melting Pots IV, Corrosion Resisting Properties, J. Soc. Glass Tech., 16, 131-142 (1932).

38. J. L. Lambelet, A Fundamental Study of the Attack of Glass on Glass Tank Refractories, Thesis, Rutgers University (1951).

39. J. E. Comoforo and R. K. Hursh, The Wetting of Al_2O_3-SiO_2 Refractories by Molten Glass I Measurement of Wetting, J. Am. Ceram. Soc., 35, 130-134 (1952), II Effect of Wetting of Penetration of Glass into Refractory, ibid, 142-8.

40. N. K. Adams, Principles of Penetration of Liquids into Solids Disc. Far. Soc., 3, 5 (1948).

41. H. Lehmann and U. S. Singh, The Influence of Surface Tension of the Melt on the Attack of Refractories, Ber. deut. keram. Ges. 35, 353 (1958).

42. W. H. Parsons and H. Insley, Attack on Refractory Clay Pots by Optical Glasses, J. Research Natl. Bur. Standards, 36, 31-45 (1946).

43. R. Rasch, Slag Penetration by Capillarity and Diffusion, Sprechsaal 88, 196,227,245 (1955).

44. H. Salmang and J. Kaltenbach, Researches on the Corrosion of Refractory Materials, VI, Feurfest 7, 161 (1931).

45. N. McCallum and L. R. Barrett, Kinetics of the Dissolution fof Corundum in Binary Silicate Slags, Silicates Ind., 17, 89 (1952).

46. H. Jebson-Marwedel (a) Remarks on the Influence of Surface Tension in the Glass Melting Process, J. Soc., Glass Tech., 21, 436 (1937), (b) The Mechanism of the Solution of Pairs of Glasses and other Liquids, J. Soc. Glass. Tech., 32, 162 (1948).

47. H. J. Tress, Some Distinctive Contours Worn on Alumina-Silicate Refractory Faces by Different Molten Glasses: Surface Tension and the Mechanism of Refractory Attack, J. Soc. Glass Tech., 38, 89 (1954).

48. C. V. Boys, SOAP BUBBLES AND THE FORCES WHICH MOULD THEM, Doubleday Anchor Books, Garden City, New York (1959).

49. F. W. Preston and J. C. Turnbull, Physics of Upward Drilling, Am. J. Sci., 239, 92-105 (1941).

50. J. Loffler, Reactions between Glass and Refractory Walls, III, Action of Bubbles in Glass on Refractories, Glas. tech. Ber., 27, 415 (1954).

51. V. W. King and A. I. Andrews, Solubility of Zirconia on Soda Borosilicate, Glasses, J. Amer. Ceram. Soc., 24, 367-72 (1941).

52. P. P. Budnikov, G. V. Kukolev and I. S. Smelyanski, Influence of Alumina Content on the Corrosion of Furnace Refractories, Glas tech. Ber., 9, 144 (1931).

53. O. Bartsh, Determination of Slag Attacks by the Crucible Method, Ber. deut. keram. ges. 19, 413-426 (1920).

54. H. H. Blau and C. D. Smith, Refractory Problems in Glass Manufacture, Bull. Amer. Ceram. Soc., 29, 6 (1950).

55. F. Day and J. P. Ambrosene, Corrosion Resistance of Pure Alumina as a Glass Refractory, J. Amer. Ceram. Soc., 37, 162,

56. C. E. Gould, Temperature Gradient in Glass Tank Melting Furnaces, J. Soc. Glass Tech., 31, 213 (1945).

57. F. F. S. Bryson, Distribution of Temperature and Block Corrosion in Glass Tank Furnaces, J. Soc. Glass Tech., 13, 140 (1927).

58. F. H. Norton, REFRACTORIES, Chapter XV, McGraw Hill Book Co., New York (1942).

59. J. H. Partridge, Testing of Refractory Blocks for Glass Tank Furnaces, J. Soc. Glass Tech., 20, 548 (1935).

60. J. J. Webber, A. C. Siefert and F. V. Tooley, Glass Corrosion Tests on Refractories, Bull. Amer. Ceram. Soc., 29, 52 (1950).

61. G. A. Loomis, Properties and Tests of Modern Flux Clay Blocks Glass Tech. Ind., 17, 122 (1936).

62. J. C. McMullen, A Miniature Glass Test Tank, Amer. Ceram. Soc. Bull., 26, 365-6 (1947).

632 F. W. Preston, Behavior and Misbehavior of Glass in Tanks, J. Amer. Ceram. Soc., 51, 36 (1932).

64. J. Part ridge and H. Bigg, Glasshouse Refractories, J. Soc. Glass Tech., 14, 63 (1930).

65. M. Jaupain, Study of the Corrosion of Refractories by examining the Fluorescence of Adjacent Glass. Verres et Refractories, 6, 356-61 (1952).

66. W. D. Kingery, Corrosion of Refractories by Liquid Melts, pgs. 126-32 of ON HIGH TEMPERATURE - A TOOL FOR THE FUTURE, Stanford Research Inst., Menlo Park, California (1956).

67. L. Prandtl, Fluid Motion with very Small Friction, Proc. III Intern. Math. Congr., Heidleberg (1904) N.A.C.A., Tech. Memo No. 452 (1928).

68. H. Schlichting, BOUNDARY LAYER THEORY, translated by J. Kestin, Pergamon Press, New York (1955).

69. L. Howarth, On the Solution of the Laminar Boundary Layer Equation, Proc. Roy. Soc., (London), A 164, 547 (1938).

70. W. G. Cochran, The Flow due to a Rotating Disc, Proc. Cambridge Phil. Soc., 30. 365 (1934).

71. T. von Karman, On Laminar and Turbulent Friction, Z. angew Math. Mech., 1, 235 (1921).

72.a E. Eckert, INTRODUCTION TO THE TRANSFER OF HEAT AND MASS, McGraw Hill, New York, (1950).

b. C. Wagner, CLASS NOTES, KINETICS OF METALLURGICAL E PROCESSES, MIT (1956).

73. Y. S. Touloukian, G. A. Hawkins and M. Jakob, Heat Transfer by Free Convection from Heated Vertical Surfaces to Liquids, Trans. ASME, 70, 13 (1948).

74. C. Wagner, The Dissolution Rate of NaCl with Diffusion and Natural Convection as the Controlling Factors, J. Phys. and Coll. Chem., 53, 1030 (1949).

75. J. Crank, MATHEMATICS OF DIFFUSION, p. 19, Oxford, (1957).

76. W. Nusselt, The Fundementals of Heat Transfer, Gesundh. Ing., 38, 277 (1915).

77. M. Eisenberg, C. Tobias and C. Wilke, Chemical Eng. Progress Symposium Series 51, No. 161, (1955).

78. H. McMurdie and F. Hall, PHASE DIAGRAMS FOR CERAMISTS, The Amer. Ceram. Soc., page 124.

79 J. Chipman, The Thermodynamic Properties of Blast Furnace Slags, to be published in Proceedings of the Symposium on Physical Chemistry of Process Metallurgy.

80. J. D. Fulton and J. Chipman, J. Metals, 6, 1136 (1954).

81. J. D. Baird and J. Taylor, Trans. Far. Soc., 54, 526 (1958).

82. R. Sakagami and Y. Matsushita, On the Construction of Constituents in the Molten Slag of the Fundamental System. Report of the Institute of Industrial Science, University of Tokyo, 7, 180 (1954).

83. K. Sanbongi and Y. Omori, Research on the Activity Components of the Fundamental System I and II, Science Reports of the Research Inst., Tohoku University, All, 244-262 and 339-351.

84. L. C. Chang and G. Derge, An Electrochemical Study of the Properties of Molten Slags of the System $CaO-SiO_2$ and $CaO-Al_2O_3-SiO_2$. Trans. AIME, 172, 90 (1947).

85. L. R. Barrett and A. G. Thomas, Surface Tension and Density Measurements on Molten Glasses in the $CaO-Al_2O_3-SiO_2$ System, J. Soc. Glass Tech., 63, 179 (1959).

86. J. Machin and Tin Boo Yee, Viscosity Studies of the System $CaO-MgO-Al_2O_3-SiO_2$, II, $CaO-Al_2O_3-SiO_2$, J. Amer. Ceram. Soc., 31, 200-204 (1948).

87. P, Kozakevich, Viscosity of Lime Alumina Silica Melts, between 1600° and 2100° C, preprint of paper presented at AIME meeting, Pittsburgh, Pa. (1959).

88. H. Towers and J. Chipman, Diffusion of Calcium and Silica in a Lime Alumina Silica Slag, Trans. AIME, 209, 1 (1957).

89. T. King and P. Koros, Diffusion in Liquid Silicates, p. 30, KINETICS OF HIGH TEMPERATURE PROCESSES, N. D. Kingery, Editor, J. Wiley and Co., New York (1959).

90. J. Henderson, L. Yang and G. Derge, Self Diffusion of Alumina in $CaO-SiO_2-Al_2O_3$ Melts, preprint AIME meeing, Februray 14, 1960, N.Y.C.

91. J. Bardeen and C. Herring, Diffusion in Metal Alloys, Atom Movements ASM Symposium (1951).

92. Y. Haven and J. M. Stevels, Note on the Mechanism of Ionic Transport in Glass, IV CONGRESS INTERNATION DU VERRE, 343, Paris 1956.

93. K. Compaan and Y. Haven, Correlation factors for Diffusion in Solids, Trans. Far. Soc., 52, 786 (1956).

94. N. Hertz and M. Knoch, Z. anorg. Chem., 45, 267 (1905.

95. Ibid,

96. M. L. Sheeley, Ind. Eng. Chem., 24, 1060 (1932).

97. I. V. Nolkowa, Z. physik. Chem., 145, 200 (1929), ibid, 147, 206 (1930).

98. International Critical Tables, Vol III. 28, McGraw Hill Book Co., New York (1928).

99. K. Holm [illegible]ver. J. Pharmacy, 94, 139 (1922).

100. P. B. Davis and H. C. Jones, Conductivity and Negative Viscosity Coefficients, Z. Phys. Chemie, 81, 68 (1912).

101. B. Levich, The Theory of Concentration Polarization, Disc. Far. Soc., 1, 37 (1947).

102. J. A. Burton and R. C. Prim and W. P. Schlicter, The Distribution of Solute in Crystals Grown from a Melt, Part I., J. Chemical Physics, 21, 1987 (1954).

103. J. Wagner, Heat Transfer from a Rotating Disc to Ambient Air, J. Appl. Phys., 19, 837 (1948).

104. J. O'M. Bockris, J. W. Tomlinson and J. L. White, The Structure of Liquid Silicates, Partial Molar Volumes and Expansivities, Trans. Far. Soc., 52, 299 (1956).

105. L. Shartsis and S. Spinner, J. Res. Nat. Bur. Stand., 46, 176 (1951).

106. J. C. Jaeger, Proc. Roy. Soc., Edin., A 61, 223 (1942)).

107. H. S. Carslaw and J. C. Jaeger, HEAT CONDUCTION IN SOLIDS, 2nd Edition, Oxford at The Clarendon Press (1959).

108. J. C. Jaeger and M. E. Clarke, Proc. Roy. Soc. Edin., A61, 229 (1942).

109. L. Boltzmann, Ann. Physik, Peipzig, 53, 959 (1894).

110. J. R. Phillip, Numerical Solution of Equations of the Diffusion Type with Diffusivity Concentration Dependent, Trans. Far. Soc., 51, 885 (1955).

111. D. D. Gregory, A. C. Riddiford, Transport to the Surface of a Rotating Disc, J. Chem. Soc., 1, 3756 (1956).

112. F. B. Hildebrand, ADVANCED CALCULUS FOR ENGINEERS, Prentice Hall, Englewood Cliffs, New Jersey (1948).

113. W. Ellenbaas, Dissipation of Heat by Free Convection, Phillips Res. Rep. 3, 338 (1948), Dissipation of Heat by Free Convection from Vertical and Horizontal Cylinders, App. Phys. 19, 1148 (1948).

114.a E. Schmidt and W. Beckmann, The Temperature and Velocity Field from Natural Convection in the Vicinity of a Heated Vertical Plate, Forsch. Ing. Wes., 1, 391 (1930).

114.b E. Pohlhausen, The Heat Exchange Between Solid Bodies and Fluids of Small Viscosity and Heat Conductivity, ZAMM, 1, 115 (1921).

115. S. A. Brayley and C. W. Rippie, Amer. Chem. Soc., 42, 1493 (1927).

116. L. Onsager, Theories of Liquid Diffusion, Annals New York Acad. of Sci., 9(XLVI) 209 (1945).

117. R. S. Bosworth, TRANSPORT PROCESS IN APPLIED CHEMISTRY, John Wiley, New York PL (1956).

118. L. Onsager, Reciprocal Relations in Irreversible Physical Processes, Phys. Revs., 38, 2265 (1931).

119. L. Onsager and S. Machlup, Fluctuations and the Irreversible Processes, Phys. Rev., 91, 1505-15.

120. L. S. Darken, Formal Basis of Diffusion Theory, Atom Movements ASM Symposium (1951).

121. R. L. Baldwin, P. J. Dunlop and L. Bosting, Interacting Flows in Liquid Diffusion, J. Amer. Chem. Soc. 77, 5236 (1955).

122. R. L. Dunlop and L. Bosting, Interacting Flows in Liquid Diffusion II: Ibid 77, 5238.

123. H. Fuhita and L. Bosting, Solution of the Equations for Free Diffusion in Three Component Systems, with Interacting Flows J. Am. Chem. Soc., 78, 1099 (1956).

124. B. S. Harley, Theory of Velocity of Diffusion of Strong Electrolytes in Dilute Solution, Phil. Mag., 12, 473,

125. L. G. Longworth, The Diffusion of Electrolytes and Macromolecule in Solution, A Historical Study, Annals N. Y. Acad. of Sci., XLVI, 209 (1945).

126. B. S. Hartley and J. Crank, Some Fundamental Definitions and Concepts in Diffusion Processes, Trans. Far. Soc., 45, 801 (1949).

127. H. Harned, Some Recent Experimental Studies of Diffusion in Liquid Systems, Disc. Far. Soc., 24, 7 (1957).

128. B. Hammond and R. H. Stokes, Diffusion in Binary Liquid Mixtures Part 3, Trans. Faraday Soc., 52, 781 (1952).